BRNO UNIVERSITY OF TECHNOLOGY
VYSOKÉ UČENÍ TECHNICKÉ V BRNĚ

FACULTY OF MECHANICAL ENGINEERING
FAKULTA STROJNÍHO INŽENÝRSTVÍ

INSTITUTE OF MACHINE AND INDUSTRIAL DESIGN
ÚSTAV KONSTRUOVÁNÍ

LARGE-SCALE ROBOTIC 3D PRINTING OF POLYMER COMPOSITES
ROBOTICKÝ VELKOROZMĚROVÝ 3D TISK POLYMERNÍCH KOMPOZITŮ

DOCTORAL THESIS
DIZERTAČNÍ PRÁCE

AUTHOR Ing. Martin Krčma
AUTOR PRÁCE

SUPERVISOR doc. Ing. David Paloušek, Ph.D.
ŠKOLITEL

BRNO 2023

ABSTRAKT

Tato disertační práce se zabývá vývojem a výzkumem 3D tiskové metody pro velkorozměrový 3D tisk komplexních, funkčních objektů z recyklovaného polymerního kompozitu. První část práce je materiálově zaměřená, zabývá se složením kompozitu, procesními parametry, materiálovými vlastnostmi a degradací během 3D tisku. Výsledkem této části je publikace v indexovaném časopise, která srovnává materiálové vlastnosti a porozitu tištěných a litých vzorků. V průběhu práce jsou definovány problémy s 3D tiskem tohoto materiálu a je navrženo jejich řešení pomocí tiskových strategií. Druhá část disertační práce se zaměřuje na návrh, provedení a vyhodnocení těchto strategií. Na toto téma byly publikovány dva články, první zaměřený na aplikaci a porovnání víceosých 3D tiskových strategií a druhý, ve kterém je popsána nová metoda 3D tisku. Byly srovnány 4 metody, kombinující neplanární slicing a orientovaný 3D tisk, z pohledu kvality povrchu, obtížnosti zpracování a vystavitelnosti. Získané poznatky byly využity při návrhu zmíněné nové metody 3D tisku, založené na principu variace výšky vrstvy v kombinaci s reorientací tiskové hlavy pro zlepšení možností velkorozměrového 3D tisku objektů s jedním perimetrem, u kterých metoda umožnuje vystavitelnost převisů přes 80°.

KLÍČOVÁ SLOVA

Extruze materiálu, Velkorozměrový 3D tisk, Víceosý 3D tisk, Polymerní beton, Kompozit

ABSTRACT

The main goal of the thesis is research and development of a 3D printing process for large-scale printing of complex, functional objects from recycled polymer composites. The first part of the thesis is material-oriented, dealing with the composite makeup, processing parameters, material properties and their degradation during 3D printing. The results of this part are summarized in a journal article comparing the mechanical properties and porosity of printed and cast samples. During this part of the thesis, material processing problems are defined, and 3D printing strategies are proposed to solve or avoid them. The second part of the thesis then deals with the design, execution and evaluation of these strategies. This is split into two articles, the first one dealing with the application and evaluation of multiaxis 3D printing strategies, and a second that proposes a new printing method. Four methods were compared, combining nonplanar slicing and oriented 3D printing and evaluating the results in terms of buildability, processing difficulty and surface quality. The insights gained during this study were then used to inform the design of the new 3D printing method that makes use of intralayer height variations and tool reorientation to enhance single perimeter printing resulting in an increase in buildability for large-scale 3D printing to over 80° of overhang.

KEYWORDS

Material extrusion, Large scale 3D printing, Multi-axis 3D printing, Polymer Concrete, Composite

BIBLIOGRAPHICAL REFERENCE

KRČMA, Martin. *Robotický velkorozměrový 3D tisk polymerních kompozitů,* Brno, 2022, / s. Brno University of Technology, Faculty of Mechanical Engineering, Institute of Machine and Industrial Design. Supervisor doc. David Paloušek, PhD.

ACKNOWLEDGEMENT

I would like to say thanks to my thesis supervisor, David Paloušek, for his leadership during my transition to research, as that was a completely new field for me. Furthermore, I would like to thank David Škaroupka, my supervisor specialist, for taking on board his team and introducing me to a new field, and I would like to say thanks to my colleagues and family for their support when I needed it.

STATEMENT OF ORIGINALITY

I hereby declare that I have written the PhD thesis *Large scale robotic 3D printing of polymer composites* on my own according to the advice of my supervisor doc. Ing. David Paloušek, Ph.D., and using the sources listed in references.

.....

Authors signature

CONTENT

1 INTRODUCTION

1.1 Motivation

Social challenge

Unusable contaminated polymer waste continues to be a major problem in the current recycling chain, because although the ratio of recycled plastic in EU countries increased significantly to 75% in 2018 [1], there are still up to 20 megatons of plastics that do not reach recycling centres in the EU alone [2]. Instead of a final thermal reclamation or landfilling the unrecycled waste, there is a way to take advantage of its good material properties, by using it as a binder in a highly filled polymer composite. These materials can be made from recycled post-consumer thermoplastics which are used to bind a majority percentage of filler – aggregate or other inexpensive material. The use of aggregate, such as sand, essentially makes these composites a type of concrete. Concrete-like recycled composites are not a new idea, and their popularity rises and falls with the cost of plastic and, respectively, oil prices. The first mentions date back to the 1980s, as shown by research [3] and patents [4]. These materials are economical while exhibiting suitable properties for construction. Highly filled polymer composites combine the ease of processing of thermoplastics with properties suitable for large-scale 3D printing, including in the construction industry.

Figure 1 A tile cast from a polymer concrete mixture based on post-consumer PET and reclaimed glass [5]

3D printing for the construction industry

The first choice of material for construction 3D printing might be concrete, but concrete is a complicated material whose behaviour makes it difficult to use for 3D printing, especially for complex, optimised parts. While using polymer concrete for 3D printing carries some obstacles, but the same time its material properties make it well suited to the process, especially for applications where using polymers alone would not be sufficient. In particular, the high filler content makes the large-scale deposition stable, as it prevents sagging and decreases warping during the printing process. The finished products inherit these properties, exhibiting high stiffness, high heat deflection temperature (HDT) and resistance to environmental influences. This makes them suitable for demanding construction applications.

Regardless of the complexity of a construction project, a large amount of waste is generated and driving it down by efficient material usage would be a significant advantage of 3D printing in construction. Efficient material usage is also one of the reasons for the utilization of multiaxis methods in this thesis, as one of their benefits is a reduction in the amount of support structures needed. They also make it possible to use the method for more complex parts, e.g. for the production of manufacturing tools, moulds or formwork.

Figure 2 Beam joint printed using polymer concrete and nonplanar toolpaths for a conference submission

1.2 Topic introduction

This thesis began to develop the idea of 3D printing polymer concrete from the ground up. During the first and second years, various extruders were designed, and some of them were built and tested in collaboration with students and staff from the Institute of Machine and Industrial Design. The screw extruder developed by J. Kočař [6] ended up being the cornerstone of this thesis, as it was able to process the material for 3D printing with sufficient results. The method and the results developed with this extruder form the first part of the thesis, which focuses on the material properties of the printed composite. The results achieved with this equipment setup are quite simple, but they were sufficient to verify the process and show its potential, and a new set of equipment is under development to further advance the process.

During the testing of the current setup, several problems came to light – warping of the prints under internal stresses, unexpected behaviour of the large molten depositions, and the limitations of printing with a screw extruder. The second part of the thesis focuses on addressing these problems specific to large-scale 3D printing using multiaxis methods, such as non-planar3D printing, oriented 3D printing, variable layer height and more. These methods were applied to the process of large-scale multiaxis 3D printing and their usability was evaluated.

The importance of some parameters, especially the layer height, became clear. This led to the development of a new method that harnesses the capabilities of material extrusion 3D printing (MEX) to significantly improve the buildability of the process while keeping material usage and processing costs low. This innovation brings the desired goal of material savings in construction closer by enabling easier buildability of optimised geometries through large-scale extrusion 3D printing with any material. When used for 3D printing of polymer concrete, the combination provides a clean building solution that utilizes recycled material, produces little waste and offers high performance. However, its usability is not limited to polymer concrete; it should prove valuable for any MEX printing process, including clay and concrete, and even for other line-by-line 3D printing processes, such as wire arc additive manufacturing.

1.3 Motivation summary

- By processing a contaminated material that would otherwise be landfilled or incinerated, more of its value is retained and recycling it into a composite is better than the alternatives.

- The material properties of the polymer composite lend themselves to high performance architecture due to its environmental resistance and increased tensile strength and fit well with the freedom of form that 3D printing offers.
- The support-free printing of the aforementioned high-performance, complex shapes enabled by multiaxis methods can significantly reduce material consumption, resulting in less waste, cost and processing time.
- Due to its material properties, the material could also replace concrete in certain applications, with significantly lower material consumption due to its tensile strength. In addition, the high CO2 emissions generated by cement processing could be reduced.

2 STATE OF THE ART

2.1 Overview of important 3D printing concepts

One of the most popular methods of 3D printing is MEX (Material Extrusion). It works by extruding liquid material through a movable nozzle and building up objects line by line and layer by layer. Its most common form is FDM (Fused Deposition Modelling), working with thermoplastic in the form of filaments.

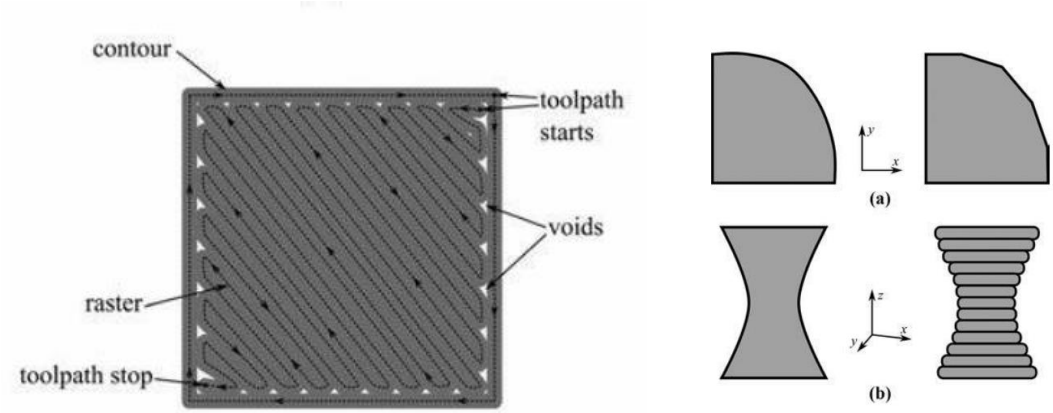

Figure 3 Raster effect in FDM creating voids in the material, Stairstep effect [7]

This manufacturing method has its inherent problems. The line-by-line, layer-by-layer manufacturing process leads to porosity between the individual deposition, due to their oval profile. Another effect of this is the inherent anisotropy of ME printing, with the build direction being the weakest and the most brittle. The layer height also influences surface quality, depending on the build direction. This is mainly caused by the surface of the deposition not perfectly describing the angled surface of the model (Fig.3). This difference is described by “cusp height”, which is the maximum deviation of the deposition from the model Layer height also influences overhang buildability (the ability of the process to build a specified geometry). The process fundamentally has limits on buildability, as it's impossible to deposit new print paths mid-air. The commonly used limit for overhang buildability is 45°, though in practice, the limit is inversely proportional to layer height, and can be as high as 60° [7–14].

Thermoplastics are most used for this process because of their ability to regain material properties after remelting. The most common ones are PLA, ABS and PETG, as their amorphous nature makes them exhibit low warpage during printing. High-performance semi-crystalline polymers can also be used, but their high shrinkage factors bring the need for a heated build chamber. Other processable fluid materials include thermosets plastics, clay, and concrete [15–17].

2.2 Use of polymer recyclate as a binder in concrete

There are occasional mentions of using plastic recyclates as the binder in a binder-sand composite – commonly called concrete [18]. A wide variety of these composites, mostly using fine-grained filler, was tested by Slieptsova [19]. Different types of PE, PET and PC were used, in combination with sand of 0.2 to 1.2 granularity. The best results were achieved using PET composites, as PET-G has low HDT, and polyolefin-based materials have lower mechanical performance. Recycled PET in flake form was also processed by Dumitrescu [20], suggesting an optimal processing temperature of 185-195°C. Using a filler ratio of 0.6 to 1.2, strength in compression of 87 MPa was achieved (Chart can be seen in Fig. 5). Alternative method of processing recycled plastic into a rough flake and then by a screw extruder is used by a partner company [5], as well as by other research teams with up to 40% aggregate infill [21]. Material prepared in this way presents good environmental resistance in regards to UV, water and acid resistance [22]. There are patents describing ways to manufacture polymer-aggregate composites, either by batch mixing or by modified screw extrusion [4, 23]. An alternative processing route is by mixing the granular materials together and heating them in the mould, before compacting them. This enables low binder content, 10% of PE was judged to perform the best, with a flexural strength of 15 MPa [24]. To increase the ratio of recycled materials, in addition to waste plastic, using recycled fibre and sand is also a possibility [25], another option would be using natural fibre which can partially bring the same benefits as GF [26].

Material properties of POLYBET (77:23, sand:PET)	POLYBET	Common concrete
Density	1950 kg/m^3	2300 kg/m^3
Median flexural strength	14,6 MPa	7 MPa
Water absorption	0%	7%
Frost resistance	1[-]	0,81[-]
Water and CHRL resistance (50 cycles)	Loss of 4 g/m^2 Undisturbed	Loss of 250 4 g/m^2 Slightly disturbed
Depth of seepage of pressurised water	0 mm	3-5 mm

Figure 4 Properties of a polymer concrete mixture [5]

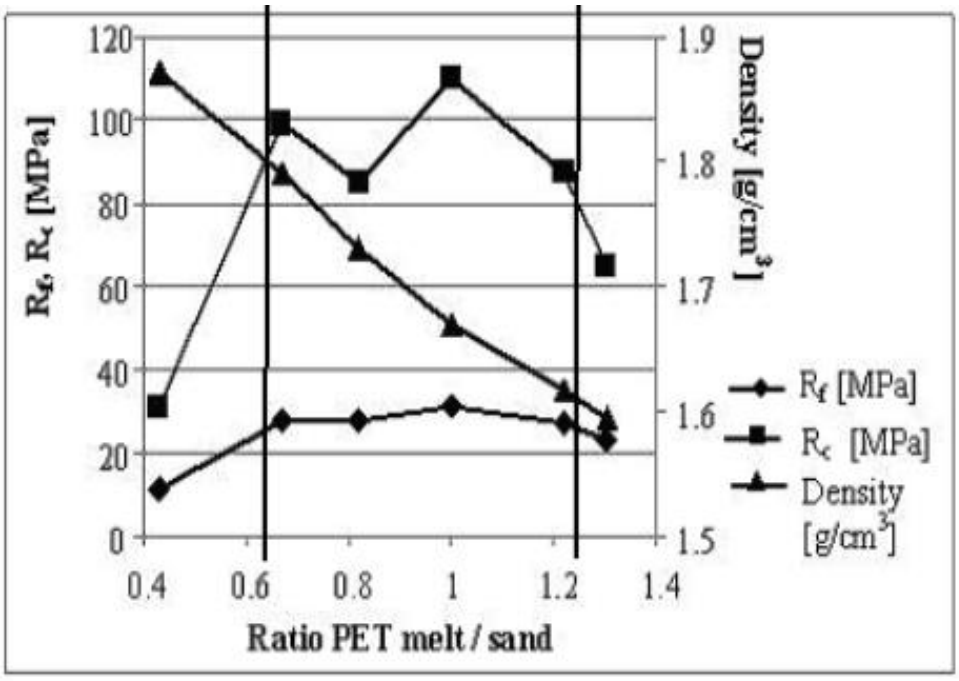

Figure 5 Influence of particulate ratio on composite strength [20]

Different fillers were tested by Hugo, finding that glass fibres and plate-like mica had better results than spherical fillers, and worked well together in a combination of 30% GF and 5% mica (Fig. 6). For the fillers to decrease the coefficient of thermal expansion (CTE), proper interfacing must be achieved by e.g. surface treatment. The 30% GF-filled composite has a CTE of 300% less than the original blend of recycled plastics by itself [27]. Exploration of sand-fibre systems was carried out by Herrera-Franco, showing that a 50% sand and 20% natural fibre composite is possible without significant loss of tensile strength with proper surface treatment, in this case, silane [28]. In another work, a clay-palm fibre system showed an increase in thermal, tensile (11%) and rheological properties, offering a more economical material with increased performance [29].

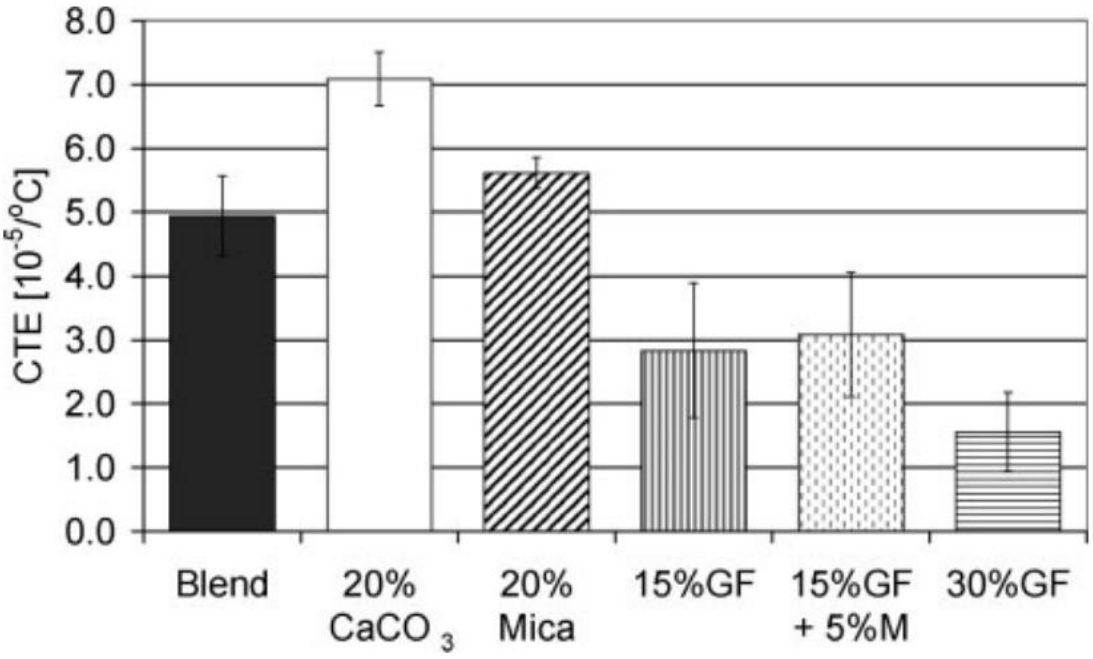

Figure 6 Comparison of filler influence on CTE [27]

The strengthening properties of glass fibre are enough to give a satisfactory mechanical performance to material made of contaminated cast-off waste, consisting of a mixture of commodity plastics and contaminants such as metal foil. 30% of GF inside the composite increases its tensile strength by 400% [30].

2.2.1 Use of composites and recyclates for 3D printing

Recycled post-consumer polypropylene was used for FDM 3D printing by Stoof [31] together with fillers, such as natural fibres and mineral particulate. The addition of the filler resulted in an increase in strength and stiffness in the raw stock, which did not completely translate to the printed samples. Most importantly, a warpage test was proposed and used to measure deformation after printing of the filled PP filament. The specimens with 30% natural fibre had a reduction in warpage up to 80%. The specimen and results can be seen in Fig. 7.

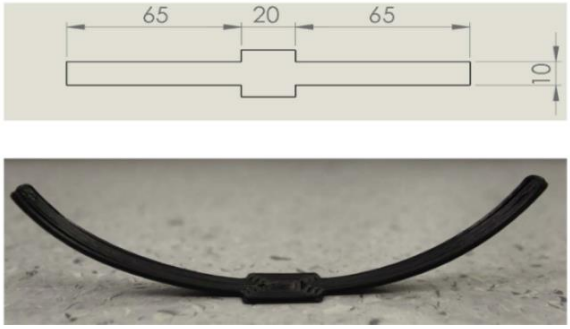

Sample	Shrinkage (%)	Net reduction (%)
Pre-consumer PP,	2.13	–
10% Hemp	1.17	45
20% Hemp	0.65	69
30% Hemp	0.47	78
10% Harakeke	1.18	45
20% Harakeke	1.2	44
30% Harakeke	0.34	84
10% Gypsum	1.53	28
20% Gypsum	1.51	29
30% Gypsum	1.39	35
40% Gypsum	1.26	41
50% Gypsum	1.15	46

Figure 7 Warpage testing specimen and shrinkage reduction of composites [31]

Another usage of recycled PP with filler, in this case using discarded tires to produce suitable material for large-scale printing, was carried out by Dominguez [32]. They used a screw extruder with a 6 mm nozzle, adapted from a plastic welder, and printed at 198°C. They achieved maximum stress of 6 MPa, according to ISO 527-4.

A commodity plastic that has a good recycling chain and was also used for 3D printing is PET [33, 34]. The bottles were mechanically processed and the resulting flakes were used in a single screw extruder. The article mentions challenges in processing PET, such as warpage, moisture and cooling dependency, varied processing requirements based on the stock and extreme brittleness, which make it challenging to use compared to common 3D printing plastics such as ABS, which can be easily adapted for the process. [35, 36]

A review of polymer composites shows that fibre material increases tensile strength, modulus, and print quality, but at the same time also increases anisotropy. Particulate has a wider scale of effects, both positively and negatively affecting mechanical performance, elasticity and anisotropy [37].

2.2.2 Large scale 3D printing

A significant part of research into large scale melt extrusion 3D printing is coming from Oak Ridge National Laboratory, in conjunction with their development of the BAAM system – Big Area Additive Manufacturing [38–40]. This is a scalable, moving gantry-based system. Instead of trying to solve shrinkage with a heated chamber, they have moved toward using a carbon fibre filled material with low shrinkage. This results in decreasing the deformation for a 1,8 m specimen from 4,5 cm for ABS to 0 cm for the material with 13% CF. The addition of 10-40% of CF to ABS increases the stiffness by a factor of 4 to 7.

They have also noted that the fibre filled materials have a higher degree of anisotropy – 50% loss of strength for ABS CF compared to 29% for virgin ABS in the build direction. The authors speculate that this is due to the fibres becoming oriented along the deposition's surface and preventing deep bonding between depositions. Anisotropy difference between the virgin and composite ABS can be seen in Fig. 8.

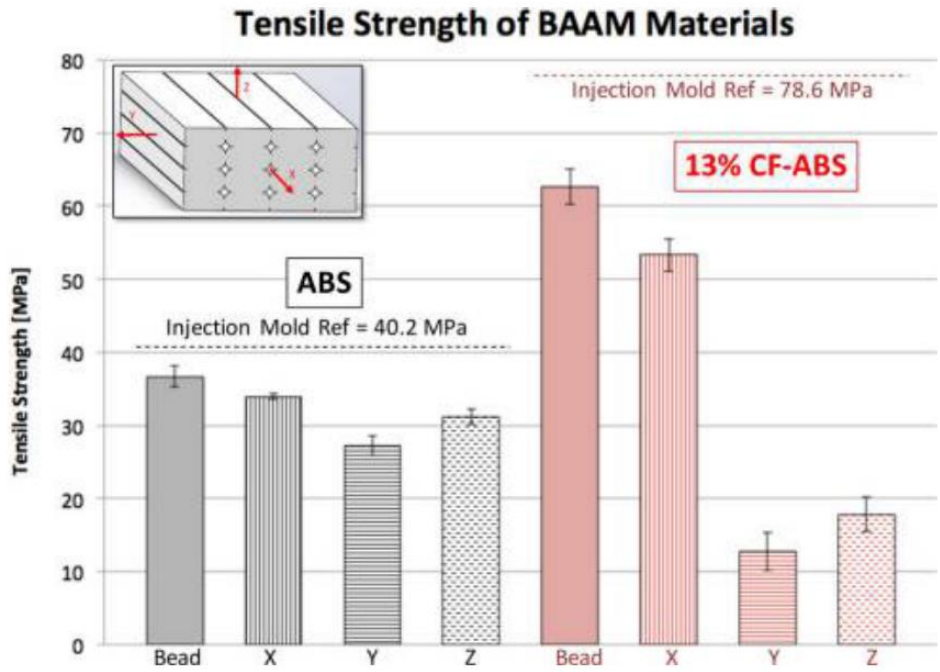

Figure 8 Increased anisotropy of fibre filled materials [39]

Melt extrusion 3D printing of PP pellets was tested out by Hertle [41]. The main takeaway was the importance of keeping the melt temperature high to achieve high mechanical performance – substrate temp. of 85°C and melt temp. of 230°C is suggested. A potential issue was highlighted – high cooling rates lead to higher potential strength but decrease material homogeneity. Warpage testing of large-scale MEX using pellets showed that even amorphous materials such as ABS have shrinkage factors high enough to cause warping and delamination during printing. Unfilled ABS exhibited shrinkage of 0.7-to 1.6%, while GF ABS exhibited 0.2-0.4% and flame retardant ABS filled with particulate exhibited 0.4-0.7%. [42]

2.3 Multi-axis 3D printing

Methods classified as multi-axis 3D printing are intended to expand the limitation of traditional 3D printing, which could even be called 2.5D printing as constant parallel layers are used. The first method would be Incline layer slicing – the model is divided into multiple segments that are printed with the most beneficial orientation. This can be done manually or algorithmically [14, 43, 44] either for a 3-axis process to the nozzle limit or for a multiaxis process with the orientation of the nozzle switching between segments. The gains realized by changing the orientation of slicing can be seen in Fig. 9. A variation on this topic is using conical surfaces – which enable 90° of printable overhang on a 3-axis and more on a 4-axis tilted head machine [45].

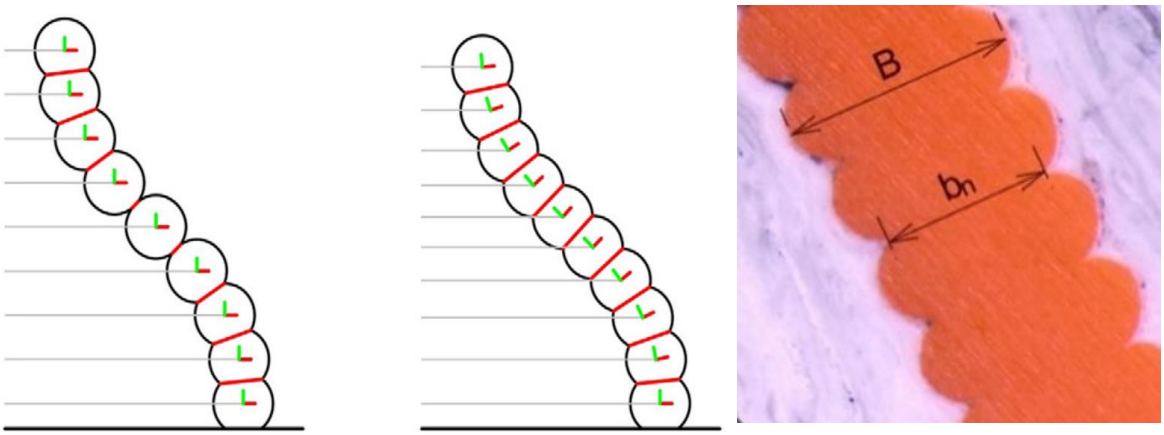

Figure 9 Oriented 3D printing Schematic [17] Real depositions [12]

The next category of methods is Curved/Nonplanar layer fused deposition modelling. CLFDM was first mentioned by Chakraborty [46] with the main goal of being able to print near-flat thin-walled parts such as propeller blades. The method is explained in Fig. 10. The main idea is generating constantly spaced print paths covering the entire model. The technique was then further developed by Huang and Singamneni over a number of publications, utilizing adaptive layers and combination with flat layer slicing as well as modelling and evaluation. [47–50] Among the main benefits of this method are increased buildability, reduced material consumption [51], increased surface quality due to elimination of stairstepping [52] and increased mechanical performance (up to 6x load [53]).

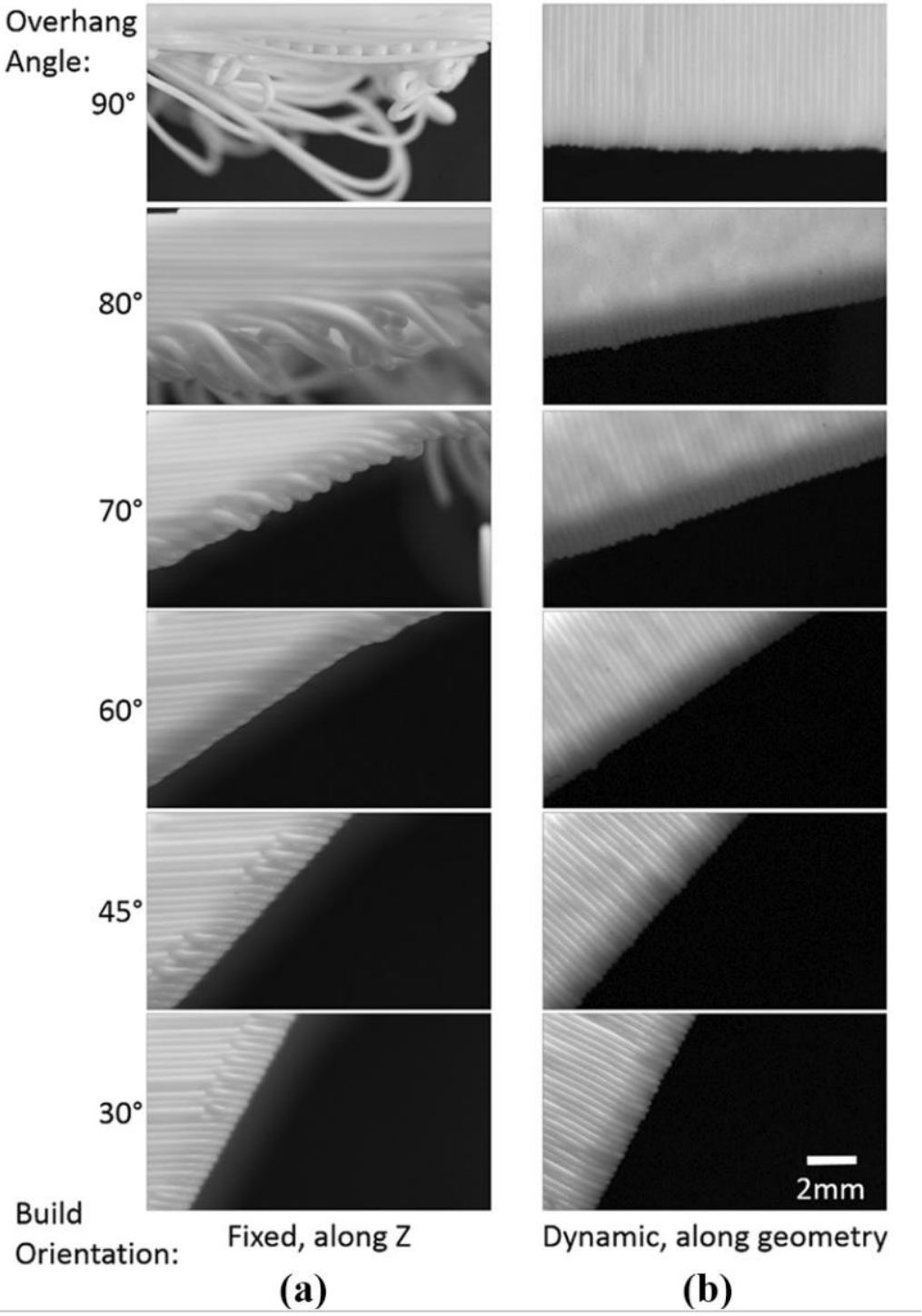

Figure 10 Buildability extension by oriented 3D printing [14]

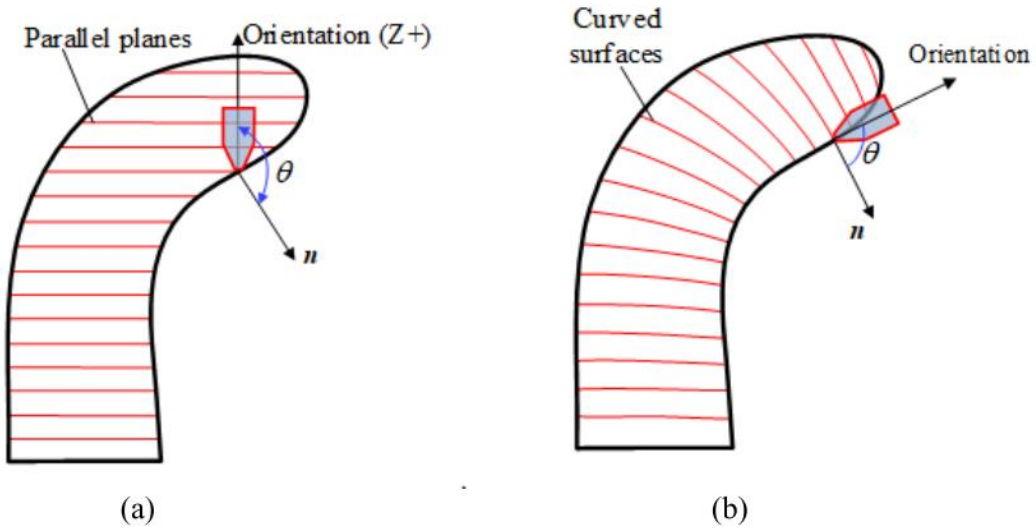

Figure 11 Difference between traditional printing (a) and non-planar oriented printing (b) [54]

The most significant challenge to using curved layers is the print path generation itself. In contrast to flat layer slicing, multiple new criteria appear [55]. The first issue is the covering of the printed part that is not taken into consideration when generating flat layers, the second is the issue of printability. Multiple approaches have been presented to the issue of surface covering [56]. The simplest of them use mathematical surface representation and divide the surfaces equally by distance. This generates perfect covering but is limited to simple forms. [57, 58] More computationally intense approaches include voxel-based marching [59] (Fig. 11), geodesic and isocurve [60] based approaches which work for general mesh representation and complex surfaces and can be further improved.

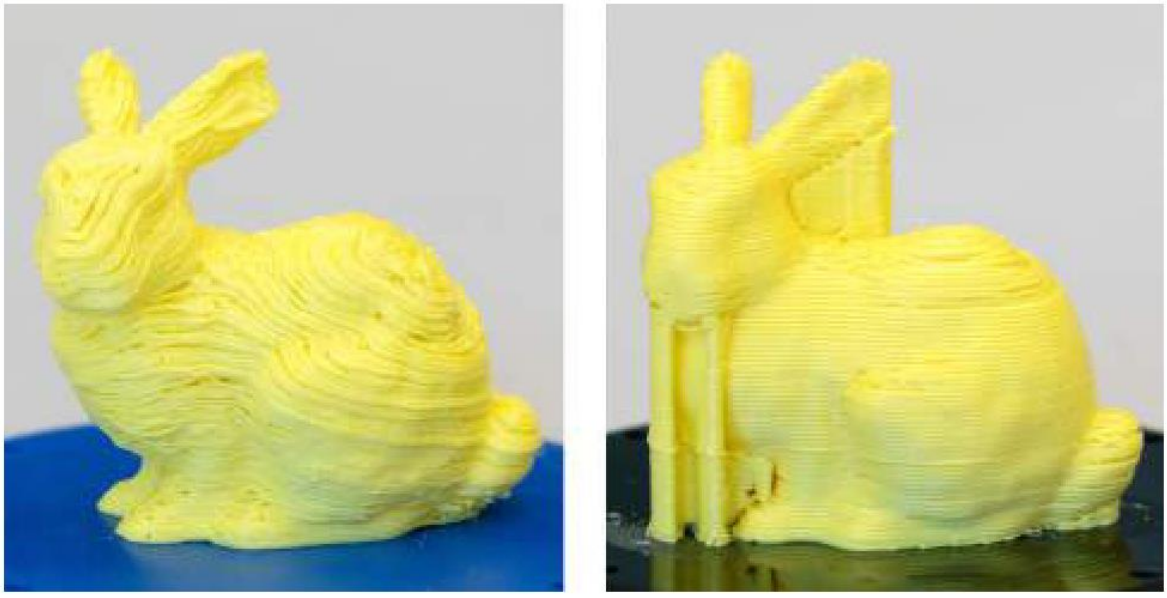

Figure 12 1. Results of CLF by voxelization 2. 2.5D Slicing and supports [59]

The second issue is printability. There is a number of possible failure states for nonplanar printing paths. These include the problem of occlusion, where the part geometry makes another area unreachable, the 3-axis problem of slope steepness limitation and the oriented 3D printing problem of geometry collision [57, 61]. Collision modes of nonplanar 3DP can be seen in Fig. 12. These problems have to be prevented by including the limitations directly in the slicing process – e.g. varying the layer height to avoid a collision, generating only convex layers for 5-axis 3D printing [59] or using a decomposition algorithm to separate and order the print in a way that makes each part printable [14, 62] Alternatively, collision check has to be performed after slicing. The solution to these problems is also partially covered in patents US20180250748A1 and US9796140B2 owned by Autodesk Inc., broadly describing curved and nonplanar printing approaches, both for buildability and surface augmentation. Adding to this, even a print without these failure states needs to be precisely controlled in terms of tool speed and orientation to prevent print artefacts or possible failure of the print [63].

The last topic to mention would be spatial 3D printing, which completely forgoes the use of layers, instead it directly prints strut structures by multiaxis motion. Commonly used to print crystalline-like structures such as BCC with a high stiffness-to-weight ratio. The difficulty of this process comes from the high number of parameters, the need to account for geometrical limitations and collision-free motion planning [64–66].

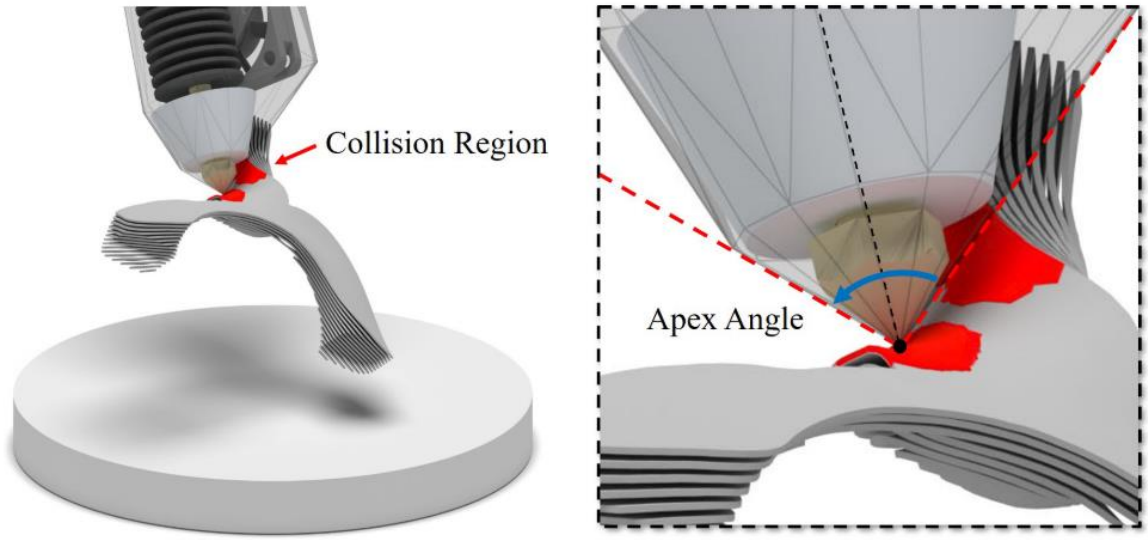

Figure 13 Geometry collision and definition of boundary cone angle/apex angle [53]

2.3.1 Layer height variation

The idea of varying layer height in between layers is thoroughly explored and implemented in current slicers. Layer heights are usually chosen according to the cusp height measure, with the layer height adapting to local geometry, either through the entire model, or locally to keep build time low [67]. The cusp height is measured as the maximum error from the original surface, measured tangentially [13]. In addition to this approach, several optimizations were developed, based on surface roughness (*Ra*) or profile analysis [68, 69]. Adaptive layer height was also combined with curved layer printing to form the Curved Layer Adaptive Slicing (CLAS) technique. This has been demonstrated to improve the surface quality and mechanical properties of specific objects [70].

In contrast to layer height variation, literature describing varying layer height during a single layer is sparse. A technique by L. Pelzer makes use of this to mechanically lock the infill together, thus improving the performance of the parts (Fig. 14), or to transition from printing slightly nonplanar top or bottom surfaces to regular printing [71], interlocking infill is also used to achieve improvement or differentiation of printed parts [72]. A similar technique is used by L. Chen to accurately print thin shells and preserve their details [73]. Related technique published under the name CONVEX focuses on varying the print path width to increase intralayer coverage and part strength perpendicular to the build direction [74].

Variation in intralayer height also occurs during iso-parametric slicing, but it does not disturb the print if the differences are small enough. Occasionally, these differences are corrected for, as in G. Schuh [75], and this is the same principle that when exploited to its full potential, could bring significant improvements to buildability.

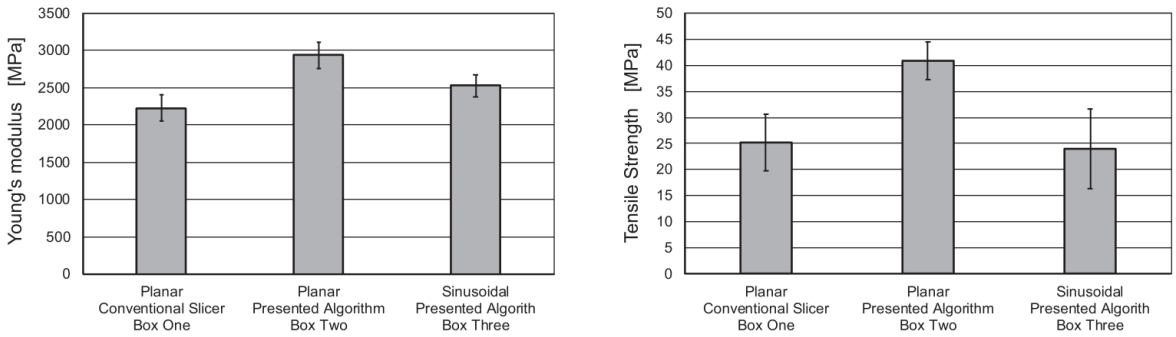

Figure 14 Youngs modulus and tensile performance comparison of conventional slicing and nonplanar slicing algorithm [71]

3 ANALYSIS OF LITERATURE

3.1 Printing of plastic and recycled composites

The amount of recycled consumer plastics has reached a significant percentage in Western European countries. However, a significant proportion of plastics continues not to be recycled, mostly due to economic reasons, as washing and separating the waste from contaminants and secondary packaging material is too costly. The amount of available material being dumped remains considerable [22, 34].

Thermal recycling of this contaminated polymer waste into a concrete composite is an economic process that is suitable for 3D printing, due to its ability to be processed by extrusion, the stability of PP in the melt [22] and the high stiffness that resists warping which would otherwise be present in the semicrystalline polymer [39]. The decreased surface quality and mediocre mechanical performance are offset by low cost, and this combination makes the material suitable for the construction industry [30]. The preferred polymer for this application is PP, as PET is difficult to process, and PE waste is usually highly contaminated [36, 41, 42].

The processing temperature range for recyclates is measured using TGA analysis and the melting point, and ranges from 160-165°C to 250°C-300°C [22]. Print temperature influences the mechanical performance of the print due to weld quality, at low temperatures the diffusion might not be sufficient [7, 10], while high temps necessitate layer cooling/other ways to manage layer temp such as interrupted printing [8, 39]. Layer height influences mechanical parameters, surface quality and partially buildability – see Figure 15., due to the decreasing contact patch size [9]. The behaviour of layer height while building overhangs was typically described with the ”cusp height measure” [13], but in this work, the concept of “actual layer height” is being used, which better explains the phenomena in single perimeter printing. Using this optic, a different approach can be devised, as you are not limited to manipulating print paths, but you can also manipulate print parameters [74, 76]. No matter the name, this leads to nonplanar printing, discussed further down, as these methods allow for the actual layer height to be kept constant [47].

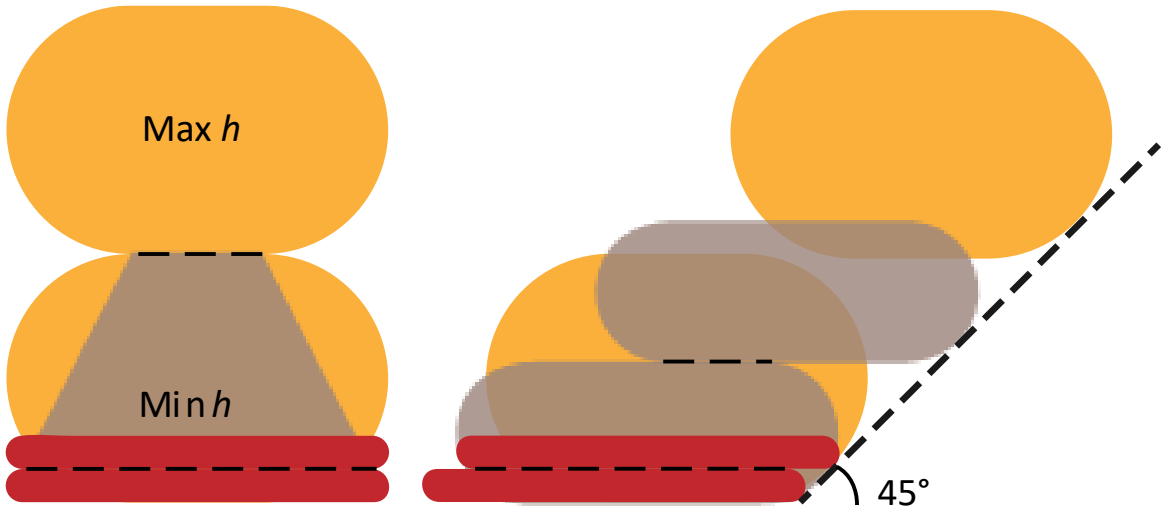

Figure 15 Layer height influence on buildability – contact patch width/actual layer height dependence on the overhang angle

3.1.1 Filler performance in composites

With an increase in particulate filler percentage, a loss of tensile strength and an increase in modulus is usually recorded [37]. However, for contaminated plastics, this loss is not linear, in some cases it is the same for a 10% fill ratio as for a 40%, thus making high fill ratios beneficial without loss of strength [20]. Especially if particulate-fibre composite is used, as fibre reinforcement has the effect of increasing tensile strength and modulus [28, 30]. Particulate filler, especially when a large particle size is used, increases performance in compression [24]. The wide range of effects of particulate fillers in plastics could be explained by binder-filler compatibility and the need for surface treatment [19, 37]. Additional benefits of using particulate-filled material in construction content are increased UV resistance and thermal stability [30]. This makes the material suitable for infrastructural usage as a replacement for wood or concrete in certain applications, especially if weather resistance is considered [27].

For large-scale printing, two effects of filler on the behaviour of the 3D prints are important to mention. First, it is the change to the melt behaviour [29], that stabilizes the deposition of post-consumer plastic [22] that otherwise wouldn’t be a good fit for extrusion at this scale. And second, it prevents warping of the print during the process by increasing the stiffness [31]. For large-scale prints, deformations on the scale of centimetres to meters would be expected without the use of filler [39], even when printing amorphous plastics that have a lower coefficient of thermal expansion as they don’t undergo crystallization [9].

3.2 Multiaxis 3D printing for large scale

The benefits of using multiaxis 3D printing are expanding buildability, improving surface quality and increasing strength [53, 75]. This is especially important in large-scale printing, as the parts are often structural, material expenditure is significant and single wall printing is often used because of material savings and extruder limitations – and this all plays against using support structures, as they are difficult to print, increase material expenditure, do not ensure high-quality surfaces and require post-processing [38, 77]. Reorientation of the print head allows for printing of significant overhang angles without material sagging, and thus without a decrease in surface quality [14, 17]. Oriented printing brings the most benefits when combined with the method of CLF (curved layer fabrication), increasing strength, surface quality and buildability [55, 78]. It also eliminates the effect of stairstepping on overhangs, significant in large-scale printing [46]. If applicable, the technique would be a good fit for polymer concrete printing.

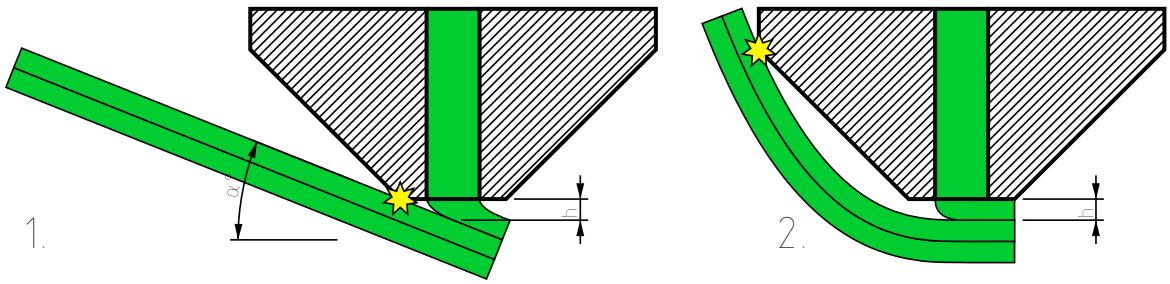

Figure 16 Self-collision modes in multiaxis 3D printing: 1. Collision due to the slope steepness 2. Collision with surrounding geometry

The limitations and difficulties in deploying CLF come from multiple factors, such as the need to use multi-axis machines, with multiple approaches to machine setup being recorded and the lack of equipment standardization that makes the development of a slicer difficult, or the need for collision checking [53]. The necessity for collision avoidance during CLF also leads to the development of custom nozzles, which further complicates deployment [55] (Types of collisions can be seen in Fig. 16). At the time of writing, there was no general-purpose slicing algorithm. There are multiple solutions described in research articles that are either limited in printable geometry, especially in the case of isocontour-based slicing [57, 78], with voxel [59] or field-based methods [60] being more flexible, but none of them are readily available. For near-flat parts, experimental features in Slic3r or CurviSlicer [76] are available and compatible with standard 3-axis FDM machines. The difficulty of the process, together with the fact that a recent review pointed out the unexplored potential of multi-axis methods should lead to consideration of other approaches that could bring benefits to large-scale composite 3D printing [56].

3.2.1 Variable layer height

One of the alternative approaches might be the combination of multiaxis 3D printing and layer height variation. This combination is underexplored in current literature, in contrast to traditional layer height variation [60, 67, 69]. Intralayer height variation was only ever used for improving top and bottom surface quality and eliminating the stair stepping effect on near-flat surfaces [71, 73, 76]. Instead of removing the variation of layer height by using curved layers, we could embrace the effect, as layer height/extrusion factor are fully controllable, and under-utilized in current 3D printing [56, 74].

3.3 Important insights

1. Polymer concrete, thanks to its composition, can be a suitable material for 3D printing, as its high filler content (> 40%) counteracts some of the problems that thermoplastic 3D printing faces as its scale increases. The main effects that could decrease its performance after 3D printing are thermal degradation and poor layer adhesion due to filler alignment.

2. Most of the problems caused by the cusp/actual layer height phenomenon, exacerbated by the large deposition height, can be solved by non-planar 3D printing, but the benefits are offset by processing difficulty. The nonplanarity of the layers themselves causes the problems– sometimes, when there are large differences in cross-sections, sharp changes in surface profile, or due to the topology of the objects, covering the object with equidistant print paths becomes impossible.

3. No publication was found that intentionally uses the variation of layer height within a single layer to counteract the decreasing patch thickness/increasing layer height. This represents a blank spot in current methods and could serve as an alternative to nonplanar methods.

4 AIM OF THE THESIS

The main goal of the thesis is the development of a 3D printing process for large-scale printing of complex, functional objects from recycled polymer composites. This method will take into account the limitations of screw extrusion and of the chosen material and will exploit the full potential of 3D printing including multiaxis methods, enabled by the use of a robotic manipulator. The aim is to improve buildability, surface quality and reduction in material expenditure through support-free printing beyond the limitations of layer-by-layer printing. The motivation for using recycled thermoplastic composite as a 3D printing material is the possibility to develop an efficient and economical manufacturing process utilizing waste material. The “polymer concrete” composite will be evaluated and possibly modified in terms of stability, buildability and mechanical performance. The goals also include defining the possible applications of the process and adapting the process to fit within the application limits.

4.1 Partial goals of the thesis

4.1.1 Experimental exploration of process parameters of polymer concrete

Finding the combination of process parameters that results in a quality deposition. This is achieved by varying the combination of deposition speed and material flow as well as layer height, extrusion temperature and others. Following that, classification of the mechanical properties of the printed highly filled material and comparison with the cast state to find the degree and source of degradation in the 3D printing process.

4.1.2 Development of a large-scale 3D printing method

Since the printing strategies of FDM are not fully suitable for large-scale printing, other strategies have to be developed. Due to the nature of the screw extruder, vase mode strategies are preferred. Deformation during printing needs to be considered, as the large deposition sizes take significant time to cool and are prone to sagging and warping. Can deformation caused by material shrinkage during the 3D printing process be mitigated by continuously changing the printhead orientation, or changing the print paths themselves?

4.1.3 Application-focused 3D printing strategies

A new multiaxis printing methods suitable for polymer concrete will be developed. This may include curved layer trajectories, varied printing orientations, spatial struts printing and other multiaxis methods. The goal of applying these methods is to improve surface quality, minimise support and reduce material usage. The outcome of this part of the research should be algorithms for slicing and for the generation of robot code.

4.2 Hypotheses and scientific questions

H1: Mechanical properties of polymer concrete are reduced by the 3D printing process compared to casting due to thermal degradation, porosity, or other factors of the process.

Is the composite made from waste thermoplastic suitable for additive manufacturing? Are the material properties after 3D printing at a level that allows the material to be used for the manufacture of functional objects [37]*? Which source of degradation (thermal degradation, porosity or anisotropy* [36, 39]*) is prevalent in the layer-by-layer process, if any, and to what degree?*

H2: The application of the oriented 3D printing technique improves buildability and surface quality beyond the level achievable with 3-axis printing, with the same benefits for large-scale 3D printing compared to desktop-scale [14, 43].

Oriented 5-axis 3D printing methods could improve surface quality and buildability beyond the common build limit of 45° [14] *by keeping the deposition walls aligned with the local surface orientation. Will the application of the oriented printing method lead to a reduction of the stairstep effect* [52]*, a reduction of the surface roughness Ra, and a reduction of the material expenditure* [51] *of large scale 3DP*?

H3: Planar slicing combined with compensation for changes in actual layer height can achieve improvements in buildability similar to those gained by nonplanar slicing.

This hypothesis is based on the results of a submitted article. It was formulated based on observations made during experiments related to the second thesis. The theory is that the reason for buildability reduction in overhanging areas is a reduction in material quantity, thus the surface coverage becomes insufficient and the print fails. If this is compensated for, can a method that offers increased buildability and supportless printing be developed, lacking the drawbacks of nonplanar methods [55, 56]*?*

4.3 Thesis structure

The core of this thesis consists of three articles published in journals indexed in the WoS database, which are attached as supplementary material. This text provides an overview of the methods used and the achieved results, as well as a background to the topic and some additional content that did not fit within the published articles or would merit its own publication.

The first article deals with the processing of polymer concrete for 3D printing and the evaluation of the results and tries to answer the first hypothesis H1. It was published in the Rapid Prototyping Journal. The second article, related to the second hypothesis H2, was published in The International Journal of Advanced Manufacturing Technology and deals with the requirements for implementing and testing the effects of various methods of multiaxis 3D printing. The third article was published in the journal 3D Printing and Additive Manufacturing and deals with the third hypothesis H3. It introduces a new method for multiaxis 3D printing with variable intralayer height and provides practical examples and verification of the method. Below you will find citations of all three articles:

1. Krčma, M., Škaroupka, D., Vosynek, P., Zikmund, T., Kaiser, J. and Palousek, D. (2021), "Use of polymer concrete for large-scale 3D printing", Rapid Prototyping Journal, Vol. 27 No. 3, pp. 465-474. https://doi.org/10.1108/RPJ-12-2019-0316
   Author's contribution: First author, 75%

2. Krčma, M., Paloušek, D. “Comparison of the effects of multiaxis printing strategies on large-scale 3D printed surface quality, accuracy, and strength.” Int J Adv Manuf Technol 119, 7109–7120 (2022). https://doi.org/10.1007/s00170-022-08685-4
   Author's contribution: First author, 90%

3. Martin Krčma, David Paloušek, David Škaroupka, Johannes Braumann, and Daniel Koutný. “Method of Multiaxis Three-Dimensional Printing with Intralayer Height Variation for Stairstep Effect Compensation”.3D Printing and Additive Manufacturing. ahead of print http://doi.org/10.1089/3dp.2022.0097
   Author's contribution: First author, 80%

5 MATERIALS AND METHODS

This chapter contains a general overview of the materials, machines and methods used in the thesis. More detailed information can be found in each of the included articles. The first part of the chapter focuses on the testing assembly used throughout the thesis to fabricate specimens, and the various testing equipment used to quantify the results. Material development, which is not a cornerstone of this thesis, but was done alongside it, is covered, together with the processing parameters used. In the second part, the software environment used to develop the slicing and printing methods is described, and the process is explained in detail, together with the tilt control.

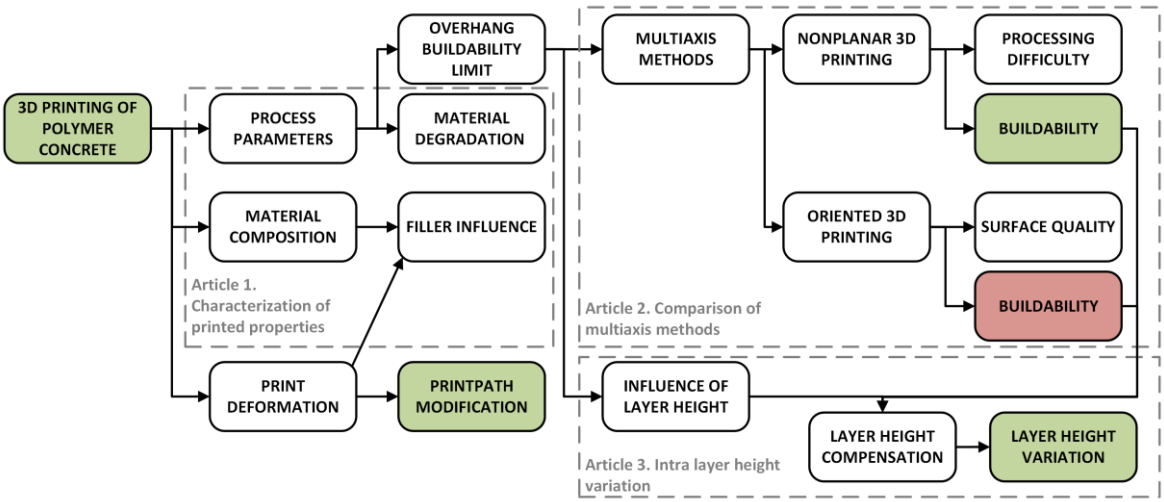

Figure 17 An overview of the thesis composition, showing the relationship between the different topics

5.1 Testing assembly

5.1.1 3D printing hardware

The extrusion equipment used in this thesis is derived from the result of the project TAČR Zéta TJ01000354. It is a constant pitch screw extruder with a diameter of 30 mm. The extruder is heated using resistive rods, the total heating output power is 3.2 kW. The extruder is driven using a NEMA 17 stepper through a planetary gearbox. The extruder can be equipped with an up to Ø10 mm nozzle, which enables filler with up to 4 mm fraction. This influences the layer height selection, as the minimum layer height has to be over the maximum particle size. Layer heights of 4-10 mm were used, with 4/5 mm being used for most of the prints.

The robotic arm used for most of the experiments is a KUKA KR60 HA, with a maximum capacity of 60 kg, reach of up to 2429 mm and accuracy of up to 0.06 mm. The whole assembly can be seen in Fig. 19.

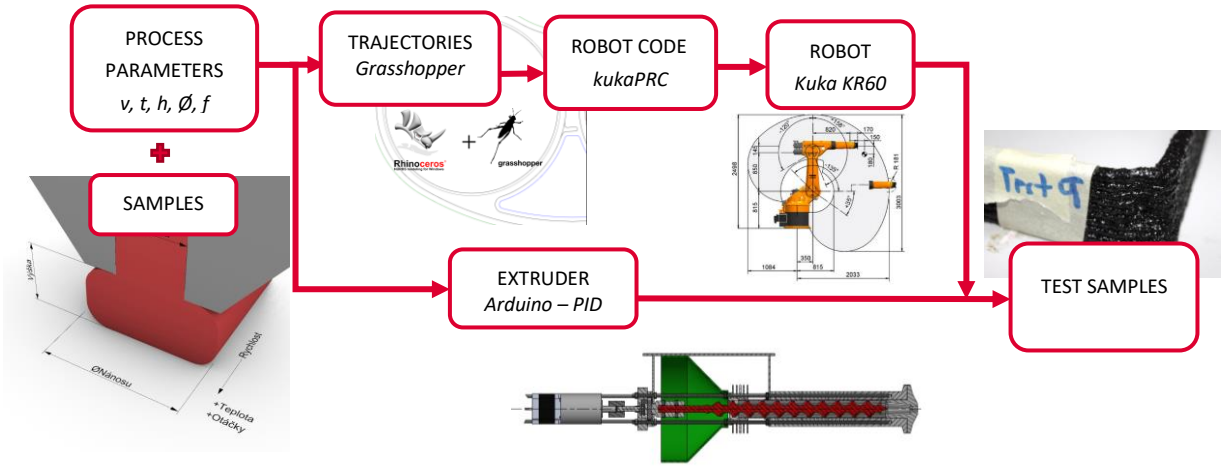

Figure 18 Scheme of material testing carried out during the first phase of the thesis

5.2 Software environment

The software environment used to develop 3D printing strategies is Grasshopper, accessible through Rhinoceros 3D modelling application or it can be accessed as an API by other applications. This enables the deployment of the developed strategies in other environments. The grasshopper environment is very suitable for this research, as it provides a wide variety of high-level geometry types and operations in its base state and is also easily expandable through plugins or direct code interpretation – using IronPython in the case of this thesis. The expandability of Grasshopper allows direct generation and simulation of robot code without leaving the environment. As KUKA robots were used, the chosen plugin is KUKA|prc [79].

Code generation workflow

The robot commands are quite similar to the traditional G-Code but have to contain all 6 movement coordinates, to account for all degrees of freedom. Other than that, there are multiple movement types – LIN, analogous to G1, PTP to G0 and CIR to G2/3, tool speeds and extruder commands depending on setup. Only LIN motion was used for 3D printing in this study. To generate the commands, oriented planes are used, as they contain all 6 degrees of freedom. They are in turn generated from an object, which is processed as follows:

1. An example GH script can be seen below in Fig. 21 a).:

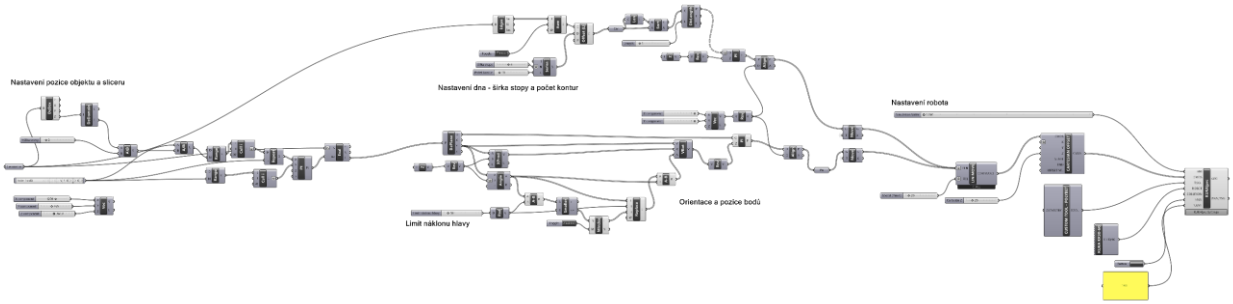

Figure 19 a) A sample code for a nonplanar oriented vase

2. Input object as mesh, or NURBS object.
3. Rem eshing, Using Quadmesh or MeshMachine function, if necessary, to gain predictable mesh resolution, aspect ratio and orientation vectors.
4. Slicing, with planar layers of constant or variable spacing, or nonplanar algorithms such as the one developed for this thesis.
5. Control points taken from the slice curves are assigned their orientation vector based on their position on the mesh, the local mesh normal and the direction of travel.
6. Motion interpolation of the vectors is performed to remove jitter and improve motion smoothness especially around sharp corners - Fig.21 c).

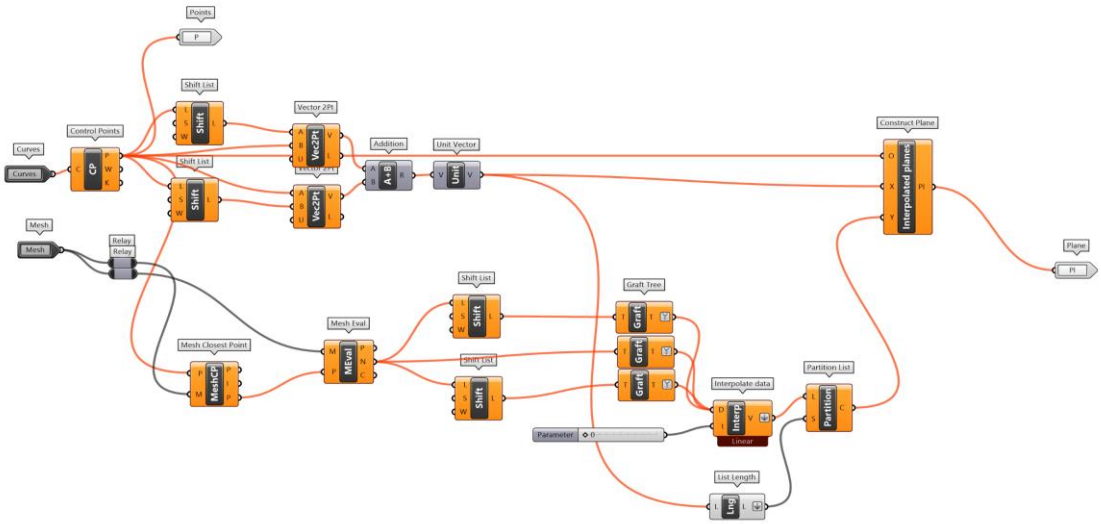

Figure 20 b) Orientation vector interpolation

7. Tilt control is performed (Explained in chapter 5.2.1) – diagram shown in Fig.21 c).

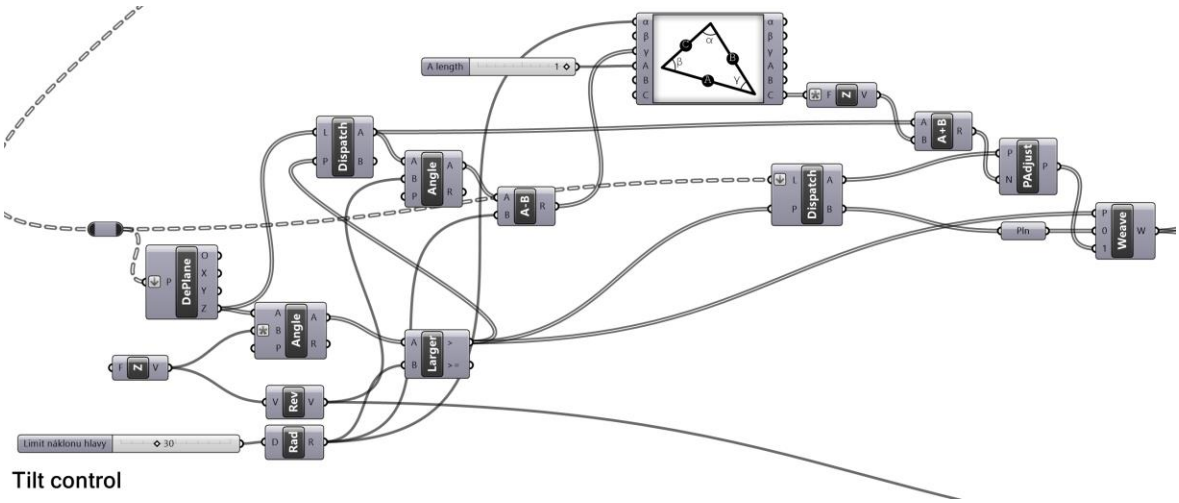

Figure 21 c) Tilt control – Detailed explanation is included in the chapter 5.2.1

8. Orientation alignment is performed – as the rotation around the Z axis of the extruder does not matter, the planes are aligned to minimize unnecessary motion.
9. The robot commands are generated using KUKA|prc, containing speed and extrusion instructions, as well as any additional information necessary for the robot setup to function.
10. Optional simulation and analysis using KUKA|prc.

5.2.1 Tilt control algorithm for oriented 3D printing

The reason for using tilt control is to avoid the possibility of self-collision and to extend the available build area. Tilt control is performed on the oriented planes before they are processed into robot commands, and it works by evaluating the angle (α° in Fig. 22) between the intended orientation of the extruder and the world Z direction and checking it against the threshold (Thresholds of 30° and 45° were used.). If the angle α exceeds the threshold, the vector is replaced by one on an identical plane (described by the World Z vector and the surface normal) with the deviation angle set at the threshold.

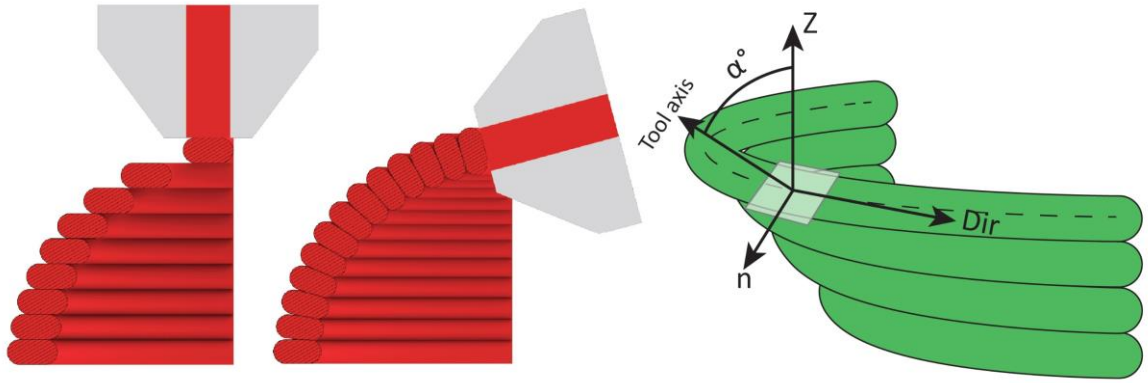

Figure 22 Tool orientation for 5-axis trajectories and the relation of the tool axis to other vectors

5.3 Specimens and testing equipment

5.3.1 Use of polymer concrete for large-scale 3D printing

Testing of mechanical degradation

Decrease of overall mechanical strength was tested by a 3-point bending test on a Zwick Z020 universal testing machine, according to the standard for testing man-made stone - ČSN EN 14617, with 3 groups of specimens, dimension 200x50x50 mm (Fig. 19) – transverse and longitudinal samples to test 3D printing effects, and a comparison cast sample. Impact testing such as a Charpy hammer was found to be unsuitable due to high granularity of the material. Print paths for the samples can be found in the attached articles.

Porosity evaluation

Porosity measurement was carried out by CT scanning of the 200x50x50 samples (µCT, GE phoenix v|tome|x L240, post-processing in VGStudio MAX 3.3.). The goal of the measurement the intra- and inter-layer increase in porosity caused by the 3D printing process.

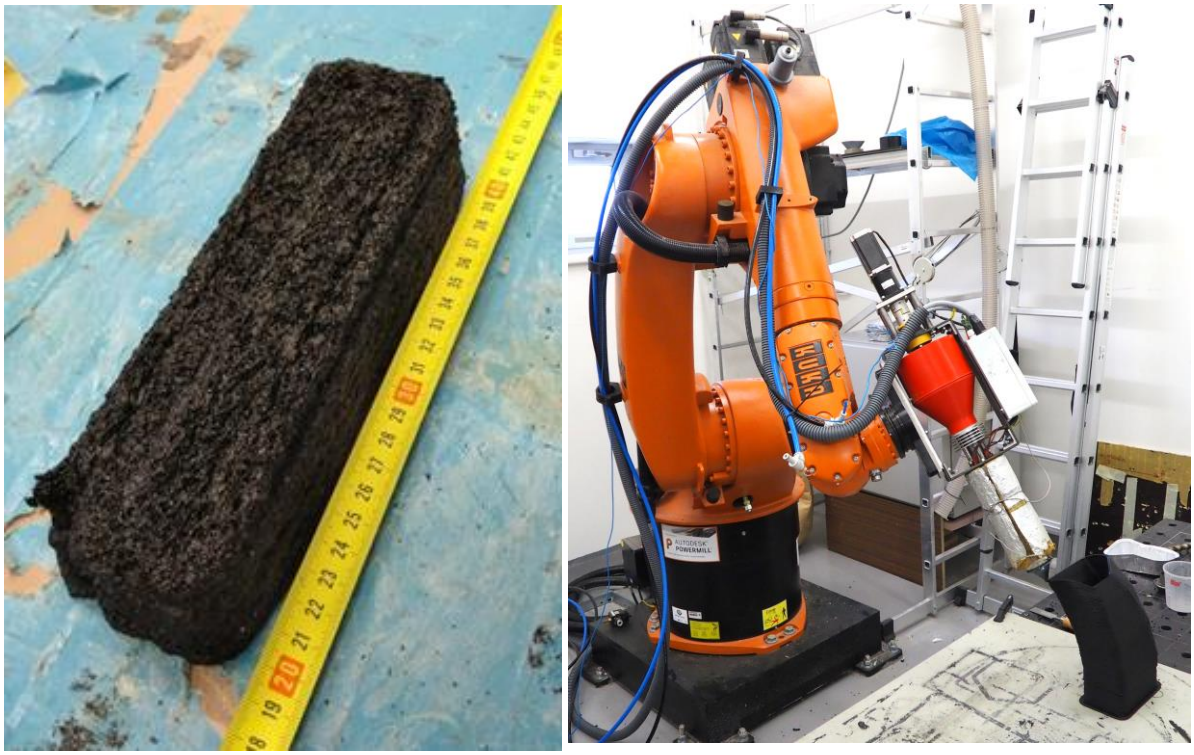

Figure 23 Left: Flexural sample in the printed state, Right: The robotic assembly during a print

5.3.2 Comparison of the effects of multiaxis printing strategies on large-scale 3D printed surface quality, accuracy, and strength

Buildability and surface quality evaluation

Changes in surface roughness and overall geometrical accuracy due to different 3D printing methods were evaluated using 3D digitalization by visible light scanning on the ATOS system scanner setup according to ‘‘VDI/VDE 2634, Part 3 Optical 3D-measuring systems, multiple view systems based on area scanning’’, and evaluation was performed in GOM Inspect. Overall geometrical accuracy was evaluated based on comparison of original model and scanned surface reconstruction. Roughness was evaluated from the scan data by extraction of surface profiles, their digital filtering to get just the roughness data, and finally evaluating the surface profile using the the digital version of the *Ra* expression.

Layer adhesion and surface quality samples were cut from purpose-designed overhang towers, enabling buildability evaluation. Layer adhesion was tested on a notched sample in tension on the Imada MX-2 universal testing stand, dimensions of the sample were 20x100x5 mm (Fig. 20). For dimensions of the test towers and the samples, as well as for more details on the measurement, please refer to the attached article.

5.3.3 Method of Multiaxis Three-Dimensional Printing with Intralayer Height Variation for Stairstep Effect Compensation

Deposition width evaluation

For the purpose of verifying the newly developed method, described in the results section, overhang towers were designed, and samples were cut from the overhanging and wall areas to verify if the method succeeds in maintaining a constant deposition width independent of the local overhang angle. Optical microscopy was used to measure and compare the deposition width – ground samples were captured on an Olympus 8ZX7 microscope equipped with a Canon EOS 1200D at 16x magnification. For measurement and statistics, its accompanying software - QuickPHOTO Micro was used.

5.4 Material

The polymer concrete mixture used in the first part of the thesis is composed of a 25:75 ratio of binder to filler, the binder is a recycled PP from the automotive industry. The filler is a mixture of quartz sand, with a fraction of 0.4-4.0 mm. The initial fill ratio is adapted from a stamp moulding mixture used by a company developing polymer concrete processing for building elements, such as flooring.

Processing the composite at the highest temperature that does not degrade the material properties is desirable for process speed and mechanical performance [41], therefore 240°C was chosen as the melt temperature [22]. Preheated state of the substrate when depositing a new layer is beneficial [80], and the deposition stability of the composite is good due to the high fill ratio, thus part cooling is omitted when it is not necessary due to the size of the printed object.

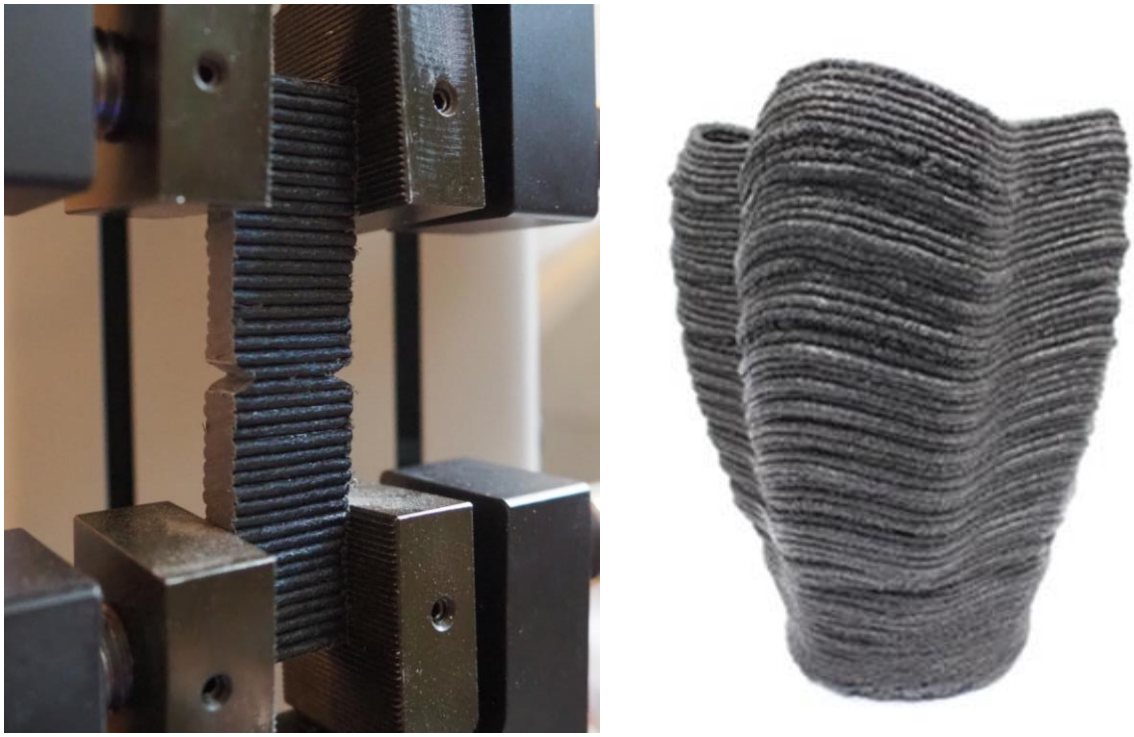

Figure 24 Left: Notched sample in the MX-2 testing stand Right: Early non-planar print made from PP GF 30 mix

Later in the thesis, a new composition was developed, using PP GF 30 or a proprietary rPP and mineral wool composite, and dropping the polymer : particulate filler ratio to 40 : 60. The fibre filler and a PP build plate are sufficient for preventing delamination and deformations for large scale prints when printing with this material.

Other materials printed during the course of thesis include various pellet thermoplastics, such as PP GF 30 and PLA, printed via the screw extruder.

6 RESULTS AND DISCUSSION

This chapter contains an overview of the results of the work carried out during this thesis. It contains the major results from the published articles, while the detailed results can be found inside the attached articles themselves, as well as some unpublished results.

6.1 Printability of polymer concrete and its properties

After the development of basic process parameters – temperature, TCP speed/Extruder speed ratio, range of usable layer heights and material flow – evaluation has started in terms of mechanical performance, deformation during printing and porosity.

Warping of prints during the process is significant, to the degree of 1 cm deformation per 10 cm of length. The high fill ratio decreases deformations significantly, but the particulate filler in the original composition of polymer concrete is not enough on its own, as the semicrystalline matrix has a high coefficient of linear expansion [31]. The replacement of the matrix for a fibre filled one, PP GF 30 or for the composition with recycled mineral insulation, is necessary to achieve large-scale printing.

The research was structured as such – three sample types were built and evaluated for mechanical performance and porosity. Two 3D printed samples, transverse and longitudinal, and comparison cast samples, with the goal of determining if layer adhesion or material degradation have a major influence on the printed material [39]. The properties of the printed material turned out favourable for the process, with the longitudinal sample being almost as strong as the cast one – 19.5 MPa to 19.7 MPa (Average force/deformation chart can be seen on Fig.23). The transverse sample has shown a significant influence of layer adhesion, as its strength was only 14.9 MPa. The porosity results by CT scanning are much less favourable to the 3D printed material – Cast material has a porosity of 1.58%, while the transverse part has a porosity of 12.59%, with multiple types of pores introduced by the 3D printing process forming continuous cavities throughout the material (See Fig. 24) [7]. Porosity reduction should be the focus of the next generation of polymer concrete processing hardware. Further details can be found in the included article "Use of polymer concrete for large-scale 3D printing".

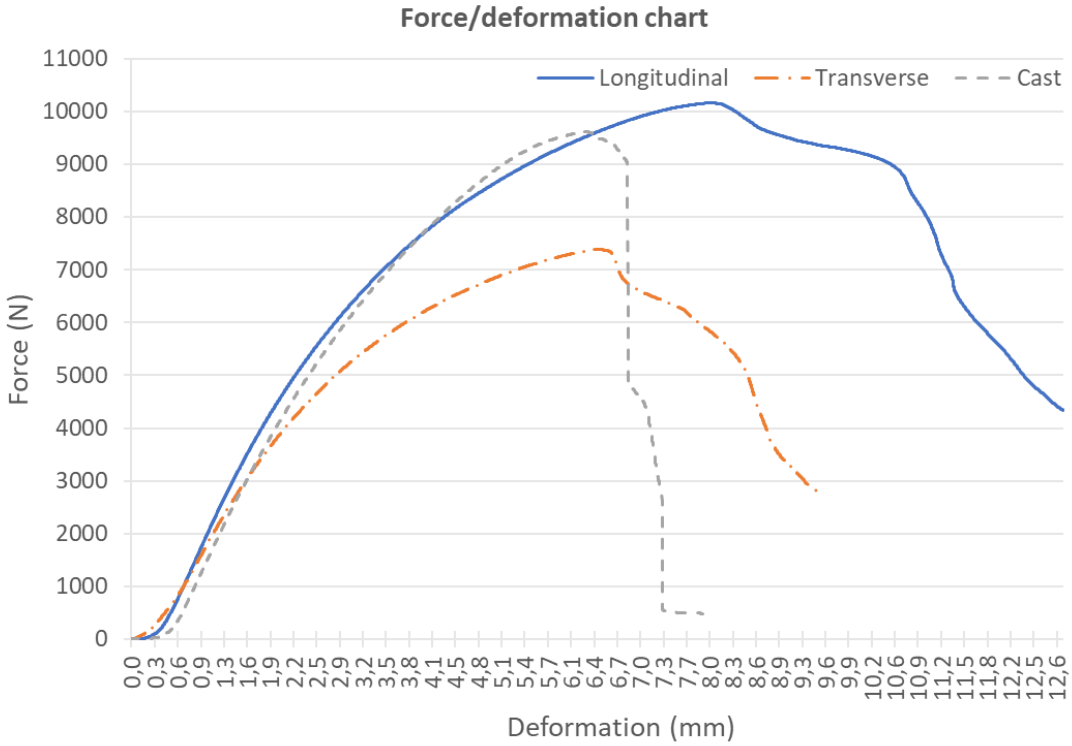

Figure 25 Results of the flexural strength tests

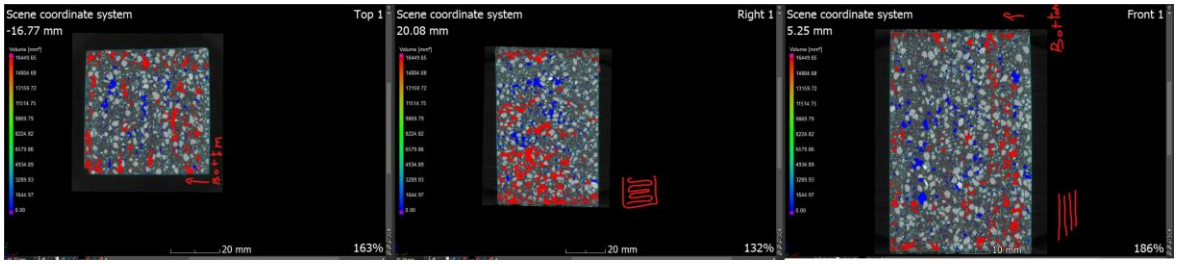

Figure 26 Typical porosity of the transverse sample, continuous voids marked in red

6.1.1 Current status of polymer concrete printing

Processing difficulties of polymer concrete that have been highlighted during the first article made further work on the topic difficult, so the focus shifted to developing methods to fix the problems, while the development of new hardware continues simultaneously. The starve feeding strategy used to print the first samples was sufficient for the first verification of the material, but as the results of CT show, lead to high inconsistency of the printed material in terms of filler distribution and porosity. By using a pelleted pre-compounded material and a significantly modified screw geometry, the goal is to decrease porosity and fill inconsistency. The limits of the current setup are simple functional objects, such as those displayed in Fig. 25.

Realised prints

Figure 27 Examples of functional objects printed during the thesis

6.1.2 Unpublished results on print deformation reduction

Changing the material composition is only one of the possible ways to lessen deformations caused by material shrinkage. An alternative approach is dissipating the residual stress inside the print by not allowing it to propagate throughout the object, by either printing with interruption to material flow, or by locally modifying the direction of deposition. The second strategy was chosen, as it fits better with the way that the screw extruder functions.

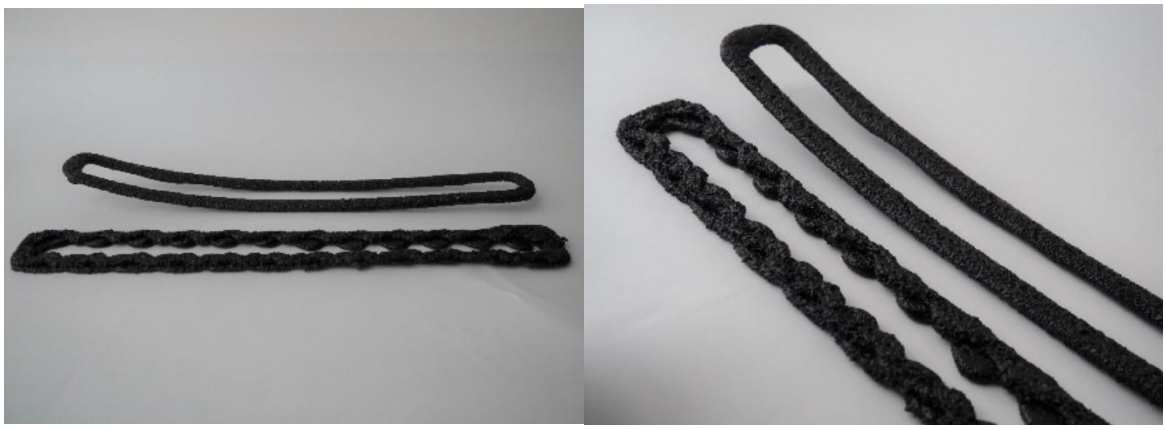

Figure 28 Effect of print path modification on warpage of polymer concrete deposition

Shrinkage testing cantilever beam test adapted from Stoof and Pickering was used to test the material [31]. These tests were carried out on 500 mm beams and used for material mixture and toolpath verification. The developed toolpath eliminates more than 90% of the deformation but has a significant effect on surface quality (Fig. 26). The results were not yet published. Similar toolpath modifications are used for decorative purposes, and to increase the stability of the depositions for fluid materials such as concrete or clay by interlocking the depositions [16]. Its use to prevent deformation was not yet recorded.

A subject deserving of coming back to and publishing is the process of printing polymer concrete by precisely dosing components of the composite to the screw extruder. Conventionally, this should not be possible, as the extruder contains no mixing zones, but the mechanism might be different due to the high filler percentage and its big fraction. The results achieved with this printing setup are convincing enough, that this direction should be explored more. At least, the process and the achieved results should be described and a possible submission title could be:

“3D printing polymer concrete by starve feeding composite constituents into a screw extruder“

6.2 Development of software methods for multiaxis printing

The next part of the thesis focuses on process planning, especially on the development of toolpath preparation algorithms. To test multiaxis methods, the process had to be put into practice, as the state of the art at the department at that time was using surface isocurves (as [57]) for toolpaths and normal vectors for tool orientation. This approach is extremely limited in terms of possible object complexity and has zero control over toolpath spacing – the layer height is directly dependent on the geometry and not controllable.

As part of the process development, a freeform nonplanar slicer had to be developed, as no solution was available at that time, except for experimental features aimed at desktop FDM. (PrusaSlicer, Curvi Slicer) [76] and solutions from research articles. The overview of the slicing algorithm can be seen in Fig. 27. This slicer is incomplete but excels at creating high-quality toolpaths. A detailed overview of the slicer can be found in the corresponding journal article: “Comparison of the effects of multiaxis printing strategies on large-scale 3D printed surface quality, accuracy, and strength”

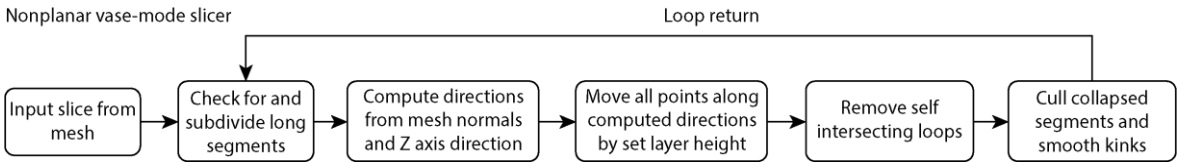

Figure 29 Flowchart of the nonplanar slicer

The disadvantage of using meshes for slicing is the discontinuous nature of normal vectors which are used for multi-axis motion. This is a benefit of using surfaces and their isocurves, as orientation vectors gained from them result in smooth motion. Jagged toolpaths and inconsistent tool orientation can result in incessant robot slowdown, affecting surface quality and accuracy. These problems can be prevented by deployment of motion interpolation. This is a complex field, but for purposes of this thesis, a mean average of consecutive tool orientation vectors in combination with a quality input mesh proved sufficient.

6.2.1 Results of testing multiaxis methods

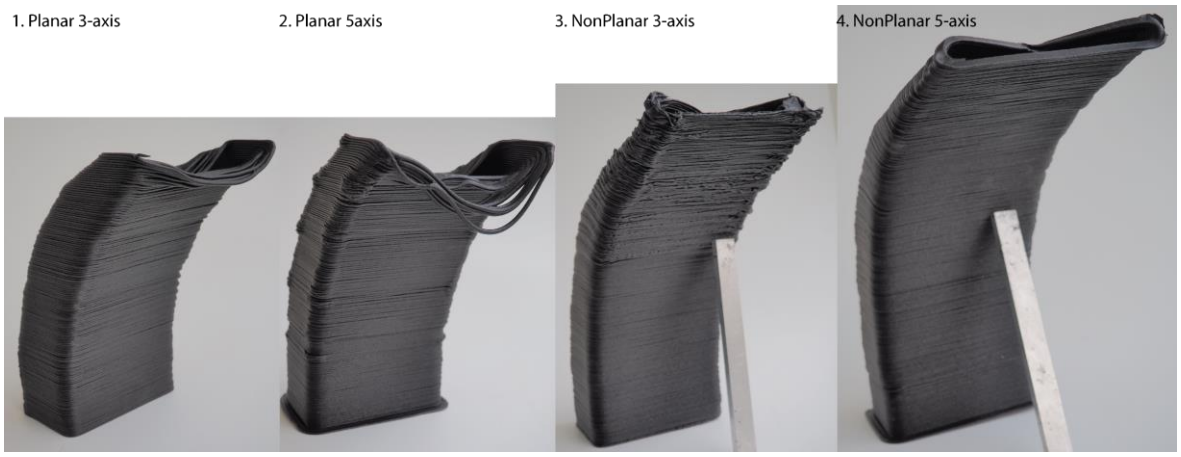

Figure 30 Comparison of different multiaxis 3DP methods: Planar 3 axis, Planar 5 axis Oriented, Nonplanar 3 axis, Nonplanar 5 axis Oriented

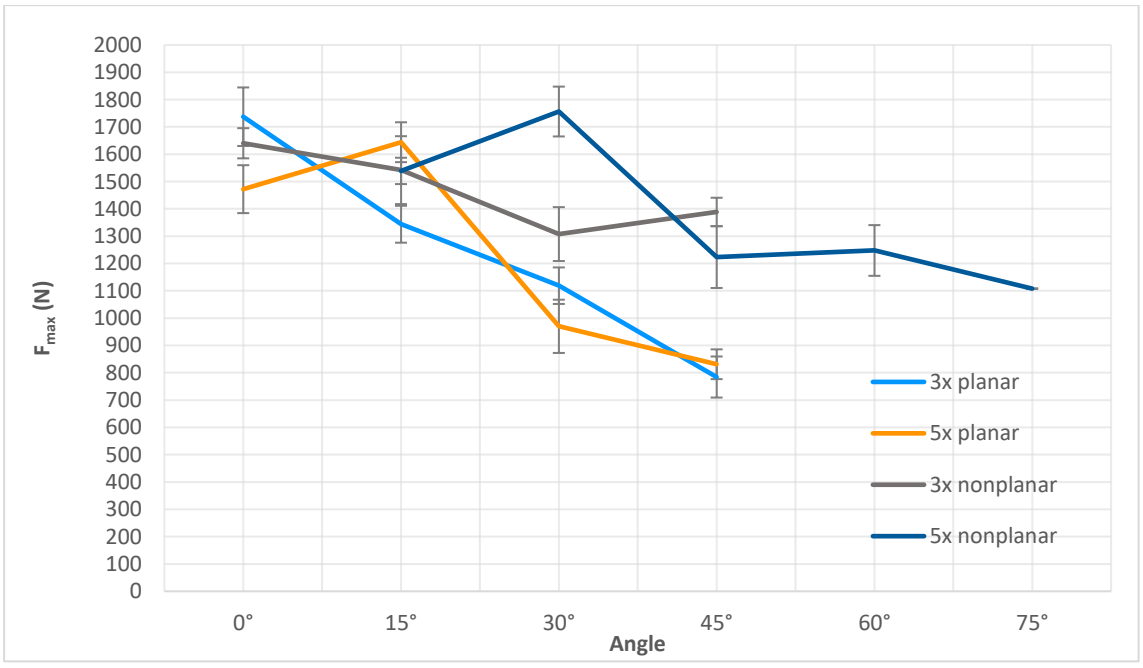

Figure 31 Delamination force chart for the different printing methods

With these methods put into practice, a comparative study connected to the second hypothesis was conducted. Properties and limitations of 4 types of multiaxis 3D printing were compared in terms of accuracy, surface quality and interlayer bond strength (The printed objects can be seen in Figure 28). The most important findings were that oriented printing by itself does not significantly increase buildability or strength. Nonplanar methods are extremely limited if combined only with 3-axis motion, even with the high layer height used [55]. If nonplanar trajectories and oriented printing are used together, buildability increases over 75° of overhang with stable wall thicknesses even for single-walled printing. Intralayer bond strength is also increased, with a 20% loss of strength compared to 50% for a 3-axis planar print. The delamination forces for all regions can be seen in Figure 29. For details, see the attached article: “Comparison of the effects of multiaxis printing strategies on large-scale 3D printed surface quality, accuracy, and strength.”

6.3 Intralayer height variation method

The findings from the comparative study of 3D printing approaches led to the conceptualization of a new method that makes use of controlled intralayer height variations in the full range of printable layer heights. The resulting depositions can be seen in Fig 30.

A detailed description of the method can be found in the attached article, and the toolpath preparation algorithm flowchart can be seen in Fig. 31. The basic principle is that the layer height is varied through each layer based on a local maximum overhang angle to keep the amount of material deposited per surface area constant. This is done over the entirety of the buildable layer height range and combined with a limited tilt to align the depositions in areas of significant overhang.

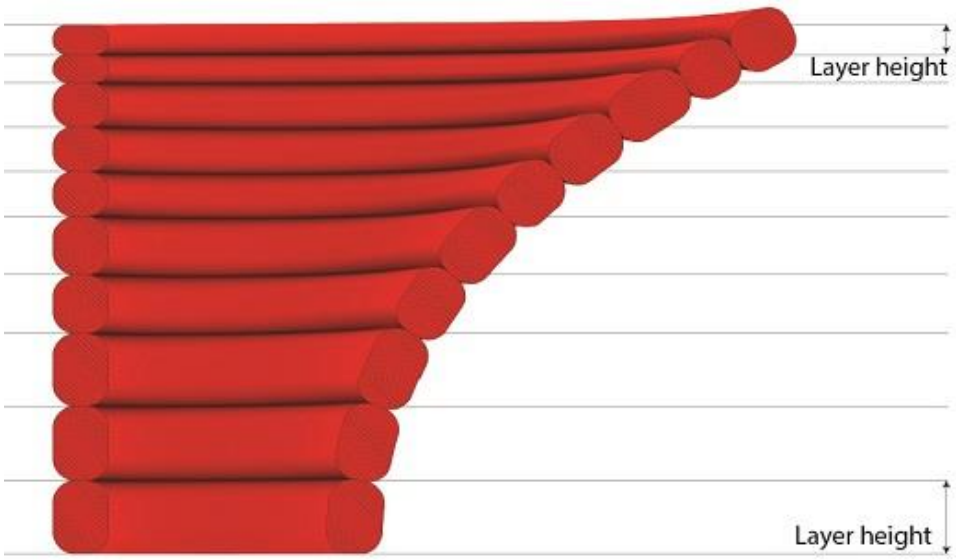

Figure 32 Depositions resulting from intralayer height variation

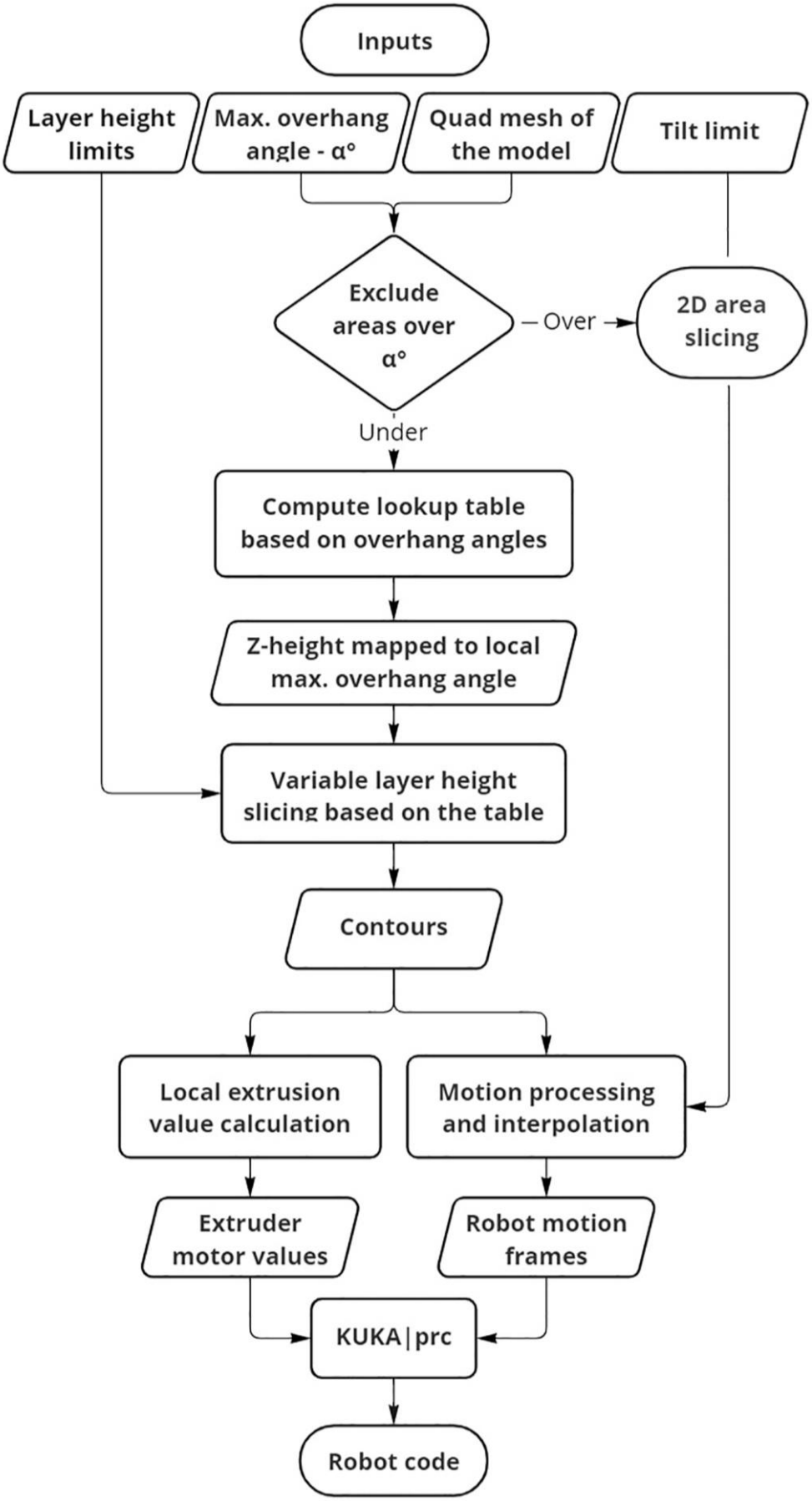

Figure 33 Algorithm scheme for the intra layer height variation method

This method, when used with large-scale single wall printing, allows for buildability of overhangs up to 82.33° for the layer height range of 10-75% of nozzle diameter, while having none of the geometry limitations of current nonplanar [57, 61] or other competing methods [45]. Wall thickness at that overhang angle only decreases by 20%, while conventionally, it would decrease to 0% at 50° if printed with the same initial layer height. The contact patch width chart can be seen in Figure 32, with the wall samples from the overhang test tower displayed in Fig. 33.

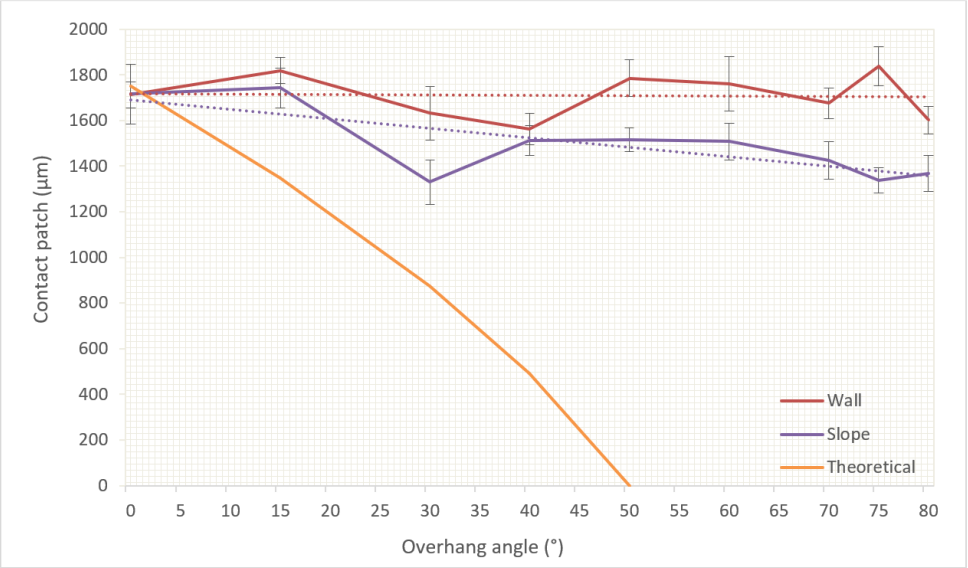

Figure 34 Contact patch thickness at various overhang angles

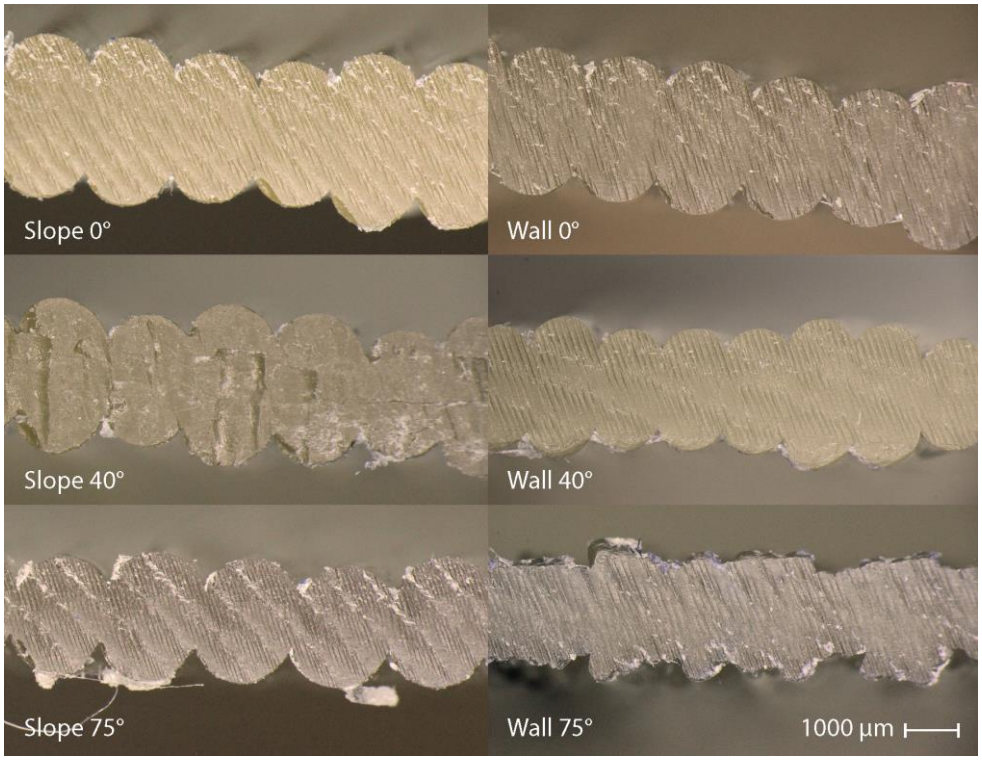

Figure 35 Microscopy of wall thickness samples

The method and its results are described in detail in the attached publication: Method of multiaxis 3D printing with intralayer height variation for stairstep effect compensation. Finally, the applicability of the method for large-scale 3DP of polymer concrete was verified by a comparative print that clearly shows the extension of buildability. An overhang tower was selected for the comparison, with overhangs from 0° to 80° with a cross-section of 200x150 mm. The 3-axis print starts to fail after 45° of overhang, while the print performed with the new method has stable deposition thickness and good buildability up to 80°, even though the resulting print is severely affected by the current hardware setup, which does not provide stable performance during extruder reorientation.

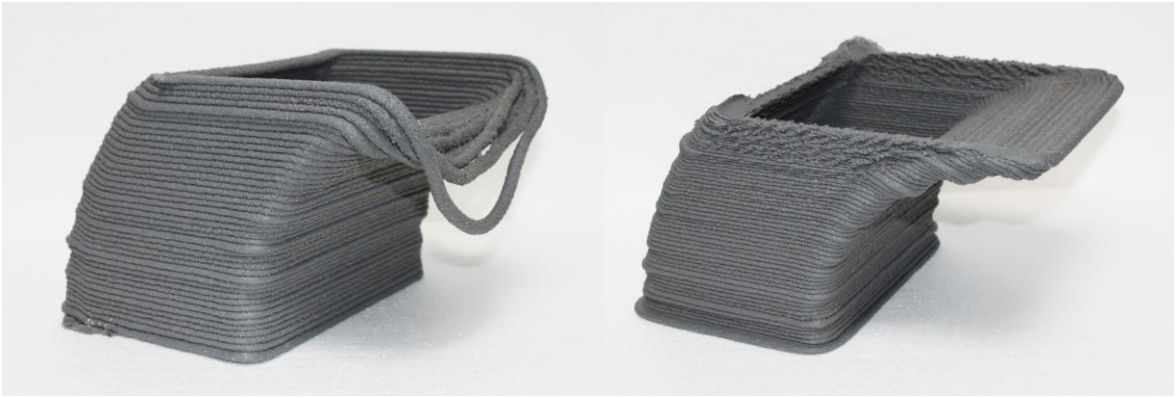

Figure 36 Buildability extension by the intralayer height variation method Left - 3-axis Right - Intralayer variation

7 CONCLUSION

This thesis deals with the topic of large-scale 3D printing of polymer concrete, with the main achievement of the thesis being a new multiaxis 3D printing method suitable for large-scale printing of polymer composites. The body of the research was published in three publications in WoS-listed journals, with the author being majority contributor and listed as the first author for all of the articles.

The material and the developed methods are intended for construction, architecture, or large-scale tooling. The material composition, the process parameters and the toolpath planning were considered. The first part of the thesis started with a focus on the material, while the latter part focused on the software processing of toolpaths, as the impact of toolpaths on 3D printing results was considered significant. This refocusing was partly due to external factors, but it has produced interesting results as it enabled the development of the method presented in the third and final article of the thesis.

The state-of-the-art summary includes an overview of the ME method, a look at the composite material that is the focus of this thesis from both the matrix and filler sides and a section about large-scale and multiaxis 3D printing methods. The materials and methods section describes the printing setup, the material compositions used, the mechanical performance and surface quality tests and includes an explanation of the software methods for robotic 3D printing and some of the processes developed as part of the work – e.g. tilt control. For more details on the state of the art, materials and methods related to specific parts of the thesis, see the attached articles.

The goals of the thesis were either fully or partially achieved. While the hardware for large-scale polymer concrete printing is still under development, the methods developed in this thesis bring a considerable extension of buildability for the process and have been demonstrated on verification prints, together with the material composition and process parameters. Process parameters were developed that enabled the fabrication of multiple functional objects such as planters, stools and vases and the properties of the printed material were characterised and compared to the as-cast state. Modifying the print path to avoid deformation proved successful, but with the caveat that this affects surface quality. This topic was not explored in depth, but the results obtained show that modification of the print path alone can reduce deformation by an order of magnitude.

Methods for large-scale 3D printing proved to be a topic with unrealised potential. Several methods related to the field of multiaxis 3D printing were realised during the thesis– such as toolhead reorientation with limited tilt, motion interpolation and a nonplanar slicing algorithm. The effects of selected methods on buildability and surface quality of large-scale printing were isolated and compared to each other, and the results were summarised in a journal article.

The last partial goal of Application-focused 3D printing strategies was achieved, with the development of the Intralayer height variation method, which takes the limitations of the robotic setup and of the screw extruders into account while significantly expanding the buildability of the process.

The methods described improve large-scale printing of complex, functional objects by increasing the buildable overhang angle, resulting in a reduction in support structures and an improvement in surface quality and strength. They also can eliminate the need for post-processing and enable the production of otherwise unfeasible parts. The goal of reducing material and time expenditure for 3D printing of polymer composites has been achieved and the results of this thesis can be applied to the growing large-scale 3DP industry. As a recent review shows, the number of companies and publications in this sector has grown rapidly in the last five years, with applications in the automotive, marine and energy industries [81]. The large-scale MEX process is not fully comparable to the desktop-scale process usually described in the literature, as it has limitations due to the material behaviour at a large scale and the use of screw extruders [39]. The methods developed and applied in this research advance the development in this industry by increasing the level of technological maturity. The future development of the methods developed in this thesis should be their application in the industry and test the economic benefits they bring by increasing buildability and improving surface quality.

7.1 Hypothesis evaluation

> H1: Mechanical properties of polymer concrete are reduced by the 3D printing process compared to casting due to thermal degradation, porosity, or other factors of the process.

The first hypothesis was rejected. Thermal degradation, due to the chosen material and the processing route used, did not prove significant. Porosity and anisotropy have an impact on the 3D printed material, but if they are kept in check, the mechanical performance can be as good as cast parts and similar performance on a 3-point bending test was recorded – 19.5 MPa for the 3d printed part to 19.7 MPa of the cast sample. The recorded porosity reached up to 12% in the transverse orientation, showing both significant intra-and inter-layer porosity, introduced by the screw extruder and the line-by-line printing process. The 3D printed parts also showed a higher degree of ductility, which may be beneficial for some applications.

H2: Application of the oriented 3D printing technique improves buildability and surface quality beyond the level achievable by 3-axis printing, with the same benefits for large-scale 3D printing compared to desktop-scale [14, 43].

It was shown that oriented 3D printing alone does not impact buildability, if used with constant layer height slicing, except for slightly improving surface quality. Using toolpaths that have a good surface coverage has proven to be more important, even when not combined with multiaxis motion – the nonplanar methods showed much more significant improvement in buildability, up to 75°compared to the original 45°. This realization was then important to the development of the Intralayer height variation method and the original hypothesis was rejected, as it was shown as incomplete.

H3: Planar slicing combined with compensation for changes in actual layer height can achieve improvements in buildability similar to those gained by nonplanar slicing.

This hypothesis was confirmed. The Intralayer height variation method brings considerable benefits to large-scale composite printing. Overhangs over 80° are printable with appropriate methods, and material sagging is sufficiently prevented by oriented 3D printing. Contact patch width only decreases by 20% at 80° of overhang, which was proven to closely correlate with layer adhesion. This is similar to results that can be achieved with nonplanar slicing, without the same processing difficulties and limited model processability.

8 LIST OF PUBLICATIONS

Conference proceedings:

Martin Krčma, doc. David Paloušek, PhD, STRUCTURAL MEMBERS MANUFACTURED BY FREEFORM DEPOSITION OF POLYMER CONCRETE, BE.AM 2020, ISBN 9798561621192, Darmstadt, 2020

Papers published in journals with impact factor:

Krčma, M., Škaroupka, D., Vosynek, P., Zikmund, T., Kaiser, J. and Palousek, D. (2021), "Use of polymer concrete for large-scale 3D printing", Rapid Prototyping Journal, Vol. 27 No. 3, pp. 465-474. https://doi.org/10.1108/RPJ-12-2019-0316

Krčma, M., Paloušek, D. Comparison of the effects of multiaxis printing strategies on large-scale 3D printed surface quality, accuracy, and strength. Int J Adv Manuf Technol 119, 7109–7120 (2022). https://doi.org/10.1007/s00170-022-08685-4

Martin Krčma, David Paloušek, David Škaroupka, Johannes Braumann, and Daniel Koutný. Method of Multiaxis Three-Dimensional Printing with Intralayer Height Variation for Stairstep Effect Compensation.3D Printing and Additive Manufacturing. ahead of print http://doi.org/10.1089/3dp.2022.0097

9 REFERENCES

1. EuRIC AISBL (2020) Recycling: Bridging Circular Economy & Climate Policy. 21
2. Plastics recyclers Europe (2022) European recyclers report low availability of sorted plastic waste. In: Packag. Eur. https://packagingeurope.com/news/european-recyclers-report-low-availability-of-sorted-plastic-waste/8355.article
3. Ramirez AP, Solis AS (1984) Development of a new composite material from waste polymers, natural fiber, and mineral fillers. J Appl Polym Sci 29:2405–2412. https://doi.org/10.1002/app.1984.070290714
4. Midland-Ross Corp (1981) Extrusion devices and methods of reclaiming scrap plastic material
5. VIA ALTA (2016) POLYBET. http://www.via-alta.cz/polybet/
6. Kočař J (2019) KONSTRUKCE EXTRUDÉRU PRO ADITIVNÍ VÝROBU VYSOCE PLNĚNÝCH TERMOPLASTŮ. BUT FME
7. N. Turner B, Strong R, A. Gold S (2014) A review of melt extrusion additive manufacturing processes: I. Process design and modeling. Rapid Prototyp J 20:192–204. https://doi.org/10.1108/RPJ-01-2013-0012
8. Turner BN, Gold SA (2015) A review of melt extrusion additive manufacturing processes: II. Materials, dimensional accuracy, and surface roughness. Rapid Prototyp J 21:250–261. https://doi.org/10.1108/RPJ-02-2013-0017
9. Cano-Vicent A, Tambuwala MM, Hassan SS, et al (2021) Fused deposition modelling: Current status, methodology, applications and future prospects. Addit Manuf 47:. https://doi.org/10.1016/j.addma.2021.102378
10. Kuznetsov VE, Solonin AN, Urzhumtsev OD, et al (2018) Strength of PLA components fabricated with fused deposition technology using a desktop 3D printer as a function of geometrical parameters of the process. Polymers (Basel) 10:. https://doi.org/10.3390/polym10030313
11. Chacón JM, Caminero MA, García-Plaza E, Núñez PJ (2017) Additive manufacturing of PLA structures using fused deposition modelling: Effect of process parameters on mechanical properties and their optimal selection. Mater Des 124:143–157. https://doi.org/10.1016/j.matdes.2017.03.065
12. Krejcirik P, Skaroupka D, Palousek D (2018) Free Directional Robotic Deposition - Influence on Overhang Printability. MM Sci J 12:2715–2721. https://doi.org/10.17973/mmsj.2018_12_2018119
13. Pandey PM, Reddy N V., Dhande SG (2003) Real time adaptive slicing for fused deposition modelling. Int J Mach Tools Manuf 43:61–71. https://doi.org/10.1016/S0890-6955(02)00164-5
14. Fry NR, Richardson RC, Boyle JH (2020) Robotic additive manufacturing system for dynamic build orientations. Rapid Prototyp J 26:659–667. https://doi.org/10.1108/RPJ-09-2019-0243
15. Laarman Joris H, Gilardi F, Geurtjens T (2016) A structure printing device for printing a three dimensional structure work piece as well as a method for controlling such structure printing device.

16. Im HC, AlOthman S, Del Castillo JLG (2018) Responsive spatial print: Clay 3D printing of spatial lattices using real-time model recalibration. Recalibration Imprecision Infidelity - Proc 38th Annu Conf Assoc Comput Aided Des Archit ACADIA 2018 286–293

17. Gosselin C, Duballet R, Roux P, et al (2016) Large-scale 3D printing of ultra-high performance concrete - a new processing route for architects and builders. Mater Des 100:102–109. https://doi.org/10.1016/j.matdes.2016.03.097

18. Abdel-Fattah H, El-Hawary MM (1999) Flexural behavior of polymer concrete. Constr Build Mater 13:253–262. https://doi.org/10.1016/S0950-0618(99)00030-6

19. Slieptsova I, Savchenko B, Sova N, Slieptsov A (2016) Polymer sand composites based on the mixed and heavily contaminated thermoplastic waste. IOP Conf Ser Mater Sci Eng 111:. https://doi.org/10.1088/1757-899X/111/1/012027

20. Dumitrescu O, Ropotă I, Bratu M, Muntean M (2011) Reuse of pet waste as thermoplastic composites. Environ Eng Manag J 10:1179–1181

21. Meyer TK, Tanikella NG, Reich MJ, Pearce JM (2020) Potential of distributed recycling from hybrid manufacturing of 3-D printing and injection molding of stamp sand and acrylonitrile styrene acrylate waste composite. Sustain Mater Technol 25:e00169. https://doi.org/10.1016/j.susmat.2020.e00169

22. KULOVANÁ E, ČERNÝ M, ONDRAČKA T, et al (2019) The utilization of plastic residues from separation for polymer concrete preparation. Waste Forum 116–122

23. Guven AH (2014) A METHOD FOR RECYCLING WASTE THERMOPLASTIC MATERIALS AND USING THIS RECYCLED THERMOPLASTIC IN COMPOSITE MATERIAL PRODUCTION. 1:1–26

24. Yi H, Oh K, Kou R, Qiao Y (2020) Sand-filler structural material with a low content of polyethylene binder. Sustain Mater Technol 25:e00194. https://doi.org/10.1016/j.susmat.2020.e00194

25. Sabau E, Bâlc N, Bere P (2013) Properties of Thermoplastics Reinforced with Foundry Sand Waste. Adv Eng Forum 8–9:309–316. https://doi.org/10.4028/www.scientific.net/aef.8-9.309

26. Kumar R, Singh T, Singh H (2015) Solid waste-based hybrid natural fiber polymeric composites. J Reinf Plast Compos 34:1979–1985. https://doi.org/10.1177/0731684415599596

27. Hugo AM, Scelsi L, Hodzic A, et al (2011) Development of recycled polymer composites for structural applications. Plast Rubber Compos 40:317–323. https://doi.org/10.1179/1743289810Y.0000000008

28. Herrera-Franco P, Valadez-Gonzalez A, Cervantes-Uc M (1997) Development and characterization of a HDPE-sand-natural fiber composite. Compos Part B Eng 28:331–343. https://doi.org/10.1016/S1359-8368(96)00024-8

29. Essabir H, Boujmal R, Bensalah MO, et al (2016) Mechanical and thermal properties of hybrid composites: Oil-palm fiber/clay reinforced high density polyethylene. Mech Mater 98:36–43. https://doi.org/10.1016/j.mechmat.2016.04.008

30. Turner RP, Kelly CA, Fox R, Hopkins B (2018) Re-formative polymer composites from plastic waste: Novel infrastructural product application. Recycling 3:1–16. https://doi.org/10.3390/recycling3040054

31. Stoof D, Pickering K (2018) Sustainable composite fused deposition modelling filament using recycled pre-consumer polypropylene. Compos Part B Eng 135:110–118. https://doi.org/10.1016/j.compositesb.2017.10.005

32. Domingues J, Marques T, Mateus A, et al (2017) An Additive Manufacturing Solution to Produce Big Green Parts from Tires and Recycled Plastics. Procedia Manuf 12:242–248. https://doi.org/10.1016/j.promfg.2017.08.028

33. Little HA, Tanikella NG, Reich MJ, et al (2020) Towards distributed recycling with additive manufacturing of PET flake feedstocks. Materials (Basel) 13:. https://doi.org/10.3390/MA13194273

34. Welle F (2011) Twenty years of PET bottle to bottle recycling - An overview. Resour Conserv Recycl 55:865–875. https://doi.org/10.1016/j.resconrec.2011.04.009

35. Liu X, Chi B, Jiao Z, et al (2017) A large-scale double-stage-screw 3D printer for fused deposition of plastic pellets. J Appl Polym Sci 134:1–9. https://doi.org/10.1002/app.45147

36. Kulovana E (2018) Vliv znečištění PET na teplotní okrajové podmínky při výrobě polymerbetonu. WASTE FORUM

37. Singh B, Kumar R, Singh Chohan J (2020) Polymer matrix composites in 3D printing: A state of art review. Mater Today Proc. https://doi.org/10.1016/j.matpr.2020.04.335

38. Love LJ, Duty CE, Post BK, et al (2015) Breaking Barriers in Polymer Additive Manufacturing

39. Duty CE, Kunc V, Compton B, et al (2017) Structure and mechanical behavior of Big Area Additive Manufacturing (BAAM) materials. Rapid Prototyp J 23:181–189. https://doi.org/10.1108/RPJ-12-2015-0183

40. Roschli A, Gaul KT, Boulger AM, et al (2019) Designing for Big Area Additive Manufacturing. Addit Manuf 25:275–285. https://doi.org/10.1016/j.addma.2018.11.006

41. Hertle S, Drexler M, Drummer D (2016) Additive Manufacturing of Poly(propylene) by Means of Melt Extrusion. Macromol Mater Eng 301:1482–1493. https://doi.org/10.1002/mame.201600259

42. Moreno Nieto D, Casal López V, Molina SI (2018) Large-format polymeric pellet-based additive manufacturing for the naval industry. Addit Manuf 23:79–85. https://doi.org/10.1016/j.addma.2018.07.012

43. Kubalak JR, Wicks AL, Williams CB (2019) Exploring multi-axis material extrusion additive manufacturing for improving mechanical properties of printed parts. Rapid Prototyp J 25:356–362. https://doi.org/10.1108/RPJ-02-2018-0035

44. Zhao H ming, He Y, Fu J zhong, Qiu J jiang (2018) Inclined layer printing for fused deposition modeling without assisted supporting structure. Robot Comput Integr Manuf 51:1–13. https://doi.org/10.1016/j.rcim.2017.11.011

45. Wüthrich M, Elspass WJ, Bos P, et al (2021) A novel slicing strategy to print overhangs without support material. Appl Sci 11:130–145. https://doi.org/10.3390/app11188760

46. Chakraborty D, Aneesh Reddy B, Roy Choudhury A (2008) Extruder path generation for Curved Layer Fused Deposition Modeling. CAD Comput Aided Des 40:235–243. https://doi.org/10.1016/j.cad.2007.10.014

47. Huang B, Singamneni S (2014) Curved layer fused deposition modeling with varying raster orientations. Appl Mech Mater 446–447:263–269. https://doi.org/10.4028/www.scientific.net/AMM.446-447.263

48. Singamneni S, Roychoudhury A, Diegel O, Huang B (2012) Modeling and evaluation of curved layer fused deposition. J Mater Process Technol 212:27–35. https://doi.org/10.1016/j.jmatprotec.2011.08.001

49. Huang B, Singamneni S (2015) A mixed-layer approach combining both flat and curved layer slicing for fused deposition modelling. Proc Inst Mech Eng Part B J Eng Manuf 229:2238–2249. https://doi.org/10.1177/0954405414551076

50. Huang B (2014) Alternate Slicing and Deposition. Strategies for Fused Deposition Modelling. 55:511–517

51. Cendrero AM, Fortunato GM, Munoz-Guijosa JM, et al (2021) Benefits of non-planar printing strategies towards eco-efficient 3d printing. Sustain 13:1–17. https://doi.org/10.3390/su13041599

52. Kalami H, Urbanic J (2021) Exploration of surface roughness measurement solutions for additive manufactured components built by multi-axis tool paths. Addit Manuf 38:101822. https://doi.org/10.1016/j.addma.2020.101822

53. Fang G, Zhang T, Zhong S, et al (2020) Reinforced FDM: Multi-axis filament alignment with controlled anisotropic strength. ACM Trans Graph 39:. https://doi.org/10.1145/3414685.3417834

54. Li Y, Tang K, He D, Wang X (2021) Multi-Axis Support-Free Printing of Freeform Parts with Lattice Infill Structures. CAD Comput Aided Des 133:1–38. https://doi.org/10.1016/j.cad.2020.102986

55. Pérez-Castillo JL, Cuan-Urquizo E, Roman-Flores A, et al (2021) Curved layered fused filament fabrication: An overview. Addit Manuf 47:. https://doi.org/10.1016/j.addma.2021.102354

56. Nayyeri P, Zareinia K, Bougherara H (2022) Planar and nonplanar slicing algorithms for fused deposition modeling technology: a critical review. Int J Adv Manuf Technol. https://doi.org/10.1007/s00170-021-08347-x

57. Ezair B, Fuhrmann S, Elber G (2018) Volumetric covering print-paths for additive manufacturing of 3D models. CAD Comput Aided Des 100:1–13. https://doi.org/10.1016/j.cad.2018.02.006

58. Zhao G, Ma G, Feng J, Xiao W (2018) Nonplanar slicing and path generation methods for robotic additive manufacturing. Int J Adv Manuf Technol 96:3149–3159. https://doi.org/10.1007/s00170-018-1772-9

59. Dai C, Wang CCL, Wu C, et al (2018) Support-free volume printing by multi-axis motion. ACM Trans Graph 37:. https://doi.org/10.1145/3197517.3201342

60. Xu K, Li Y, Chen L, Tang K (2019) Curved layer based process planning for multi-axis volume printing of freeform parts. CAD Comput Aided Des 114:51–63. https://doi.org/10.1016/j.cad.2019.05.007

61. Allen RJA, Trask RS (2015) An experimental demonstration of effective Curved Layer Fused Filament Fabrication utilising a parallel deposition robot. Addit Manuf 8:78–87. https://doi.org/10.1016/j.addma.2015.09.001

62. Wu C, Dai C, Fang G, et al (2020) General Support-Effective Decomposition for Multi-Directional 3-D Printing. IEEE Trans Autom Sci Eng 17:599–610. https://doi.org/10.1109/TASE.2019.2938219

63. Shembekar A V., Yoon YJ, Kanyuck A, Gupta SK (2019) Generating robot trajectories for conformal three-dimensional printing using nonplanar layers. J Comput Inf Sci Eng 19:1–13. https://doi.org/10.1115/1.4043013

64. Hack N, Lauer WV (2014) Mesh-mould: Robotically fabricated spatial meshes as reinforced concrete formwork. Archit Des 84:44–53. https://doi.org/10.1002/ad.1753

65. Eichenhofer M, Wong JCH, Ermanni P (2017) Continuous lattice fabrication of ultra-lightweight composite structures. Addit Manuf 18:48–57. https://doi.org/10.1016/j.addma.2017.08.013

66. De Guevara ML, Borunda L, Ficca J, et al (2019) Robotic free-oriented additive manufacturing technique for thermoplastic lattice and cellular structures. Intell Inf - Proc 24th Int Conf Comput Archit Des Res Asia, CAADRIA 2019 2:333–342

67. Mani K, Kulkarni P, Dutta D (1999) Region-based adaptive slicing. CAD Comput Aided Des 31:317–333. https://doi.org/10.1016/S0010-4485(99)00033-0

68. Mao H, Kwok TH, Chen Y, Wang CCL (2019) Adaptive slicing based on efficient profile analysis. CAD Comput Aided Des 107:89–101. https://doi.org/10.1016/j.cad.2018.09.006

69. Wasserfall F, Hendrich N, Zhang J (2017) Adaptive slicing for the FDM process revisited. IEEE Int Conf Autom Sci Eng 2017-Augus:49–54. https://doi.org/10.1109/COASE.2017.8256074

70. Huang B, Singamneni SB (2015) Curved layer adaptive slicing (CLAS) for fused deposition modelling. Rapid Prototyp J 21:354–367. https://doi.org/10.1108/RPJ-06-2013-0059

71. Pelzer L, Hopmann C (2021) Additive manufacturing of non-planar layers with variable layer height. Addit Manuf 37:101697. https://doi.org/10.1016/j.addma.2020.101697

72. Khurana JB, Dinda S, Simpson TW (2020) Active - Z printing: A new approach to increasing3D printed part strength. Solid Free Fabr 2017 Proc 28th Annu Int Solid Free Fabr Symp - An Addit Manuf Conf SFF 2017 1627–1644

73. Chen L, Chung MF, Tian Y, et al (2019) Variable-depth curved layer fused deposition modeling of thin-shells. Robot Comput Integr Manuf 57:422–434. https://doi.org/10.1016/j.rcim.2018.12.016

74. Moetazedian A, Budisuharto AS, Silberschmidt V V., Gleadall A (2021) CONVEX (CONtinuously Varied EXtrusion): A new scale of design for additive manufacturing. Addit Manuf 37:1–19. https://doi.org/10.1016/j.addma.2020.101576

75. Schuh G, Bergweiler G, Lukas G, et al (2020) Feature-based Print Method for Multi-Axis Material Extrusion in Additive Manufacturing. Procedia CIRP 93:85–89

76. Etienne J, Ray N, Panozzo D, et al (2019) Curvislicer: Slightly curved slicing for 3-axis printers. ACM Trans Graph 38:. https://doi.org/10.1145/3306346.3323022

77. Xu K, Chen L, Tang K (2019) Support-Free Layered Process Planning Toward 3 + 2-Axis Additive Manufacturing. IEEE Trans Autom Sci Eng 16:838–850. https://doi.org/10.1109/TASE.2018.2867230

78. Nisja GA, Cao A, Gao C (2021) Short review of nonplanar fused deposition modeling printing. Mater Des Process Commun 3:0–3. https://doi.org/10.1002/mdp2.221

79. Braumann J, Brell-Çokcan S (2011) Parametric Robot Control. Proc 31st Annu Conf Assoc Comput Aided Des Archit 242–251. https://doi.org/https://doi.org/10.52842/conf.acadia.2011.242

80. Yang C, Tian X, Li D, et al (2017) Influence of thermal processing conditions in 3D printing on the crystallinity and mechanical properties of PEEK material. J Mater Process Technol 248:1–7. https://doi.org/10.1016/j.jmatprotec.2017.04.027

81. Pignatelli F, Percoco G (2022) An application- and market-oriented review on large format additive manufacturing, focusing on polymer pellet-based 3D printing. Prog Addit Manuf 7:1363–1377. https://doi.org/10.1007/s40964-022-00309-3

10 LIST OF SYMBOLS AND ABBREVATIONS

3DP - 3D printing

ABS – acrylonitrile butadiene styrene

BAAM – Big Area Additive Manufacturing

CT – Computer Tomography

CTE – Coefficient of thermal expansion

CLF – Curved Layer Fabrication

FFF – Freeform Filament Fabrication

FDM – Fused Deposition Modelling

MEX – Material Extrusion

.stl – stereolithography, data format

PP, rPP – polypropylene, recycled polypropylene

PET – polyethylene terephthalate

PE, HDPE – polyethylene, high density polyethylene

PEI - polyetherimide

PC - polycarbonate

PEEK – polyether ether ketone

HDT – heat deflection temperature

TCP – tool centre point

11 LIST OF FIGURES AND TABLES

12 ATTACHEMENTS

1. Diagram of the nonplanar slicer in Grasshopper

Page 64

2. Krčma, M., Škaroupka, D., Vosynek, P., Zikmund, T., Kaiser, J. and Palousek, D. (2021), "Use of polymer concrete for large-scale 3D printing", Rapid Prototyping Journal, Vol. 27 No. 3, pp. 465-474. https://doi.org/10.1108/RPJ-12-2019-0316

Pages 65 - 75

3. Krčma, M., Paloušek, D. "Comparison of the effects of multiaxis printing strategies on large-scale 3D printed surface quality, accuracy, and strength." Int J Adv Manuf Technol 119, 7109–7120 (2022). https://doi.org/10.1007/s00170-022-08685-4

Pages 76 – 87

4. Martin Krčma, David Paloušek, David Škaroupka, Johannes Braumann, and Daniel Koutný. Method of Multiaxis Three-Dimensional Printing with Intralayer Height Variation for Stairstep Effect Compensation.3D Printing and Additive Manufacturing. ahead of print http://doi.org/10.1089/3dp.2022.0097

Pages 88 – 100

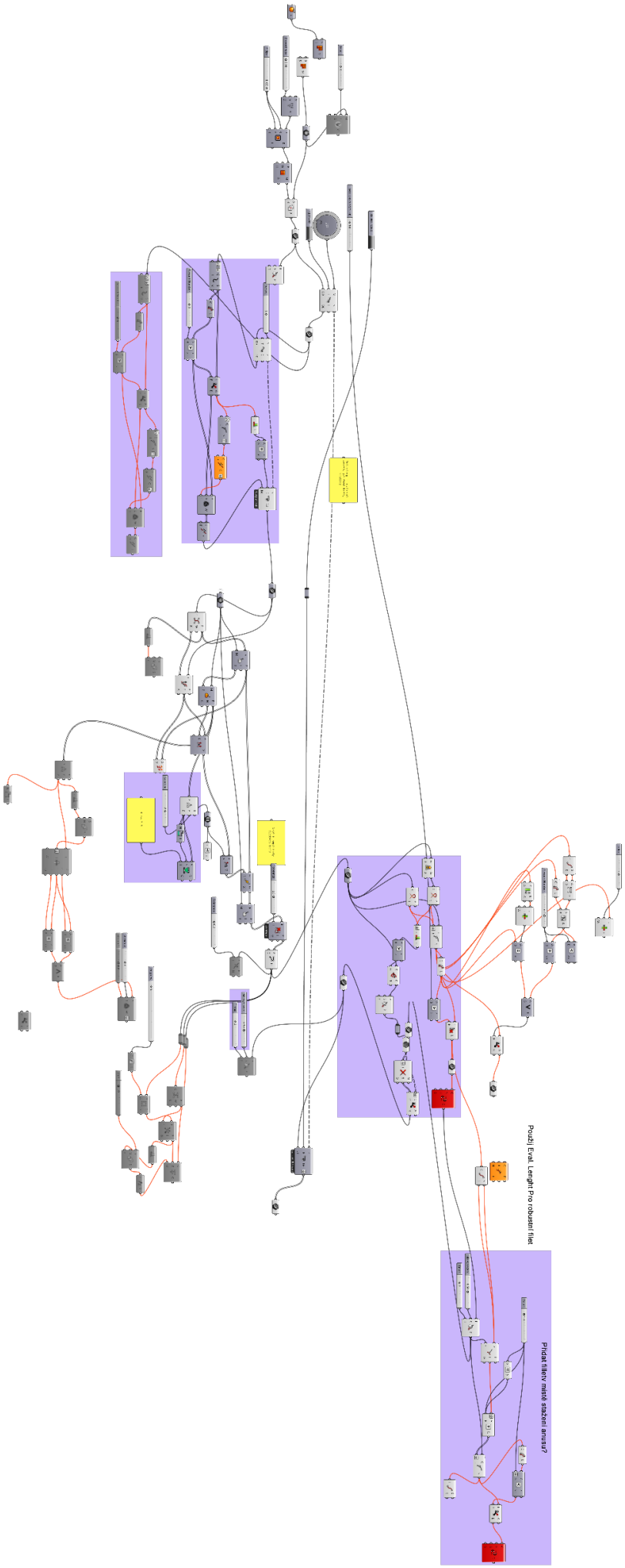
Použij Eval. Length Pro robustní fitet
Přidat fitety mezi stažení emusu?

Use of polymer concrete for large-scale 3D printing

Martin Krčma, David Škaroupka and Petr Vosynek
Faculty of Mechanical Engineering, Brno University of Technology, Brno, Czech Republic
Tomáš Zikmund and Jozef Kaiser
Central European Institute of Technology, Brno University of Technology, Brno, Czech Republic, and
David Palousek
Faculty of Mechanical Engineering, Brno University of Technology, Brno, Czech Republic

Abstract

Purpose – This paper aims to focus on the evaluation of a polymer concrete as a three-dimensional (3D) printing material. An associated company has developed plastic concrete made from reused unrecyclable plastic waste. Its intended use is as a construction material.

Design/methodology/approach – The concrete mix, called PolyBet, composed of polypropylene and glass sand, is printed by the fused deposition modelling process. The process of material and parameter selection is described. The mechanical properties of the filled material were compared to its cast state. Samples were made from castings and two different orientations of 3D-printed parts. Three-point flex tests were carried out, and the area of the break was examined. Computed tomography of the samples was carried out.

Findings – The influence of the 3D printing process on the material was evaluated. The mechanical performance of the longitudinal samples was close to the cast state. There was a difference in the failure mode between the states, with cast parts exhibiting a tougher behaviour, with fractures propagating in a stair-like manner. The 3D-printed samples exhibited high degrees of porosity.

Originality/value – The results suggest that the novel material is a good fit for 3D printing, with little to no degradation caused by the process. Layer adhesion was shown to be excellent, with negligible effect on the finished part for the longitudinal orientation. That means, if large-scale testing of buildability is successful, the material is a good fit for additive manufacturing of building components and other large-scale structures.

Keywords 3D printing, Robotic fabrication, Polymer concrete, Recycled thermoplastic

Paper type Research paper

Introduction

As three-dimensional (3D) printing technology matures, so rises the number of its applications. Recently, there has been a significant growth in projects focusing on 3D printing in the construction industry. The progress is driven mostly by architects, who desire the freedom of form made possible by additive manufacturing. At first, cement concrete may appear as a viable choice of material for 3D printing, but its specific properties make it hard to process using extrusion manufacturing (EM). Cement concrete is also known as a great contributor to the carbon dioxide (CO_2) emissions worldwide. Thermoplastics commonly used for 3D printing are costly and present a substantial burden on the climate. An associated company has presented a novel composite material, consisting of recycled polypropylene waste with sand serving as a filler. Being comprised mostly of filler, the material may be viable for use in the construction industry for both its mechanical and economical qualities. Its suitability for 3D printing will be evaluated.

The current issue and full text archive of this journal is available on Emerald Insight at: **https://www.emerald.com/insight/1355-2546.htm**

Rapid Prototyping Journal
 [ISSN 1355-2546]
[DOI 10.1108/RPJ-12-2019-0316]

State of the art

This section explores the current works on topics of thermoplastic composites from recycled material, their use for 3D printing and large-scale 3D printing in general.

Common processing methods for recycling plastic that achieve a product of the same quality as virgin plastic are currently unavailable at a comparable cost. As a result, plastic waste is stored in landfills in megatons (Welle, 2011). The first mention of a more economic method to process this waste is a patent from Midland Ross Corp., which describes a process based on re-melting scrap plastic in large-scale extrusion device, mixing it with an additive and reusing it (Midland-Ross Corp, 1981). The process on which this article is based on is quite similar at its core, but the mixture is prepared in a reactor, which also dries and preheats it. That mixture is then melted and mixed by a screw extruder and used for casting building components. The system is variable, capable of processing

This work was carried out in cooperation between Faculty of mechanical engineering BUT and VIA ALTA a.s. company supported by grant TJ01000354 and internal faculty project FSI-S-17-4144. TZ and JK thank to MEYS CR projects CEITEC 2020 (LQ1601) under the National Sustainability Programme II and CzechNanoLab Research Infrastructure (LM2018110).

Received 13 December 2019
Revised 5 June 2020
27 August 2020
Accepted 22 September 2020

various thermoplastics and working with filler ratios of 0–80%. The compressive strength is 29 MPa, the flexural strength is 14.6 MPa, double of conventional concrete. The material does not absorb water and produces minimal runoff when subjected to running water or chlorine solution – 4 g/m^2 after 50 cycles (VIA ALTA, 2016).

Similar materials were tested in laboratory conditions. Slieptsova *et al.* produced a variety of different compositions based of polyesters and polyolefins filled by 50–80% of 75 mesh sieved building sand. Components were tested for various mechanical properties and for heat deflection temperature (HDT). In general, components based on polyesters behaved better than components based on polyolefins. Flexural strength and HDT generally increased, while tensile strength and elongation declined with increased fill percentage. Also, several surface and matrix treatments were described, such as treating sand with silane and addition of polycarbonate to polyethylene terephthalate (PET), with great results. The resulting composites appear to be suitable for rigid, thin-walled, temperature-stable parts (Slieptsova *et al.*, 2016). The range of processing parameters and possible material combinations appear to be quite wide, as other authors reported that 0.62/1.22 mix of PET with contaminated blasting sand reached values as high as 87 MPa in compression and 27 MPa in flex, with temperature of processing extruder set between 185 and 195°C (Dumitrescu *et al.*, 2011).

Similar materials have been used for 3D printing in a wide variety of process scales. On a small scale, composite filament has been produced from recycled PP containing natural fibres or pulverized gypsum in percentages of 10–50%. High increase in tensile strength and rigidity was reported for the filament with natural fibre, but the results did not completely translate to 3D printed tensile specimens. The gypsum content only significantly increased rigidity. However, there was a significant change in thermal shrinkage, important for stability of 3D prints. Filament with 30% of harakeke fibre reduced the shrinkage to 1/6th of the control (Stoof and Pickering, 2018). This is only one composition; large selection of fillers ranging from recycled organic material to carbon nanotubes was already studied (Singh *et al.*, 2020). On a larger scale, a mixture of 40% recycled PP and 60% granulate from used tires was used for 3D printing. This mixture is fed into a screw extruder with a compression zone and external heating elements. This combination is affixed to a Yaskawa Motoman robotic arm. Single-layer test prints were carried out, with maximal tensile strength and elongation measured 6 MPa and 0.03%. Analysis of thermal flow during melting and crystallization was carried out, with the filled material having less severe crystallization peaks compared to unfilled PP (Domingues *et al.*, 2017).

Crystallization and shrinkage mentioned in the previous paragraph are two of the most difficult aspects of large-scale 3D printing of recycled consumer plastic, which is mostly semi-crystalline in nature. The method has not been fully developed, but there are some projects dealing with the issue, such as Print your city by Zero waste lab, which has been able to thermally recycle consumer PE packaging to print outdoor furniture (The New Raw, 2018).

A much more mature process is large-scale printing from amorphous plastics, mainly Acrylonitrile butadiene styrene (ABS). Two different approaches have been noted. The first, using logic and machine design common in FDM, are scaled-up machines, such as the Big Area Additive Manufacturing (BAAM). It is a large, up to 2.4 × 16.5 in platform dimensions, gantry-based system, with a screw extruder moving at high speeds up to 12.7 mm/s. To decrease warping and shrinkage, ABS filled by 10% of carbon fibre is used. The amount of extruded material is up to 5,000 cm^3/h, using a 7.5Ø mm nozzle (Love *et al.*, 2015). Designing for a large-scale manufacturing systems has a unique set of requirements, mainly the increased time needed to cool a layer. This has led to the requirement of variable printing speed based on length of the print path (Roschli *et al.*, 2019). The second approach is again using a robotic arm as a positioning system, printing ABS reinforced with carbon fibre to print cellular structures (Boyd *et al.*, 2017).

In contrast to large-scale plastic 3D printing, construction 3D printing from cementitious materials is currently developing technology being worked on several research institutions and approaching commercialisation. One well-recognised method is called contour crafting, developed by B. Khoshnevic. The method works with large nozzles and layer heights but produces smooth material finish, using adjustable trowels. It is limited to 2.5 D shapes (Khoshnevis *et al.*, 2001). Full 3D printing of ultra-high-performance concrete is possible, especially if aided by five axis tilt of the printing head, as demonstrated by Gosselin *et al.* Large scale of the layers presents a new set of challenges compared to traditional FDM knowledge, making new printing strategies necessary (Gosselin *et al.*, 2016).

The challenge shared by most of concrete 3D printing methods is the absence of reinforcement in the finished structures. Steel elements used in traditional reinforced concrete structures provide them with much of their mechanical properties. There are two approaches that attempt to solve this for material extrusion methods. First is either automated or manual incorporation of reinforcements between layers. This approach still faces the issue of lacking interconnection between parts, which results in decreased strength of the final structure. One solution is automated welding of the reinforcement during the build (HACK *et al.*, 2016). Another solution is using external reinforcement structure applied after the build (Asprone *et al.*, 2018).

Competing with these material extrusion methods are powder- and binder-based methods, like VoxelJet or DShape. They offer freedom of shape because of the powder bed process, combined with high surface quality without significant layer lines. They are, however, limited by machine build volume, and the addition of reinforcements is not possible during the process (Teizer *et al.*, 2016).

Methods

Material selection

Following up previous studies performed by project partners, three main types of post-consumer plastic waste were identified using differential scanning calorimetry (DSC) analysis – PP, PET and various types of PE, shown in Figure 1 (KULOVANÁ *et al.*, 2019). PE is quite a poor candidate for 3D printing, exhibiting problems with self-adhesion and warping. PP and PET were selected as main candidates. We were unable to produce consistent prints using the extruder

Figure 1 DSC analysis of a discarded PE mix, showing different melting points for differing amounts of PE types present in the mix

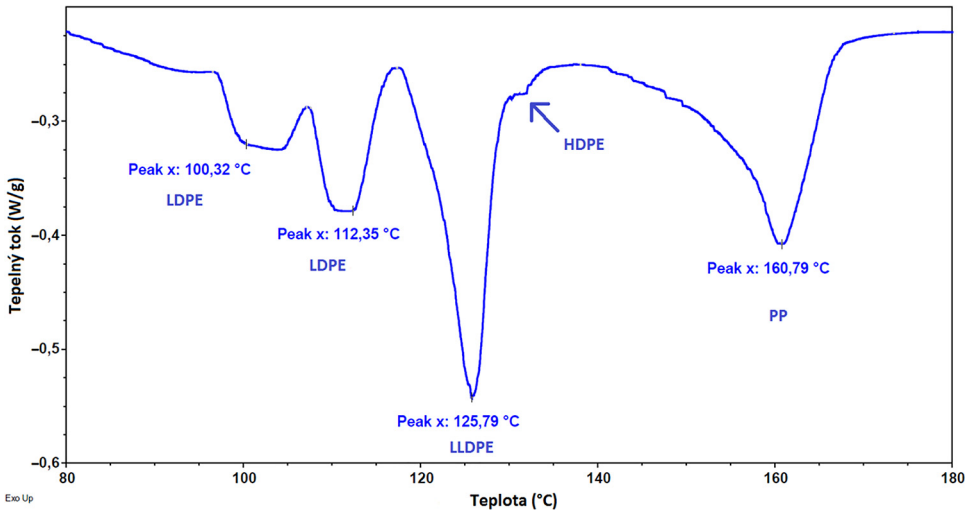

described further in the text, with ground-contaminated PET bottle flakes as a material.

The material used was a composite of PP and sand. PP, serving as a binder, was sourced from rejected injection-moulded parts intended for automotive, which were then shredded. For filler, two types of sand were used, common building sand and silica sand (brand Silico, fraction 2–4 mm). They were mixed directly in the extruder with the PP: silica sand: building sand ratio being 4:4:2 by weight.

Filler selection was a compromise between printability and price of the filler. Originally, we intended to use recycled filler from different sources, the main being glass panels. We ran into issues using the recycled glass for printing, first, with shape of the ground glass particles and, second, with grain distribution. Roughly ground glass sieved to 4 mm exhibits sharp edges and long grain aspect ratio, leading to problems during extrusion (4 mm filler was selected as maximum during the extruder design). Finely ground glass includes large quantities of extremely fine particles, which clog the extruder during printing. Sieving them out greatly reduces yield. Usage of recycled filler was postponed, and we opted to use commercially available aggregates. We selected common building sand because of its low price, and silica sand intended for filters, because of its grain shape and availability in different fractions. Our target fill ratio was 75%, but the extrusion was unstable due to the oscillating fill ratio caused by batch supply of raw materials to the extruder, so the fill ratio vas dropped to 60%.

Printing assembly and parameters

The extruder used in this work was purpose-built at our department (Kočař, 2019). It is a constant compression rate, 30 mm diameter single-screw extruder, heated by four heating cartridges, with the total heating power of 3.2 kW, driven by a NEMA stepper via a helical transmission. The output temperature and rotations per minute of the output shaft were controlled by an Arduino. The extruder was attached to an industrial arm robot by a universal mounting plate. The assembly can be seen in Figure 2.

Experiments were performed by industrial robot KUKA KR60 with KRC 2 HA, pictured in Figure 3. The maximum reach of the robot arm is over 2 m, and the maximum payload at this distance is 25 kg. Due to low speeds used, the robot is able to trace the generated print paths with accuracy and without vibrations. The available build envelope with the extruder attached is about 2 × 1 × 1 m, or bigger if the object is able to fit in the spherical shell traced by the end effector (KUKA Roboter GmbH, 2017).

The strategies and robot code were generated in Rhinoceros 5.0 (McNeel) using the Grasshopper programming environment and KUKA|prc plugin to generate both the print paths and the subsequent code.

Prints were done at 200°C; at this temperature, the PP flows readily. The boundaries for temperature came from thermogravimetric analysis (TGA) performed by project partner, seen in Figure 4, which shows that the recycled PP starts undergoing degradation at 250°C. The bottom limit is the melting point of PP – 160–165°C.

Samples were printed with the following process parameters: the layer height was 4.2 mm, with Ø10 mm nozzle. The system was running at reduced speed, velocity of the printing head was set to 9 mm/s. To ensure adhesion, the print surface from MDF

Figure 2 Single screw extruder mounted on KUKA robot arm, shown during a test print

Figure 3 Kuka KR 60 HA, dimensions and maximum reach

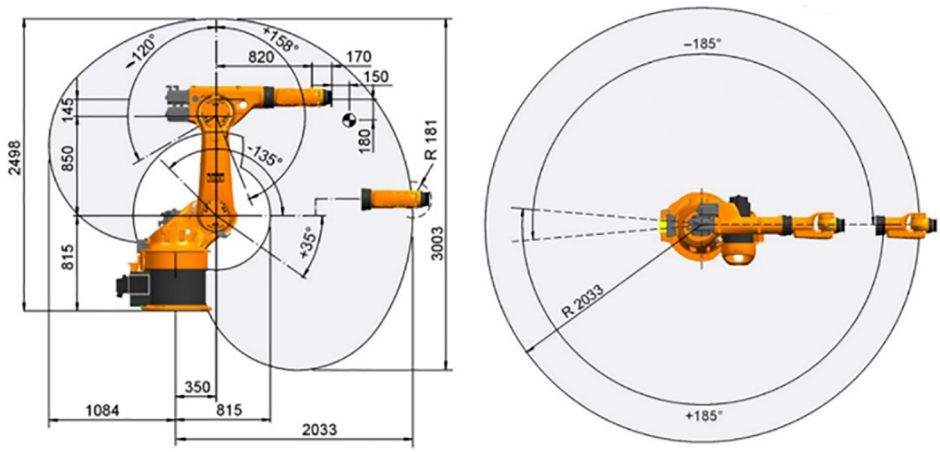

Figure 4 TGA analysis of PP used in this study, showing weightloss with increasing temperature

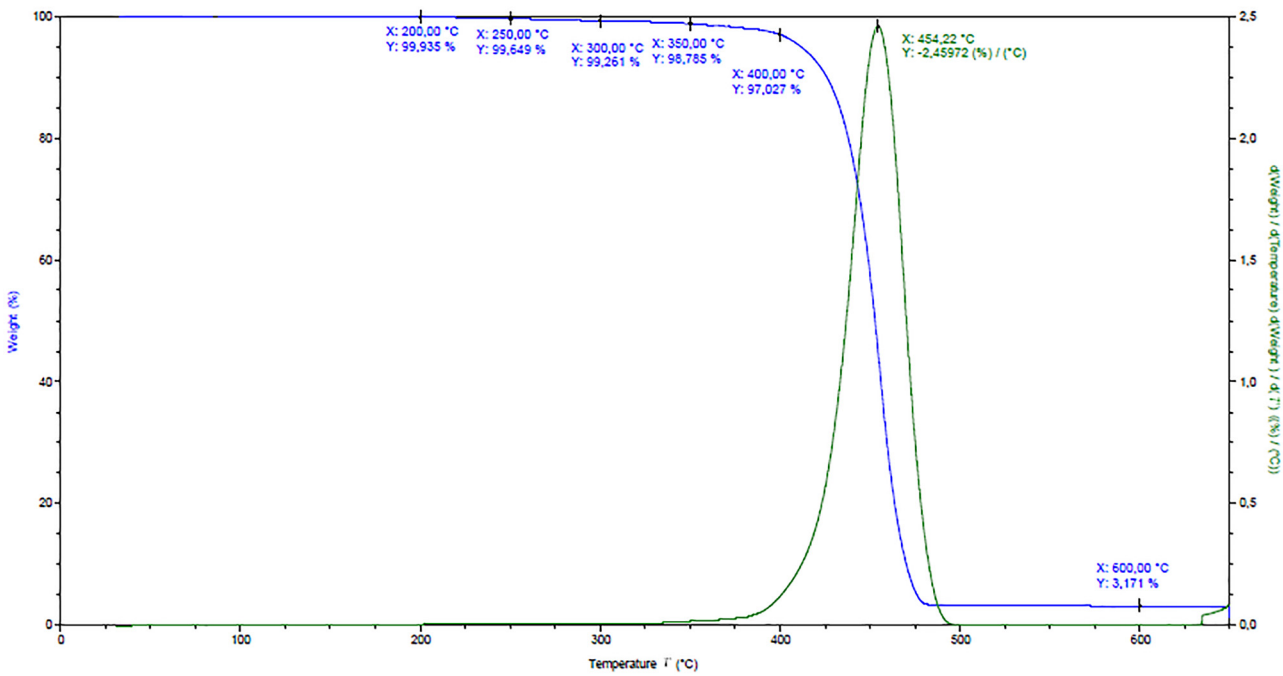

was preheated with a hot-air gun to 90°C. After the first layer, the print was cooled by compressed air. Having cooled, the samples were taken to the final dimension using a diamond-bladed table saw with a water circuit and a surface grinder.

Specimen design

The three-point flexural test was selected for the purpose of comparison between the printed and cast states. The material granularity is too high to be tested with the ISO standard for 3D printed parts (ISO 17296) (Forster, 2015). Instead, a standardised test for artificial stone was selected according to ČSN EN 14617.

A test specimen for the three-point flexural test according to the standard is a slab with the dimension of at least $50 \pm 0.3 \times 200 \pm 0.3$ mm, with thickness of the intended part, placed in the testing machine on rolling pins, spaced by 20 mm from edge of the part. The specimen thickness was selected to be 50 mm, maximum that the standard allows for a specimen of this width:

$$\mathbf{R_{tf}} = \frac{3FI}{2bh^2} \tag{1}$$

The flexural strength is determined by equation (1), where F is maximum force (N), I is distance between supports (mm), b is width of the specimen (mm) and h is the thickness (mm). Young's modulus is also calculated from the measured force/deformation.

To test the effect of material degradation as well as the decreased mechanical properties resulting from poor interlayer adhesion and voids in final part, two 3D printing strategies were designed and were compared to cast comparison samples. The strategies have been dubbed transverse and longitudinal, and their layout is shown in Figure 5. The ratio of the area to length of print path was within a 2% margin for these strategies, and both of these parts are designed to be fully solid A longitudinal sample after printing is shown in Figure 6. The longitudinal sample consists of outlines and should exhibit higher strength because of lesser number of interfaces between print roads. The transverse sample is more complex, using a with common strategy using one perimeter and infill, made up from parallel lines placed a nozzle width apart, and oriented perpendicular to the longest dimension of the part.

Casting for comparison

Process parameters for cast comparison parts were as follows: sand was dried and preheated in a furnace to a temperature of 250°C. The PP was then separately heated to a temperature of 150°C, added to the sand, mixed and left to melt at a temperature of 200°C. A wooden mould was preheated, and the melted composite was cast and pressed into the mould with pressure of 100 kg. After cooling, the resulting slab was cut into specimens using a diamond-bladed table saw with a water circuit.

Figure 5 Longitudinal and Transverse sample trajectories

Figure 6 Longitudinal sample after printing, still on its print surface

Specimen testing

Testing was carried out on a Zwick universal testing machine, Z020, equipped with a 20 kN load cell. The machine was unable to produce the specified 0.25 MPa/s in the selected sample size. Instead, commonly used loading speed of 2 mm/min was used. A sample after failure can be seen in Figure 7.

Each set of samples consisted of three specimens, except for the cast comparison parts. Internal voids created by the imperfect casting process led to reduced yield, and of the five planned cast specimens, only two were fit for testing. Other factors influencing the results are inaccuracies by machining to final dimensions. These were outside of the specified range of ±0.3 mm, so the flexural strength of each sample was recalculated using real measured dimensions.

The samples were analysed using computed tomography (μCT, GE phoenix v|tome|x L240). The main used parameters of the X-ray tube were voltage 160 kV, current 180 μA and filter of 0.5 mm thin copper plate. The measurement was focused only on selected region, which allowed to reach 40 μm linear voxel resolution. The CT reconstruction (based on filtered back-projection algorithm) was performed in the Datos 2.6 reconstruction software. All subsequent post-processing was performed in the software VGStudio MAX 3.3.

The aim of software analyses was to determine the porosity ratio and amount of high-density material. Porosity was compared between the cast and printed specimens, with a follow-up discussion considering the ways voids are created in the printed specimens.

Results and discussion

In Table 1, the average flexural strength is listed. Specimens displayed predicted behaviour during testing, and the area of

Figure 7 Sample after failure during the bending test

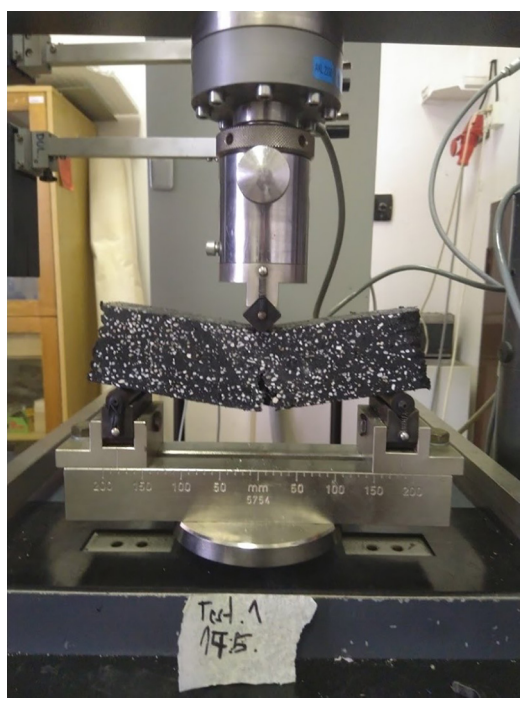

break was located in the middle of the part. The highest recorded deformation before break was around 10 mm, exhibited by the longitudinal samples. All configurations, except the transverse samples, exhibited higher strength than the values reported by the company, which is 16 MPa. This is expected, as the formulation used for 3D printing in this test has a slightly lower fill ratio. Usually, the company uses 25:75% ratio of binder: filler by weight, but for these tests, the ratio of 40% binder to 60% filler was used (the filler consists of 40% of silica sand, 20% building sand). For the transverse orientation, 25% loss of strength was recorded, which is less than in parts printed on regular-scale 3D printing machinery (Dizon *et al.*, 2018).

Less expected was the mechanical performance of the longitudinal samples. Similar material degradation was expected, as all of the material went through re-melting and mechanical incorporation of the filler before being formed into samples. However, based on knowledge of mechanical behaviour of FDM-printed parts, the layer-based process of 3D printing introduces break initiators and internal voids, and these contribute to anisotropy and decreased strength. In contrary to this expectation, longitudinal samples had the same flexural strength as cast parts. This shows that both inter- and between-layer adhesion was good, and that porosity introduced by the process had not negatively impacted strength of the parts. It is also possible that the 3D printing process has a positive effect on the orientation of the filler particles and the crystalline structure within the polymer.

There was a marked difference between the cast and 3D printed samples in fracture behaviour, as seen in Figure 8. The cast parts failed with expected brittle failure mode, with a crack rapidly propagating through the entire cross section. The 3D-printed parts failed with much more tough behaviour, with the crack advancing slowly layer by layer, with slight staircase like effect. This is confirmed by the difference in Young's modulus of elasticity,

Table 1 Average flexural strenght

Sample group	R_f *(MPa)*	SD
Longitudinal	19.5	0.631
Transverse	14.9	0.265
Cast	19.7	0.194

Figure 8 Difference in crack propagation, with cast sample at the top and longitudinal sample at the bottom

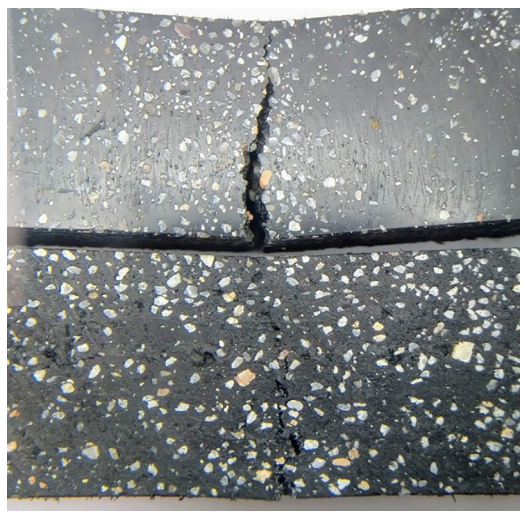

Figure 9 Stress/strain chart for all the samples included in this study

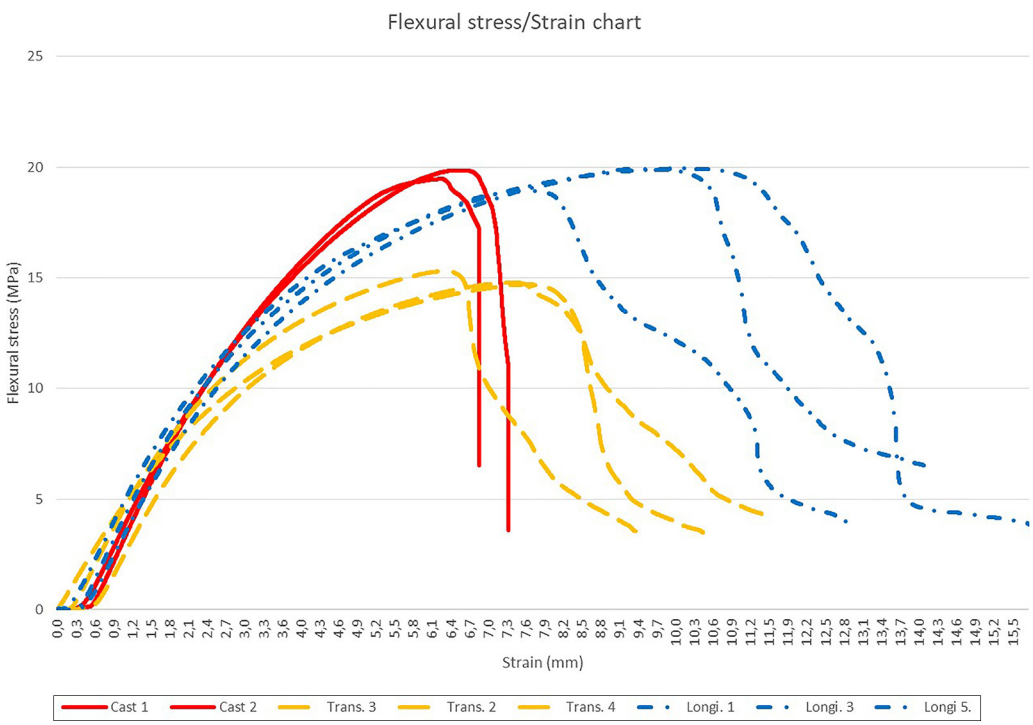

which is approximately 222 MPa for the 3D-printed samples, and 332 MPa for the cast samples, showing the rigider behaviour. Stress/strain charts for all the samples are displayed in Figure 9.

Typical slices for a cast part and both 3D-printed orientations can be seen in Figure 10, with porosity highlighted by solid colours depending on the pore size. Pictograms were added to identify layer orientation in 3D-printed parts. In large sections of the 3D-printed parts, the voids form a continuous cavity similar to open a foam structure. Alongside small voids mostly under 10 mm^3 – with a few voids up to 200 mm^3 – there are continuous voids displayed in red in both figures, interconnected throughout the entire part, both in longitudinal and transverse orientations. This makes the material water-permeable. These large cavities can be seen on the porosity distribution charts in Figure 11.

Transverse and longitudinal samples had porosity ratio of 12.59 and 10.54%, respectively, while the cast sample had porosity ratio of 1.58%. The large difference in porosity does not match with the similar flexural strength. It is possible that the material is brittle enough that the difference in porosity does not affect its strength much. Voids are displayed in Figure 12, with all the voids present in the cast part displayed, and only with voids larger than 10 mm^3 displayed for the 3D-printed parts to better show the shape of the continuous voids (displayed in red).

Cast parts are lightly porous, exhibiting a typical porosity pattern, with small, oblique voids. Rarely present are faults resulting from the molten material being poured into moulds. These faults happen when melt flow fronts trap pockets of air resulting in larger internal voids.

3D-printed parts manufactured via the FDM technology typically present porosity between individual lines and layers. This porosity is present here, especially in the transverse part, caused by the more complex infill pattern. One type of a problematic area in these parts is the sharp U-turns in the parallel infill paths. Generally, the sharper the turns, the greater the chance of porosity increase.

However, there is another cause of porosity present on the inside of the print roads themselves. The biggest infill particles were dragged in the direction of the print, leaving significant voids oriented along the print direction. This suggest that composition and shape of the filler particles might have to be addressed, or that minimal layer thickness must be increased.

Void distribution along the build direction can be seen on Figures 13 and 13_1. The chart shows a regular repetition along the entire height of the part, with peaks corresponding to layer thickness. This suggests interlayer voids as an important

Figure 10 Typical slices for all orientations, arranged in rows. Pore size is displayed by color, with individual scales included. Slice orientation is marked with axes and diagram of layers when applicable

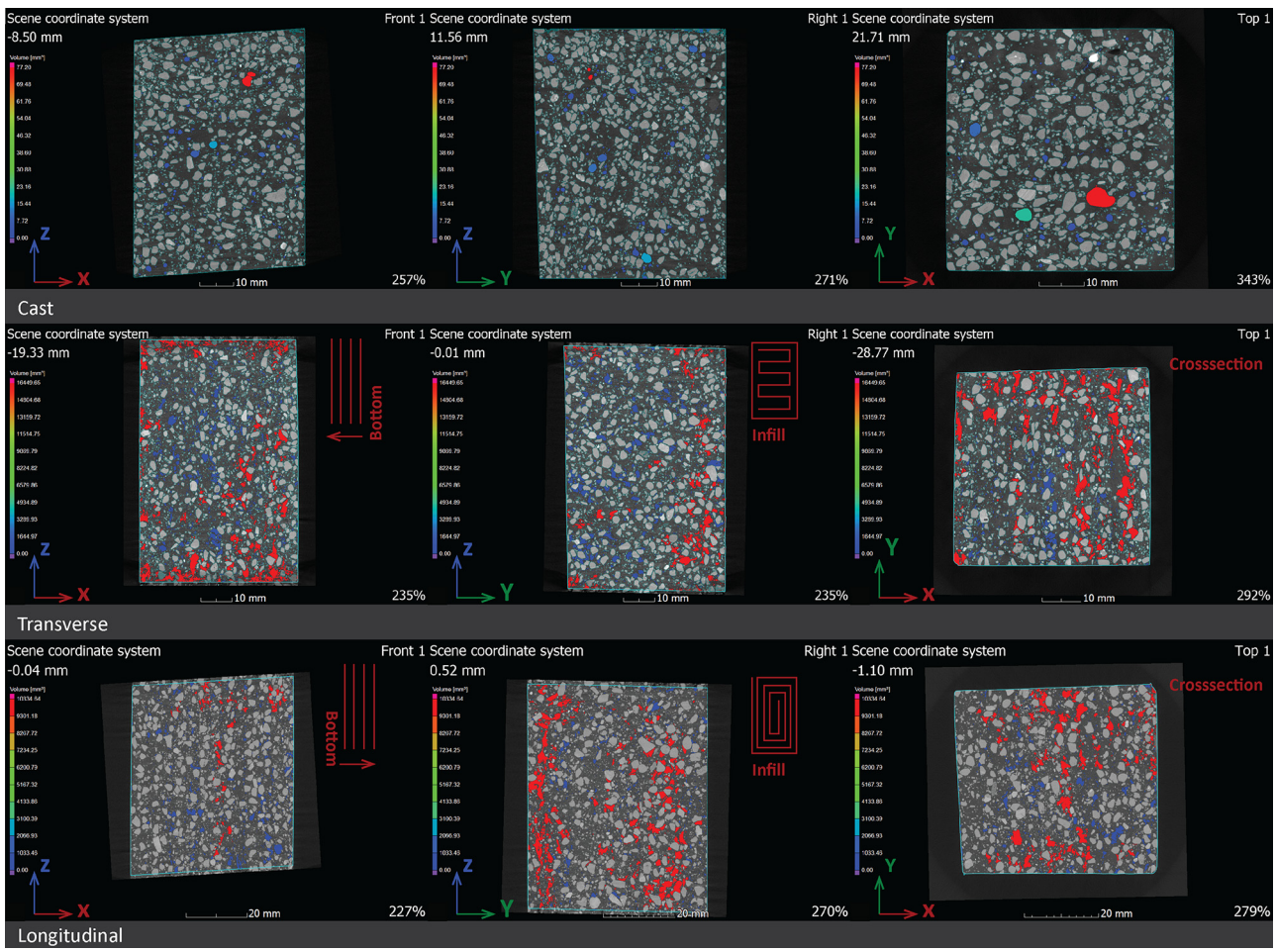

Figure 11 Pore size distribution for all sample types. Note the difference in X axis scale caused by the continuous void displayed in red for 3D printed samples

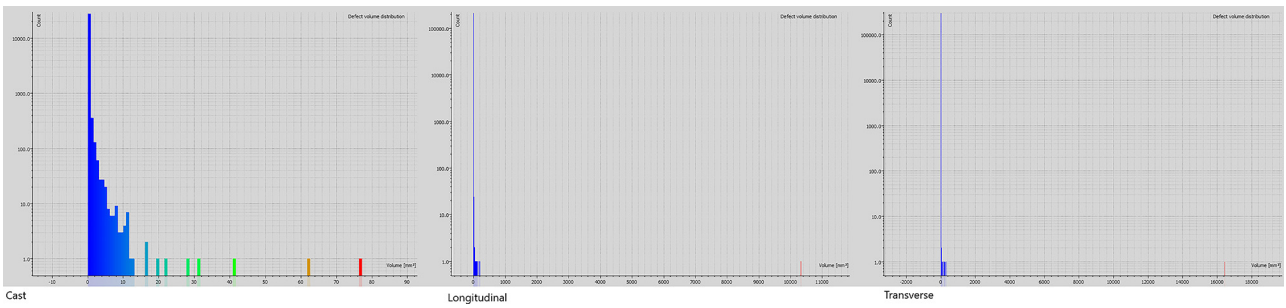

Figure 12 Rendering of voids in all sample types. Continuous voids in 3D printed samples displayed in red

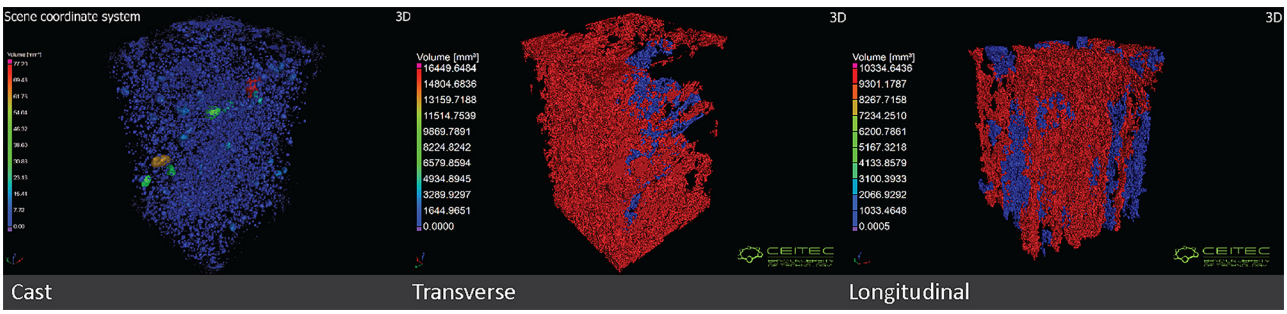

source of porosity, as well as consistent process parameters across the entire print, with most obvious deviations lying close to the build platform. This chart is not perfectly representative of total porosity distribution throughout the whole part, as a large part of the porosity forms a single void.

There are two main ways to control porosity in the finished parts, the first is by improving the extruder design, and the second is by improving the printing strategies. A correct screw extruder design should not incorporate extra air into the mixture and, ideally, should compress extra air out of the melt. To lower porosity by printing strategy, it is important to correctly set extrusion ratio (speed of movement/volume of extrusion). A slight over-extrusion can be beneficial to lower porosity and improve mechanical properties (Turner and Gold, 2015). This can be selectively applied to problematic areas, such as sharp bends, where the print road tends to deform due increased nozzle contact.

As a side note, it is important to ensure that the material used in extrusion is properly dried before printing to eliminate porosity caused by water vapour.

Possible uses for the material, considering its high toughness and fitting properties for large scale 3D printing, in combination with good water resistance of PP used as filler, would be as a formwork for pouring concrete construction. The manufacture of this formwork is usually quite costly, both in terms of materials and labour. This is true especially for double-curved formwork. The 3D printing process could reduce both requirements, without any restraints on the complexity of geometry.

After the initial testing stage, several functional artefacts were produced using the technology. Two of them can be seen in Figure 14, the first being a garden stool, the second being a lost formwork segment. The stool is fully functional right after printing and easily supports weight of two adults. During printing, several layers had partially delaminated due to material shrinkage.

Conclusions

In this paper, the influence of large-scale 3D printing process on a polymer concrete has been evaluated. Two printing orientations were compared to control cast part to examine the loss of mechanical quality during printing. Two possible sources of degradation of mechanical properties were evaluated – poor layer adhesion and material degradation. This was done by comparison of samples, with one having better print road orientation with regard to mechanical strength.

The mechanical properties of all three sample types were similar, with a slight decrease for the transverse orientation. The average flexural strength of the longitudinal and cast samples was 19.5 MPa and 19.7 MPa, and 14.9 MPa for the transverse orientation. The quality of the 3D prints was evaluated using CT, and porosity analysis was performed. Cast parts had a porosity ratio of 1.58%, while the 3D-printed parts exhibited porosity up to 12.59% in the transverse part, with pores created by multiple factors of the 3D printing process.

This suggests that the material is a good fit for 3D printing, with little to no degradation caused by the process. Layer adhesion was shown to be excellent, with negligible effect on the finished part for the longitudinal orientation. The process still has room for improvement due to the high porosity present in the specimens. Currently, any prints produced might not be waterproof, and the process is not ready for its intended use.

Figure 13 Porosity distribution charts for 3D printed samples

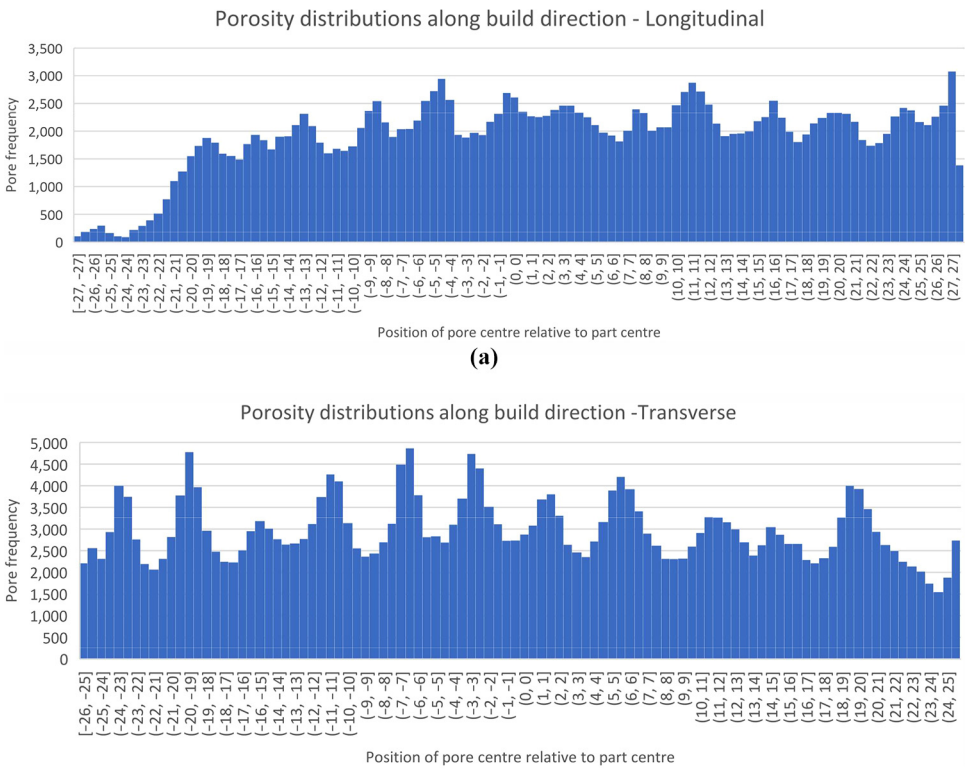

Figure 14 Prototypes produced by the technology. First is a functional garden stool, second is a mock up of a lost formwork segment

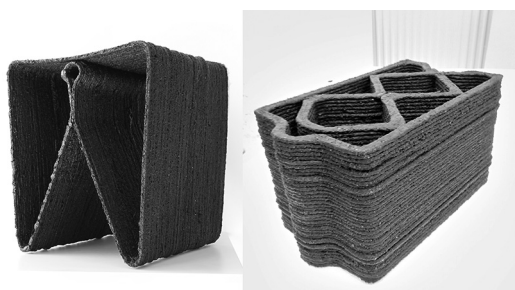

These results warrant further study of possibilities of printing with the material. The area of break should be investigated, and the comparison with cast material should be carried out again with a statistically significant set of samples. And, finally, large-scale testing of buildability should be carried out to evaluate possibility of using recycled plastic concrete for construction scale 3D printing .

References

Asprone, D., Auricchio, F., Menna, C. and Mercuri, V. (2018), "3D printing of reinforced concrete elements: technology and design approach", *Construction and Building Materials*, Vol. 165, pp. 218-231, doi: 10.1016/j.conbuildmat.2018.01.018.

Boyd, R.P., IV, Weller, C., DiSanto, A., Rees, M. and Hilbert, B. (2017), 'Cellular Fabrication And Apparatus For Additive Manufacturing', U.S. Patent 10,618,217.

Dizon, J.R.C., Espera, A.H., Jr, Chen, Q. and Advincula, R.C. (2018), "Mechanical characterization of 3D-printed polymers", *Additive Manufacturing*, Vol. 20, pp. 44-67, doi: 10.1016/j.addma.2017.12.002.

Domingues, J., Marques, T., Mateus, A., Carreira, P. and Malça, C. (2017), "An additive manufacturing solution to produce big green parts from tires and recycled plastics", *Procedia Manufacturing*, Vol. 12 No. December 2016, pp. 242-248, doi: 10.1016/j.promfg.2017.08.028.

Dumitrescu, O., Ropotă, I., Bratu, M. and Muntean, M. (2011), "Reuse of pet waste as thermoplastic composites", *Environmental Engineering and Management Journal*, Vol. 10 No. 8, pp. 1179-1181.

Forster, A.M. (2015), "Materials testing standards for additive manufacturing of polymer materials: state of the art and standards applicability", *Additive Manufacturing Materials: Standards, Testing and Applicability*, pp. 67-123.

Gosselin, C., Duballet, R., Roux, P., Gaudillière, N., Dirrenberger, J. and Morel, P. (2016), "Large-scale 3D printing of ultra-high performance concrete - a new processing route for architects and builders", *Materials & Design*, Vol. 100, pp. 102-109, doi: 10.1016/j.matdes.2016.03.097.

Hack, N.P. *et al.* (2016), "Method of fabricating a 3-dimensional structure, mesh formwork element for fabricating a 3-dimensional structure, and method of fabricating the same", available at: www.google.com/patents/US20160207220.

Khoshnevis, B., Russell, R., Kwon, H. and Bukkapatnam, S. (2001), "Crafting large prototypes", *IEEE Robotics and Automation Magazine*, Vol. 8 No. 3, pp. 33-42, doi: 10.1109/100.956812.

Kočař, J. (2019), "konstrukce extrudéru pro aditivní výrobu vysoce plněných termoplastů. BUT fme",

KUKA Roboter GmbH (2017), "Robots KR 30, 60 HA with C variants specification", pp. 1-171.

Kulovaná, E., *et al.* (2019), "The utilization of plastic residues from separation for polymer concrete preparation", *Waste Forum*, No. 2, pp. 116-122.

Love, L.J. Duty, C.E. Post, B.K. Lind, R.F. Lloyd, P.D. Kunc, V. Peter, W.H. and Blue, C.A. (2015), "Breaking barriers in polymer additive manufacturing", available at: www.osti.gov/servlets/purl/1185467.0.

Midland-Ross Corp (1981), "Extrusion devices and methods of reclaiming scrap plastic material".

Roschli, A., Gaul, K.T., Boulger, A.M., Post, B.K., Chesser, P. C., Love, L.J., Blue, F. and Borish, M. (2019), "Designing for big area additive manufacturing", *Additive Manufacturing*, Vol. 25 No. September 2018, pp. 275-285, doi: 10.1016/j.addma.2018.11.006.

Singh, B., Kumar, R. and Singh Chohan, J. (2020), "Polymer matrix composites in 3D printing: a state of art review", *Materials Today: Proceedings)*, doi: 10.1016/j.matpr.2020.04.335.

Slieptsova, I., Savchenko, B., Sova, N. and Slieptsov, A. (2016), "Polymer sand composites based on the mixed and heavily contaminated thermoplastic waste", *IOP Conference Series: Materials Science and Engineering*, Vol. 111 No. 1, doi: 10.1088/1757-899X/111/1/012027.

Stoof, D. and Pickering, K. (2018), "Sustainable composite fused deposition modelling filament using recycled pre-consumer polypropylene", *Composites Part B: Engineering*, Vol. 135 No. June 2017, pp. 110-118, doi: 10.1016/j.compositesb.2017.10.005.

Teizer, J., Blickle, A., King, T., Leitzbach, O. and Guenther, D. (2016), "Large scale 3D printing of complex geometric shapes in construction", *33rd International Symposium on Automation and Robotics in Construction, ISA 2016, i(Isarc)*, pp. 948-956. doi: 10.22260/ISARC2016/0114.

The New Raw (2018), "Print your city – Thessaloniki", available at: https://thenewraw.org/Print-Your-City-Thessaloniki (Accessed: 20 June 2019).

Turner, B.N. and Gold, S.A. (2015), "A review of melt extrusion additive manufacturing processes: II. Materials, dimensional accuracy, and surface roughness", *Rapid Prototyping Journal*, Vol. 21 No. 3, pp. 250-261, doi: 10.1108/RPJ-02-2013-0017.

VIA ALTA (2016), "POLYBET", available at: www.via-alta.cz/polybet/.

Welle, F. (2011), "Twenty years of PET bottle to bottle recycling – An overview", *Resources, Conservation and Recycling. Elsevier B.V*, Vol. 55 No. 11, pp. 865-875, doi: 10.1016/j.resconrec.2011.04.009.

Corresponding author

Martin Krčma can be contacted at: 152781@vutbr.cz

The International Journal of Advanced Manufacturing Technology
https://doi.org/10.1007/s00170-022-08685-4

ORIGINAL ARTICLE

Comparison of the effects of multiaxis printing strategies on large-scale 3D printed surface quality, accuracy, and strength

Martin Krčma[1] · **David Paloušek**[1]

Received: 16 September 2021 / Accepted: 4 January 2022

Abstract
The purpose of this study is to determine impact of several multi-axis 3D printing strategies on buildability, surface quality, accuracy, and strength of large scale single-walled object (printed in a so called vase mode). To achieve this goal, test objects were printed using four different printing strategies by an industrial robotic arm and a pellet-fed screw extruder. The strategies tested in this study are regular 3-axis deposition with planar layers, 5-axis deposition with planar layers, 3-axis deposition with nonplanar layers, and 5-axis deposition with nonplanar layers. Custom scripts for nonplanar slicing and for tilt control during multiaxis printing were developed to achieve these prints and are explained in this study. The results were evaluated using 3D scanning and mechanical testing, and surface accuracy, surface roughness, and layer adhesion strength were compared. The most important findings are (1) 5-axis motion alone does not improve the results of the printing; (2) while nonplanar printing can improve surface quality, its usability is geometry dependent; and (3) multi-axis nonplanar printing, even with partial tilt (30°) can expand printability with enhanced quality to at least 75° overhang angle. The future potential of these methods and the requirements to achieve them are discussed.

Keywords Robotic · 3D printing · Additive manufacturing · Nonplanar · Multi-axis

1 Introduction

The limitations of layer-by-layer processes, such as FDM (fused deposition modelling) are well known to its users and partially result from the slicing process that uses equally spaced parallel layers. This causes anisotropy and reduced surface quality due to stair stepping [1], both which depend on the build orientation [2]. Lately, a wide range of publications pushing these limitations has been published, in areas of multi-axis printing [3], supportless printing [4–7], and nonplanar printing [8, 9] strategies. One possible approach is the deconstruction of the model into parts with different slicing directions based on local geometry [10, 11]. The second study is closely related to another area of research, and that is nonplanar, or curved layer printing. Current publications focus mainly on the data preparation and path planning aspects of the processes. The presented study aims to analyse the impact of these strategies on the resulting objects more closely and discuss the usability of these strategies for expanding the application boundary of layer-by-layer extrusion printing methods. Other areas where multi-axis printing was used are DED using a robotic arm [12] or UV resin-based accumulation processes [13].

The focus of this study is on the usability and evaluation of these methods for large-scale printing (Fig. 1), because this area could benefit more from reducing the overall amount of material used and the support structures needed than desktop scale machinery [14]. Large-scale prints are commonly only single-walled, and the contact area between subsequent layers has a much greater impact on the print quality; the surface roughness due to stair stepping is significantly more noticeable for large layer heights, as are the errors that retractions can cause.

The main difficulty in nonplanar printing lies in the multifaceted problem of slicing/path planning for such a method. Universal slicing algorithms have only recently been presented by researchers and utilize computationally difficult and user inaccessible voxel accumulation based or iso-parametric/gradient based methods [15, 16]. Previously, more accessible approaches used transformation-based

✉ Martin Krčma
martin.krcma1@vut.cz

[1] Institute of Machine and Industrial Design, Faculty of Mechanical Engineering, Brno University of Technology, Brno, Czechia

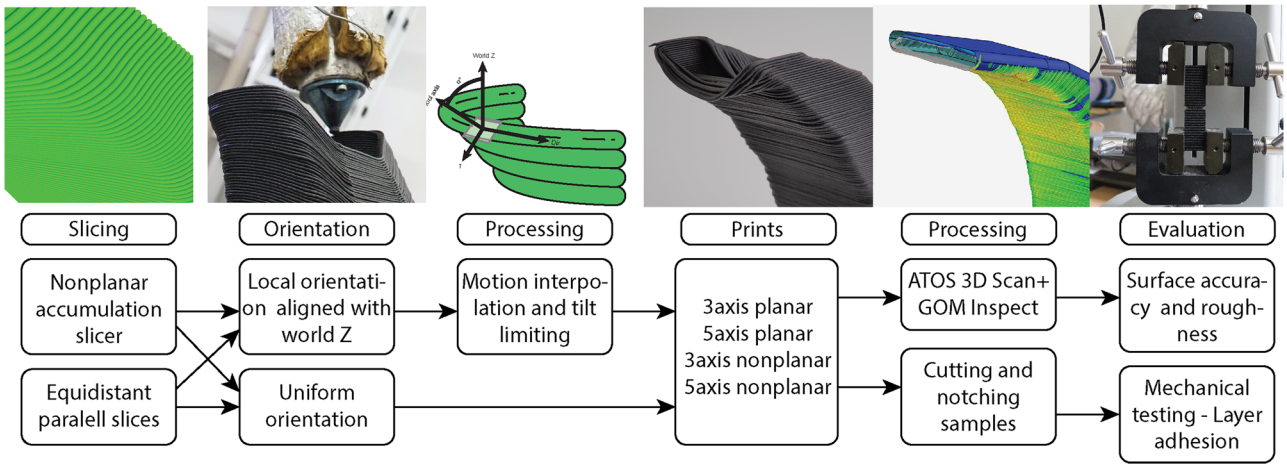

Fig. 1 Graphical abstract

methods, often utilizing a constant slicing geometry, either an arbitrary one or one extracted from the part, for the entirety of the build. These methods were suitable only for simple geometries and often had to make significant sacrifices in surface quality.

2 State of the art

The improvement in buildability that can be gained by varying the build orientation was demonstrated by Zhao et al. using incline layer slicing [10] or by Kubalak et al. using a multi-axis system [17]. Earliest mention of a technique for printing curved layers was made under the name CLFDM (curved layer fused deposition modelling), with the main benefit of printing near-flat thin walled parts such as turbine blades [18]. CLDFM was then developed by B. Huang and S. Singamneni over multiple publications, focusing on topics such as process modelling and evaluation, and alternative slicing methods with combined strategies or variable layer heights [19–23]. Approachable methods for generating curved print paths by cylindrical transformation are described by Zhao et al. [24].

Schuh et al. described the problem with varying layer heights and stair-stepping on angled surfaces and demonstrated a method to eliminate it by printing along local surface orientation with adaptive layer heights [25]. Limitations of layer stacking and nozzle reach for volumetric print paths, as well as multiple methods to generate such paths, are described in Ezair et al. [26].

The method for printing curved top surfaces on a 3-axis delta-type robot was presented by Allen and Trask [27]. The slope angle of the computed slices is a limitation, especially for 3-axis printers, and must be controlled to avoid collision. An algorithm that can decompose whole objects for printing on 3-axis machines was published under the name CurviSlicer [28]. The limitation can be overcome by using multi-axis motion to reorient the build orientation, either by dividing the model into parts that can be printed with parallel layers [5, 17], or by using local tangent direction and nonplanar trajectories. Xu et al. also described a method for computing these trajectories [29].

Fang et al. presented an algorithm for nonplanar volumetric slicing and showed that printing nonplanar layer oriented along stress lines can increase strength of prints by more than 6x [30]. Dai et al. describe voxel based nonplanar slicing algorithm for support less printing, that ensures printability for multi-axis printing by generating convex shells [31].

3 Methods

To evaluate usability of the different methods, a test object was designed, and 4 different print strategies were prepared, manufactured, and evaluated. The strategies are 3-axis deposition with planar layers, 5-axis deposition with planar layers, 3-axis deposition with nonplanar layers, and 5-axis deposition with nonplanar layers. The 5-axis deposition methods are intended to improve surface quality by orienting the extruder nozzle along the local surface tangent. The nonplanar strategy focuses on keeping the actual layer height, measured along surface orientation, constant for the entire build. The actual layer height is directly proportional to "cusp height."

3.1 Samples and trajectories

The test object used for the comparison is an overhang tower, stepped by 15° from 0 to 75°. The tower dimensions are in

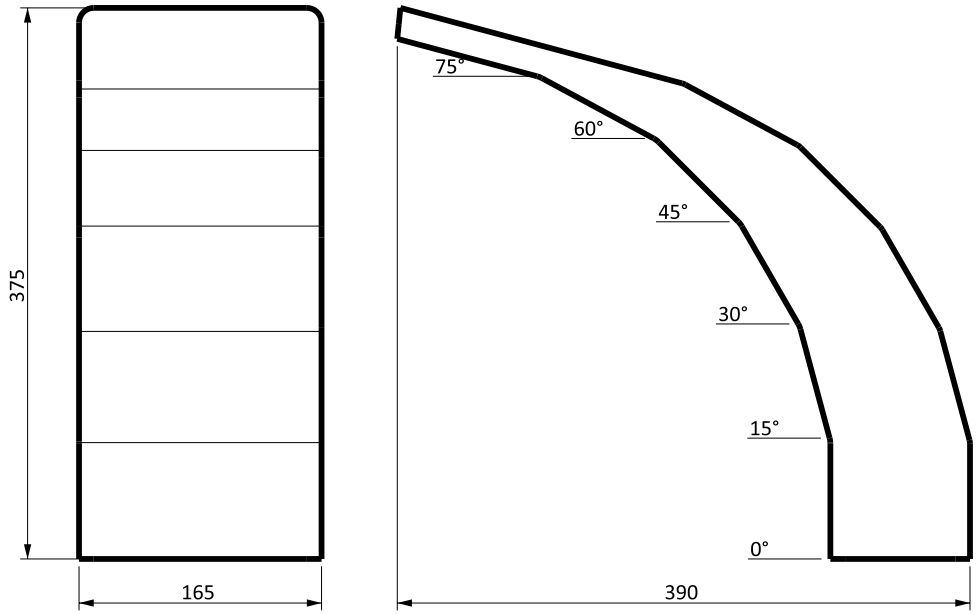

Fig. 2 Dimensions of the test tower

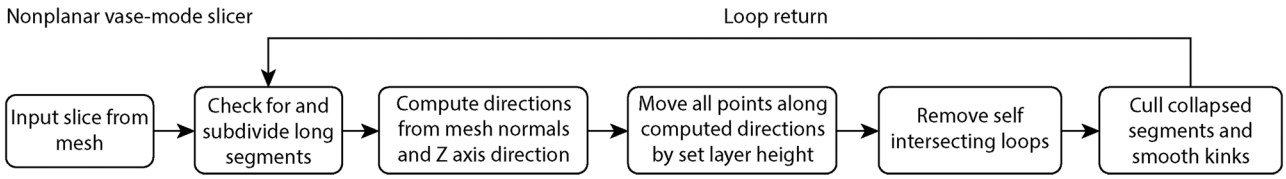

Fig. 3 Scheme of the nonplanar slicing algorithm

Fig. 2. The tower is designed in such a way that the trajectories are arrayed in straight, parallel layers on the inside overhang surfaces for all towers and these surfaces are then used for analysis and comparison. The tower cross section is constant to keep layer printing times for 3 axis methods constant as well. They vary slightly for nonplanar methods (the nonplanar trajectory is 6.4% longer at the 60° segment) but not enough to warrant designing a different test object.

The test objects were modelled, sliced, and the resulting robot motions programmed in Rhinoceros 3D and the Grasshopper environment, with the kuka.prc [32] plugin being used for robot code generation. Custom algorithms were developed for slicing and motion planning in the Grasshopper environment.

The nonplanar slicing algorithm works iteratively, calculating the position of the next layer from the last layer to keep the actual layer height the same as the nominal layer height for all points. The basic workflow can be seen in Fig. 3. Figure 4 shows both used trajectories, and Fig. 5 displays deviation from nominal layer height for both approaches, with points with spacing of < 2 mm coloured in green and > 2 mm coloured in red. The range of distances is 2 to 7.72 mm for the planar trajectories and 0.7 to 4.1 for the nonplanar approach. The actual layer height, sorted from lowest to highest, is also displayed on the charts as a part of Fig. 5. Layer height variation in the planar trajectories is easily explained by the overhang angle, as the *Actual layer height* = *nominal layer height/cos(overhang°)*. Any significant layer height deviations in the nonplanar trajectories come from slicing artifacts around sharp corners, and these are rare outliers, as can be seen in the point distribution chart.

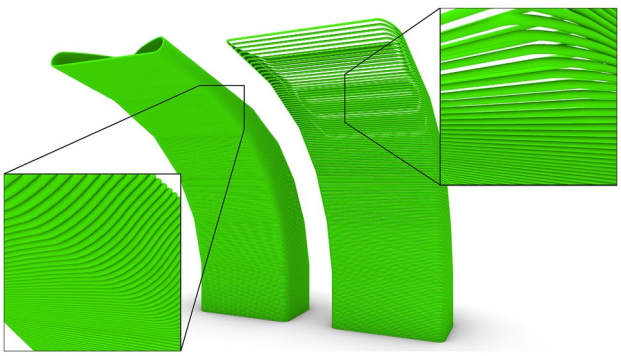

Fig. 4 Comparison of the two trajectories used. Open loops are excluded

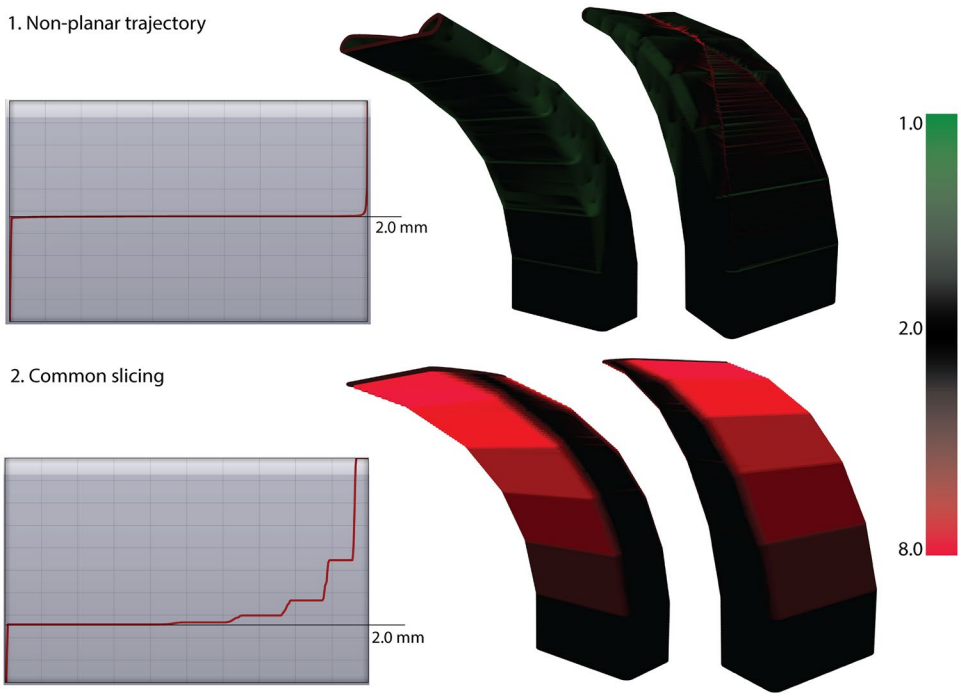

Fig. 5 Visualization of the deviation from set layer height for both trajectories using a plot of distances between all adjacent points and coloured visualization on the mesh

The planar trajectory is 88,227 mm long (est. print time 4 h 55 m), and the nonplanar trajectory, without the top extension needed to avoid open loops and thus covering the same surface area, is 113,711 mm (6 h 15 m). Both trajectories were printed using both the regular 3-axis printing and the 5-axis printing, where the extruder is oriented along the local surface tangent and perpendicular to the trajectory. The maximum allowed angular deviation from the world Z axis is set to 30°, mainly to ensure proper gravity feeding of the granulate from the hopper and to increase the usable build envelope. This limit is enforced by the tilt control script, explained in the next section.

The motion planning is carried out as follows: First, the orientation frames are calculated for each point as a cross product of the direction of the trajectory as the first vector and the local normal as the second vector (Fig. 6). Then, simple interpolation is applied by averaging each point orientation with its closest neighbours to ensure smooth robot motion even in sharp corners. Before calculating the final set of robot frames, tilt control is performed.

The tilt control script works by evaluating the angle (α° in Fig. 6) between the intended orientation of the extruder and the world Z direction and checking it against the threshold. If the angle α exceeds the threshold, the vector is replaced by one on an identical plane (described by the World Z vector and the surface normal) with the deviation angle set at the threshold.

3.2 Materials

The robotic arm used as a 3D printer gantry was Kuka KR 60 HA, with KRC 2 controller. The extruder is a custom-built single screw extruder with a diameter of 30 mm. Nozzle diameter is 5 mm, with an extended tip in order to increase clearance when printing a nonplanar paths. The tool speed was reduced to 5 mm/s to allow sufficient cooling of the deposited layer before another one is deposited [33]. The assembly can be seen in Fig. 7.

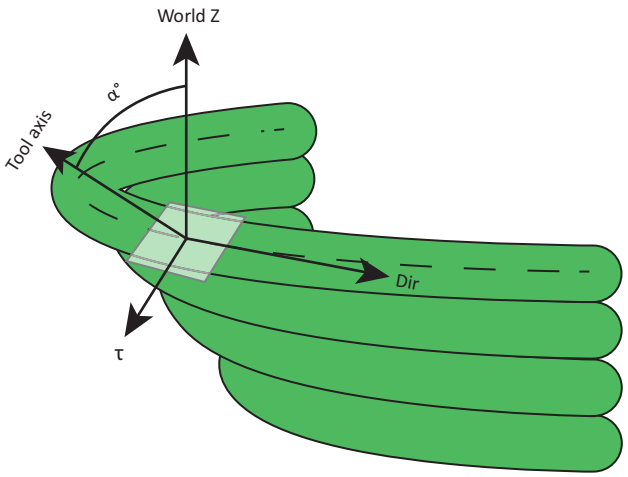

Fig. 6 Tool orientation for 5-axis trajectories

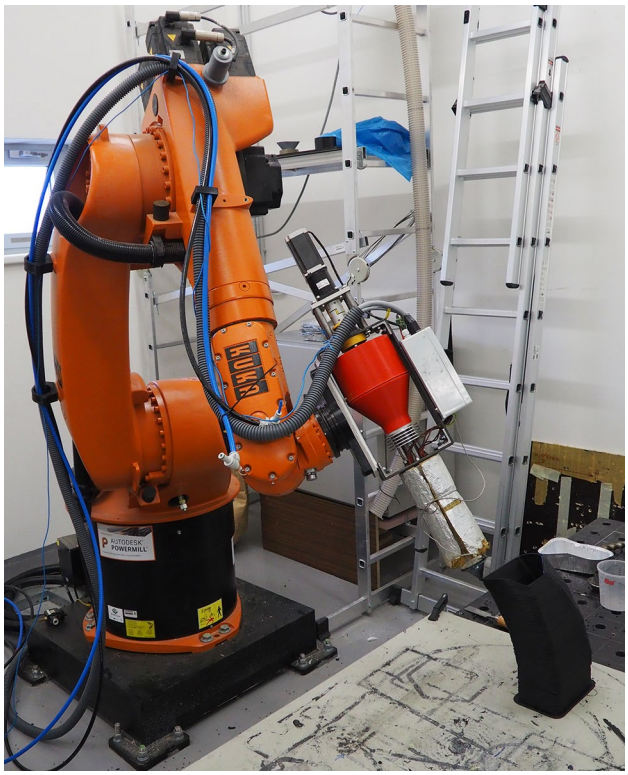

Fig. 7 Robotic arm with the screw extruder during a multi-axis print

Table 1 Summary of print parameters

	Planar	Nonplanar
Temperature	230 °C	
Layer height	2 mm	N/a
Actual layer *h*	Variable	2 mm
Nozzle Ø	5 mm	
Tool speed	5 mm/s	

The test objects were printed using Remark Plast Remapylen GF 30 (rPP GF 30). This material is a widely available engineering plastic that promises economical printing and is very resistant to degradation in the melt extrusion. The semicrystalline nature of the polymer makes it prone to warping during the printing process; this behaviour is reduced by the high percentage of fibre filler [34]. The extruder temperature was set at 230 °C, the layer height at 2 mm. The process parameters are summarized in Table 1.

The resulting specimens were then 3D scanned using an ATOS Triple scan optical scanner. 3D optical digitization is based on active fringe projection and triangulation.

Process of 3D data digitization:

1. Surface matting with chalk spray.
2. Reference points placement on the part surfaces.
3. 3D digitizing with a rotation table.
4. Post-processing and evaluation of deformations.

The measurements were performed with the scanner setup according to "VDI/VDE 2634, Part 3 Optical 3D-measuring systems, multiple view systems based on area scanning." Measurements in this study were made using MV560 lenses (560×420×420 mm) calibrated in a standard arrangement. The measuring point distance is 0.176 mm, i.e. 6 points/mm, the recommended reference point diameter is 3 mm, measuring distance 830 mm, camera angle 27°, focal length of camera lenses 24 mm, and focal length of projector lens 30 mm.

CAD alignment (Fig. 8) was based on fitting planes in the 0° overhang sections of the printed objects and aligning them with the original CAD surfaces. This method was chosen instead of the best-fit method to properly represent the progressive deviation that occurred during the prints. The point cloud reconstruction, alignment to the nominal CAD model, and deviation analyses were performed in GOM Inspect.

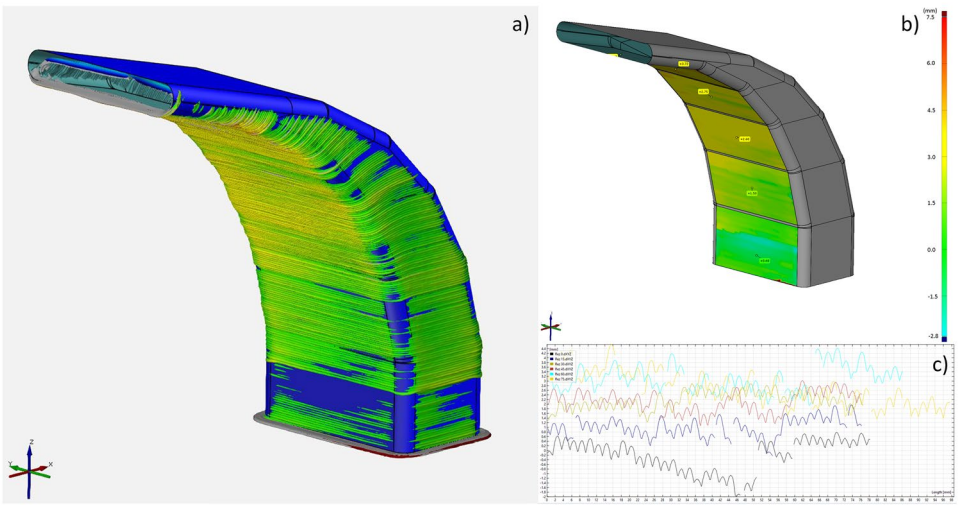

Fig. 8 **a** 3D scanned mesh reconstruction of the 5-axis nonplanar test object aligned with the nominal CAD data. **b** The surfaces evaluated for deviation analysis. **c** A set of profile curves exported from GOM Inspect

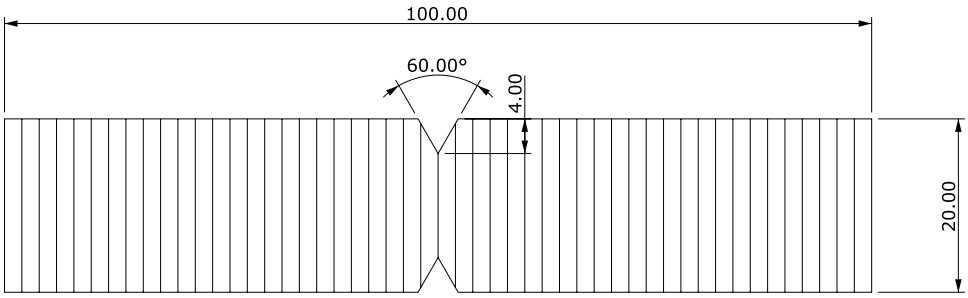

Fig. 9 Dimensions of the layer adhesion sample

Table 2 Overview of printing results by overhang angle

	0°	15°	30°	45°	60°	75°
3-axis planar	Pass	Pass	Pass	Pass	Fail	Fail
5-axis planar	Pass	Pass	Pass	Pass	Fail	Fail
3-axis nonplanar	Pass	Pass	Pass	Fail	Fail	Fail
5-axis nonplanar	Pass	Pass	Pass	Pass	Pass	Pass

On the resulting meshes, mean surface deviation analysis and surface profile extraction for surface roughness (Ra — arithmetic average height) calculation were performed. For the surface deviation analysis, the mean absolute deviation from the nominal CAD model is presented. The evaluated surfaces can be seen in Fig. 8b. For surface roughness, profile curves were extracted and *Ra* was calculated using Formula 1, which is the digital version of the *Ra* expression. The profile curve was filtered using sliding average with a wide window to eliminate the influence of possible geometric surface defects such as waviness [12]. After this, the mean *m* and the resulting *Ra* were calculated.

$$Formula\ 1: Ra = \left(\left|Z_1 - m\right| + \left|Z_2 - m\right| + \cdots + \left|Z_N - m\right|\right)/N$$

3.3 Layer adhesion testing

Slabs were cut from each tier of the overhang towers on the internal wall where the layers run in parallel for both slicing approaches. Layer adhesion samples were then cut and ground from these slabs, dimensions $100 \times 20 \times 5$, notched in the middle along a layer boundary to ensure delamination in the preferred position. The specimen can be seen in Fig. 9. The V-shaped notch was broached, 4 mm in depth, and with 60° tip angle. Specimens were kept sealed with a desiccant for 14 days.

The samples were then tested for layer adhesion on an Imada MX2 test stand, equipped with a 2.5 kN load cell, with the loading speed being 10.0 mm/min. Maximum force was recorded, and the fracture surface was measured. A test sample loaded in parallel jaws can be seen in Fig. 10.

4 Results

4.1 Printing results

Of the four builds, the only one to finish printing was the 5-axis, nonplanar build (Table 2). All the prints before testing can be seen in Fig. 11. Both planar builds failed

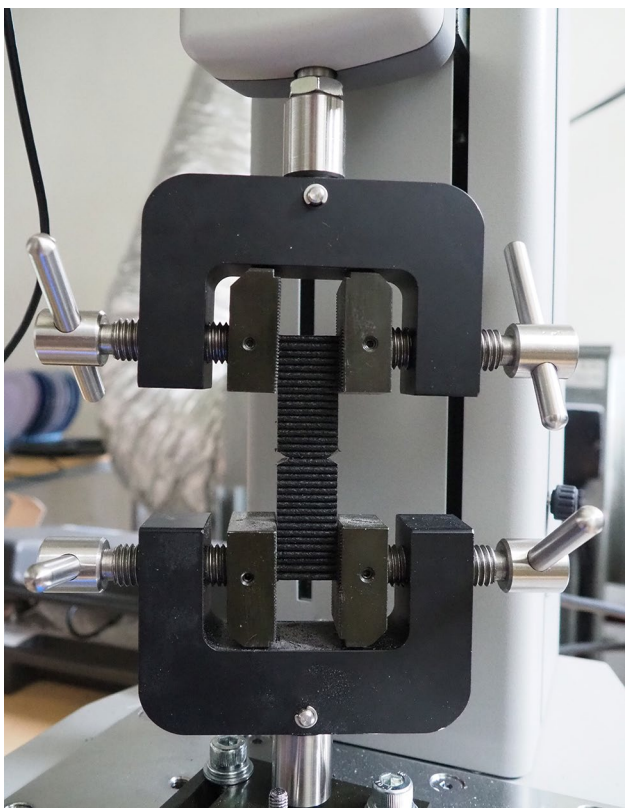

Fig. 10 A layer adhesion specimen loaded in the testing machine

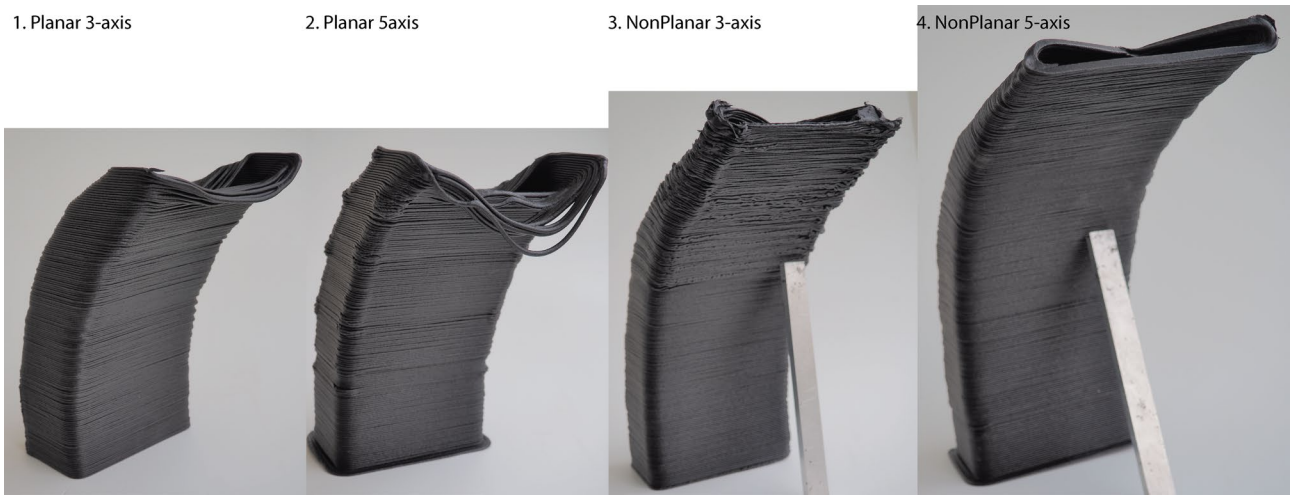

Fig. 11 All the prints side by side, from left to right: planar 3-axis, planar 5-axis, nonplanar 3-axis, nonplanar 5-axis

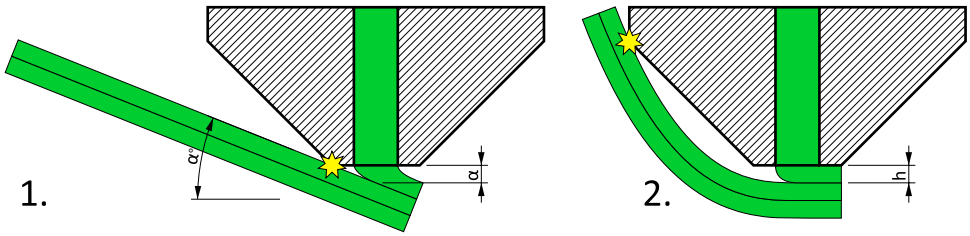

Fig. 12 1. Collision due to the slope steepness. 2. Collision with surrounding geometry

after 45° of overhang due to failure to stack subsequent layers. The 3-axis nonplanar test failed after 30° when the nozzle contacted the previous layer, due to the slope angle being too steep. The build appeared to continue, but it had partially separated from the build platform and shifted. This has caused the segments after the 30° overhang to be printed out of alignment with the underlying geometry.

Notable issues recorded during printing: Feeding issues, causing under extruded segments in the 5-axis builds. The under extruded areas were excluded from all analyses. Both 5-axis samples had overextruded areas in the corners of the transitions between overhang angles. This is due to a slicing error, the double curved surface patches generated a large number of points, causing the robotic arm to slow down. The last, 75° overhang segment of the nonplanar 5-axis print is underextruded, as the nozzle was close to contacting the previous segment and reaching failure state.

The results show that using multi-axis printing with conventional slicing technique does not improve printability on its own, as well as showcasing the problems that arise with the use of nonplanar trajectories. The nonplanar 3-axis method is especially limited and failed because of slope angle limitations. The nonplanar 5-axis method has a much wider area of applicability, but also increased requirements due to possibility of collision. Geometric limitations are displayed in Fig. 12. Figure 13 shows near collision due to local geometric limitation in the 5 axis test object.

4.2 Accuracy

The comparisons of the four test objects can be seen in Figs. 14–16. The 3-axis nonplanar test object is evaluated even beyond the point of print failure when possible; otherwise, it is excluded.

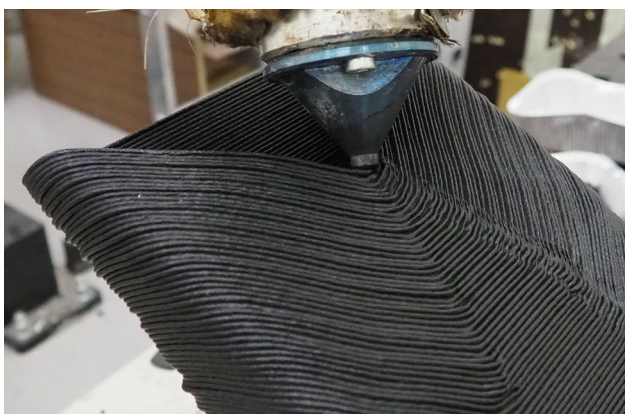

Fig. 13 Nozzle near contacting local geometry during the 75° segment

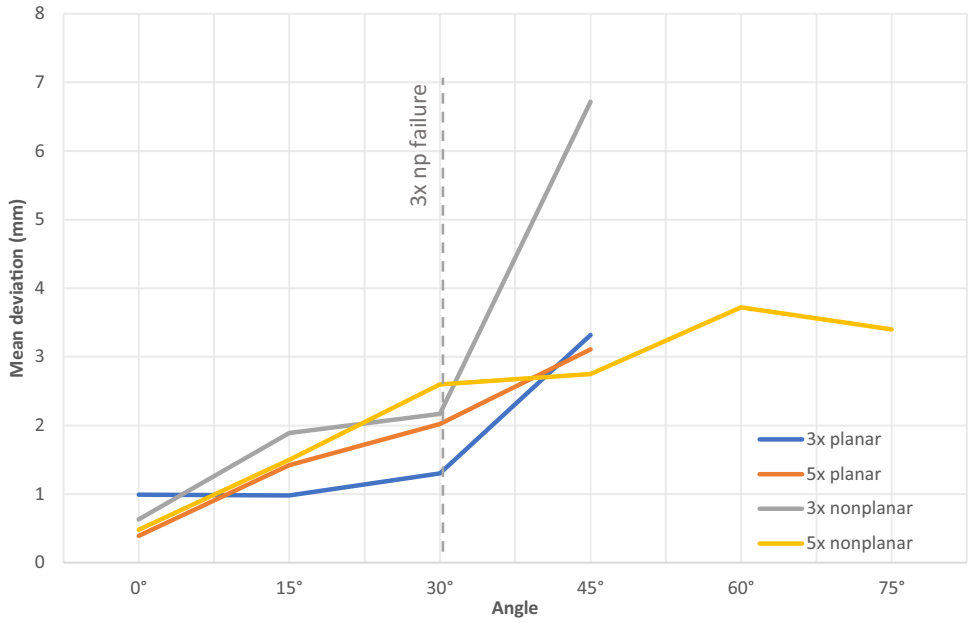

Fig. 14 Mean deviation chart

Figure 14 shows the total mean deviation, including the deviations caused by geometric deviation, surface roughness and the deviations caused by technology — such as differences in print path width. The initial deviation, caused by the thickness of the actual deposition, lies between 0.4 and 1.0 mm. The deviation increases for each method until its respective point of failure, with the deviation of the last correctly printed segment lying between 2 and 4 mm for all methods.

The surface roughness can be seen in Fig. 15. After the first segment, the surface roughness starts to increase for the 3-axis planar method starting at 0.22 mm and reaching 0.41 mm. The 5-axis and nonplanar methods, while sometimes worse at low overhang angles, manage to keep lower surface roughness at high overhangs until the tilt control allowance runs out. Surface roughness is the only area where the 5-axis planar strategy appears to bring benefits, as the print finished with nearly the same roughness as at the start.

4.3 Mechanical testing

The maximum average delamination force (F_{max}) can be seen in Fig. 16. Slight initial differences between the test objects could be due to slicing errors, but the percentual differences between different overhang angles of the same test object

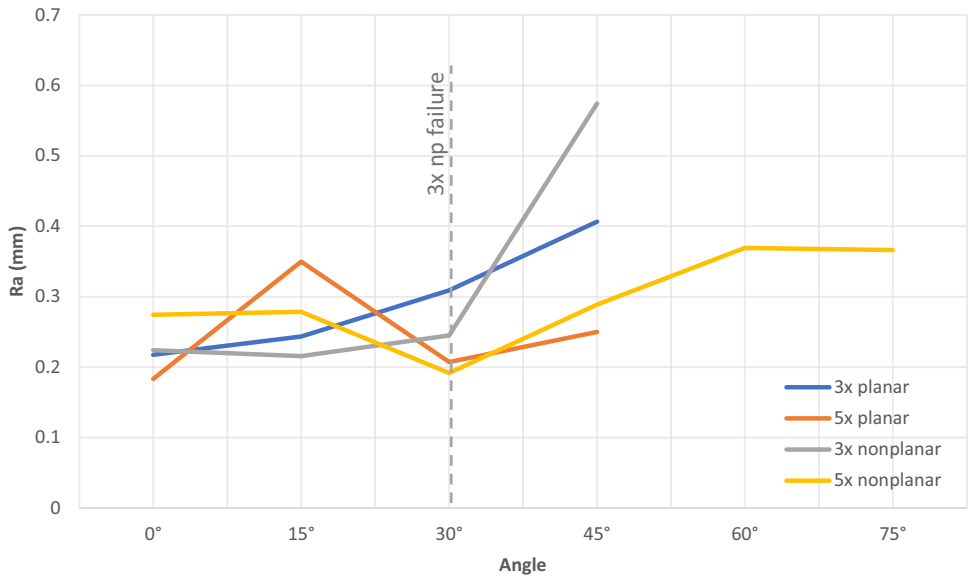

Fig. 15 Surface roughness chart

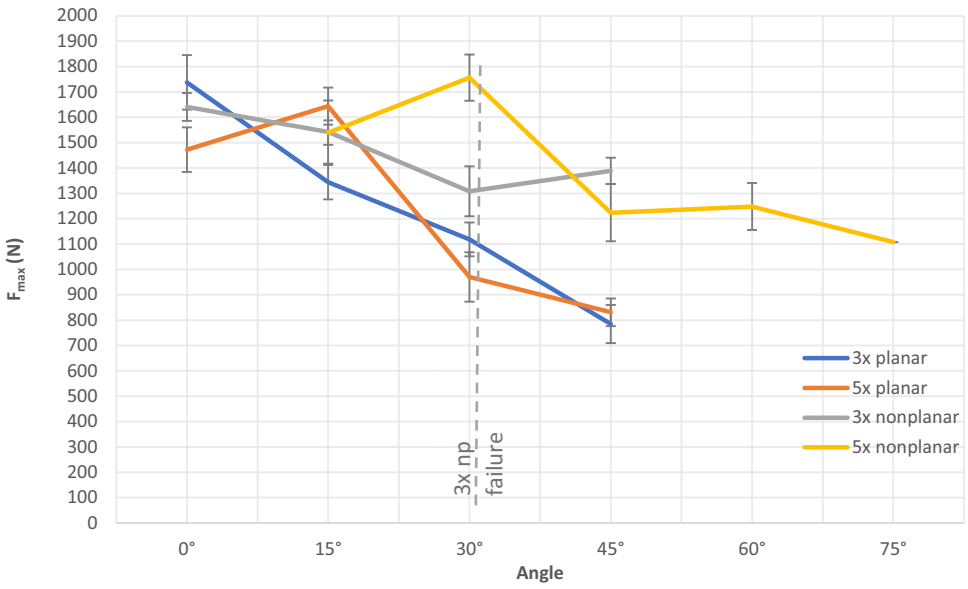

Fig. 16 Maximum delamination force chart

can still be evaluated. The planar slicing methods showed a rapid decline in the delamination force (from 1737.4 N to 784.5 N), which can be explained by the decrease in contact area between adjacent print paths. The 5-axis planar test lost approximately 46% F_{max} and did not show significant improvement over the 3-axis test, which lost approximately 54% F_{max}.

For the nonplanar tests, some decrease in F_{max} was present, but to a much lesser degree. The 3-axis nonplanar test object lost 25% F_{max} at the 45° overhang segment, while the 5-axis lost 20% at the same segment and 30% at the 75° segment. The decrease in delamination force is much more gradual for nonplanar printing methods. These methods could be promising for preserving strength in the vertical direction of prints, which is the direction most susceptible to anisotropy in FDM and similar methods [2]. This anisotropy is even more prominent in fibre filled materials such as the PP GF 30 used in this study [35]. The method would also bring consistency to printed parts by decreasing the dependence of mechanical properties on the overhang angle.

5 Discussion

This study explores the impact of individual multi-axis printing methods. Slicing for such methods must acknowledge the problems of geometry collision, either due to slope steepness or due to local geometry (Fig. 12). For the process to be reliable, either the slicer has to generate trajectories with the geometric constraints included in the process, or each layer has to be collision checked. A possible approach to generate guaranteed collision free trajectories could be separating areas of the layer into multiple levels, based on the local steepness, similar to CAM finishing strategies for shallow areas. Another approach to generating layers for 5-axis processes with guaranteed printability is to generate "convex hull layers" [31] (Fig. 17).

The slicing algorithm used in this study is incomplete. It is only suitable for slicing vase mode objects with a single continuous perimeter. It also does not include any precalculation to ensure that the calculated trajectories cover the entire object. If the sliced object has areas with much greater geodesic surface distance than others, it is possible that the algorithm will fail or will not cover the entire surface. This can be overcome by calculating layers with variable height. The nonplanar trajectories used in the study did not cover the entire test tower; the upper area of the tower was excluded to avoid printing partial perimeters with retraction. Due to its ability to cover horizontal areas and even negative overhangs, the slicer can still be used for a wide variety of geometry. The computational intensity of the presented nonplanar slicing algorithm is higher than that of a constant layer height slicing. It is influenced to a high degree by density of the input mesh and user set parameters, mainly the max. length of a segment before subdivision. Regular slicing of the test object takes roughly 6 s, while the runtime of the nonplanar slicer is about 90 s on an i7 7700 equipped

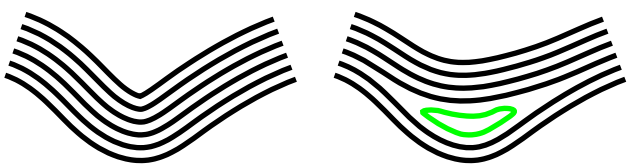

Fig. 17 Suggested technique for sharp corner prevention by partial layer insertion

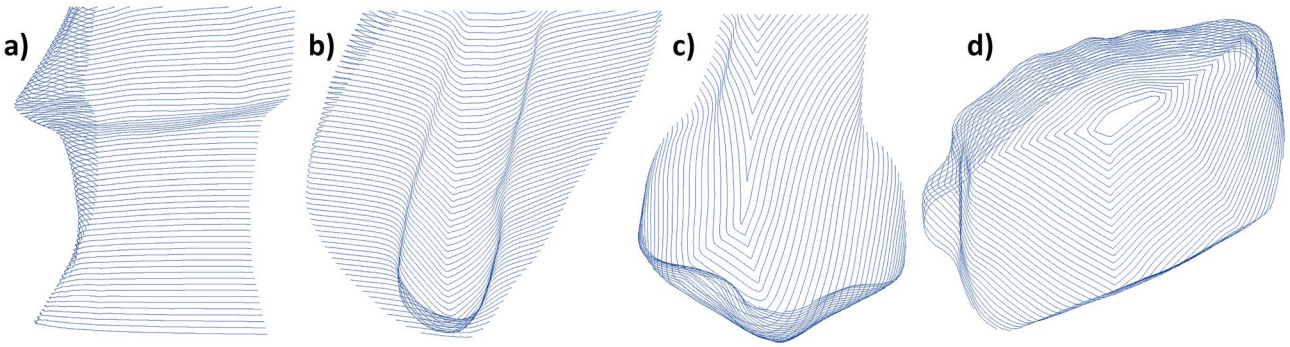

Fig. 18 Demonstration of the nonplanar slicer used on an organic mesh. **a**, **b** Correctly arrayed trajectories around narrow parts and overhangs. **c** A tight corner with trimmed loops. **d** Failure to cover tight area at the end of the print

machine. Demonstration of the slicer on a sample geometry can be seen in Fig. 18.

An important part of the nonplanar slicing script is the clean-up after a layer shift. The most problems arise in areas that have significantly smaller curvature radius than layer height, and after rapid decrease in cross section area. These areas can produce self-intersecting loops in the trajectory that the clean-up process has to detect and eliminate, as shown in Fig. 19. Alternatively, precautions have to be taken, such as preventive filleting of detected sharp corners.

The main reason for using this transformation based method instead of isocurve/isoparametric based one is the ability to easily calculate trajectories for multi-surface or mesh objects and the ability to generate continuous curves for vase mode printing of single walled objects, without the need to check surface coverage and insert additional curve segments as in other methods [36] and without the need for support structures.

The improvements in mechanical performance should mostly be attributed to the nonplanar trajectories keeping the amount of material deposited nearly constant independent of the overhang angle. The area density of the samples (shown on Fig. 20) partially supports this claim. The influence of different layer orientations on tensile stress between the 3-axis and 5-axis strategy is harder to establish. Literature suggests that for regular scale FDM, angled parts (the 3-axis methods in this case) have higher strength than vertical ones [37]; however, it is unclear how this translates to single-walled prints.

Fig. 19 Loop creation on sharp corners and prevention by filleting

The comparison was carried out for a single set of parameters. For a different set, the basic relationships between methods should stay the same, but the proportional differences might change. The most significant changes are expected to come with varying the layer height. The expectation is that the buildability of planar methods will increase with decreasing layer height and the buildability of nonplanar method will decrease because the allowable slope angle will decrease. The exact relationship could be a topic for further research.

The 5-axis tilt influences the accuracy of tool endpoint, and this is shown in the slight decrease in accuracy and surface quality in the beginning stages of the prints. This is compensated for by preservation of quality at higher overhang angles. Still, in future work, it could be beneficial to restrict tilt even under the currently set tilt limit of 30° and use it only when beneficial. For example, if we take 15° as the boundary under which multi-axis printing brings zero benefits, we should then exclude areas under 15° overhang from tilt and use only necessary amount of tilt in areas over that limit.

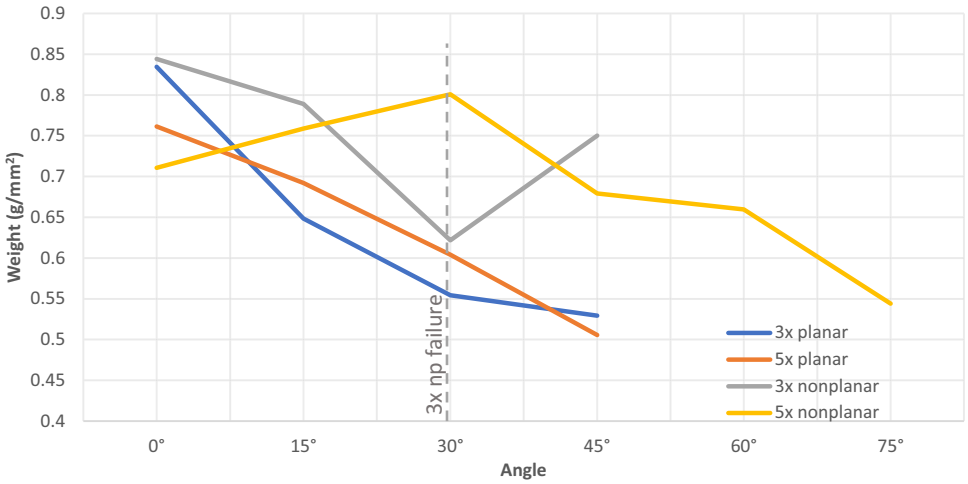

Fig. 20 Area density of the delamination samples

6 Conclusions

Four different 3D printing methods were compared and the techniques required to perform them were presented. This includes the transformation based nonplanar vase mode slicing algorithm and the method of tilt limit for multi-axis robotic 3D printing along surface tangent. The goal of these methods was to preserve layer height and print path orientations at all overhang angles, increasing surface quality and strength. The mean deviation, surface roughness, and layer adhesion strength were evaluated using 3D scanning and mechanical testing.

One of the most important takeaways is the fact that using 5-axis motion alone does not bring noticeable improvements over the common 3-axis approach. And while nonplanar trajectories can bring improvements in strength and surface quality, the approach, if used on a conventional 3-axis printing setup, is very limited in terms of printable geometry. Objects have to be either divided into parts based on reach of the nozzle, or 5-axis motion has to be used. Path planning for 5-axis motion brings another set of complications, in mainly due to the need for collision checking.

But the combination of nonplanar trajectories and multi axis motion brings real expansion of capabilities for large-scale FDM style printing. When printing large-scale objects with large nozzle sizes, single line walls are often all that is necessary to achieve desired structural performance and this, combined with the limited ability of screw extruders to perform retractions, leads to the vase mode printing being a suitable choice. Using these methods, stable wall thickness and large overhang angles of at least 75° are achievable and the quality of single walled objects is increased in terms of surface roughness at overhang angles over 15° and mechanical strength, with 20% loss of maximum average delamination force for 5-axis nonplanar trajectory at 45° compared to 50% loss for 3-axis planar trajectory.

Supplementary information The online version contains supplementary material available at https://doi.org/10.1007/s00170-022-08685-4.

Acknowledgements The Moai Head model (Used in Fig. 18) was used under CC licence from: https://www.myminifactory.com/object/3d-print-moai-or-mo-ai-75141.

Funding This research was partially funded by a faculty project of FME BUT, FSI-S-20–6296.

Availability of data and material Included as a supplementary file.

Code availability Included as a supplementary file.

Declarations

Conflict of interest Not applicable.

References

1. Ngo TD, Kashani A, Imbalzano G et al (2018) Additive manufacturing (3D printing): a review of materials, methods, applications and challenges. Compos Part B Eng. https://doi.org/10.1016/j.compositesb.2018.02.012
2. Thrimurthulu K, Pandey PM, Reddy NV, Venkata Reddy N (2004) Optimum part deposition orientation in fused deposition modeling. Int J Mach Tools Manuf 44:585–594
3. Jiang J, Newman ST, Zhong RY (2021) A review of multiple degrees of freedom for additive manufacturing machines. Int J Comput Integr Manuf 34:195–211. https://doi.org/10.1080/0951192X.2020.1858510
4. Xu K, Chen L, Tang K (2019) Support-free layered process planning toward 3 + 2-axis additive manufacturing. IEEE Trans Autom Sci Eng 16:838–850. https://doi.org/10.1109/TASE.2018.2867230
5. Fry NR, Richardson RC, Boyle JH (2020) Robotic additive manufacturing system for dynamic build orientations. Rapid Prototyp J 26:659–667. https://doi.org/10.1108/RPJ-09-2019-0243
6. Li Y, Tang K, He D, Wang X (2021) Multi-axis support-free printing of freeform parts with lattice infill structures. CAD Comput Aided Des 133:1–38. https://doi.org/10.1016/j.cad.2020.102986

7. Jiang J, Ma Y (2020) Path planning strategies to optimize accuracy, quality, build time and material use in additive manufacturing: A review. Micromachines 11. https://doi.org/10.3390/MI11070633
8. Nisja GA, Cao A, Gao C (2021) Short review of nonplanar fused deposition modeling printing. Mater Des Process Commun 3:3. https://doi.org/10.1002/mdp2.221
9. Pérez-Castillo JL, Cuan-Urquizo E, Roman-Flores A et al (2021) Curved layered fused filament fabrication: an overview. Addit Manuf 47. https://doi.org/10.1016/j.addma.2021.102354
10. Zhao HM, He Y, Fu YZ, Qiu JJ (2018) Inclined layer printing for fused deposition modeling without assisted supporting structure. Robot Comput Integr Manuf 51:1–13. https://doi.org/10.1016/j.rcim.2017.11.011
11. Yang Y, Fuh JYH, Loh HT, Wong YS (2003) Multi-orientational deposition to minimize support in the layered manufacturing process. J Manuf Syst 22:116–129. https://doi.org/10.1016/S0278-6125(03)90009-4
12. Kalami H, Urbanic J (2021) Exploration of surface roughness measurement solutions for additive manufactured components built by multi-axis tool paths. Addit Manuf 38:101822. https://doi.org/10.1016/j.addma.2020.101822
13. Pan Y, Zhou C, Chen Y, Partanen J (2014) Multitool and multi-axis computer numerically controlled accumulation for fabricating conformal features on curved surfaces. J Manuf Sci Eng Trans ASME 136. https://doi.org/10.1115/1.4026898
14. Gosselin C, Duballet R, Roux P et al (2016) Large-scale 3D printing of ultra-high performance concrete — a new processing route for architects and builders. Mater Des 100:102–109. https://doi.org/10.1016/j.matdes.2016.03.097
15. Bi D, Xie F, Tang K (2021) Generation of efficient iso-planar printing path for multi-axis fdm printing. J Manuf Mater Process 5. https://doi.org/10.3390/jmmp5020059
16. Mitropoulou I, Bernhard M, Dillenburger B (2020) Print paths key-framing: design for non-planar layered robotic FDM printing. Proc - SCF 2020 ACM Symp Comput Fabr. https://doi.org/10.1145/3424630.3425408
17. Kubalak JR, Wicks AL, Williams CB (2019) Exploring multi-axis material extrusion additive manufacturing for improving mechanical properties of printed parts. Rapid Prototyp J 25:356–362. https://doi.org/10.1108/RPJ-02-2018-0035
18. Chakraborty D, Aneesh Reddy B, Roy Choudhury A (2008) Extruder path generation for curved layer fused deposition modeling. CAD Comput Aided Des 40:235–243. https://doi.org/10.1016/j.cad.2007.10.014
19. Huang B, Singamneni SB (2015) Curved layer adaptive slicing (CLAS) for fused deposition modelling. Rapid Prototyp J 21:354–367. https://doi.org/10.1108/RPJ-06-2013-0059
20. Huang B, Singamneni S (2014) Curved layer fused deposition modeling with varying raster orientations. Appl Mech Mater 446–447:263–269. https://doi.org/10.4028/www.scientific.net/AMM.446-447.263
21. Singamneni S, Roychoudhury A, Diegel O, Huang B (2012) Modeling and evaluation of curved layer fused deposition. J Mater Process Technol 212:27–35. https://doi.org/10.1016/j.jmatprotec.2011.08.001
22. Huang B (2014) Alternate slicing and deposition. Strategies for Fused Deposition Modelling 55:511–517
23. Huang B, Singamneni S (2015) A mixed-layer approach combining both flat and curved layer slicing for fused deposition modelling. Proc Inst Mech Eng Part B J Eng Manuf 229:2238–2249. https://doi.org/10.1177/0954405414551076
24. Zhao G, Ma G, Feng J, Xiao W (2018) Nonplanar slicing and path generation methods for robotic additive manufacturing. Int J Adv Manuf Technol 96:3149–3159. https://doi.org/10.1007/s00170-018-1772-9
25. Schuh G, Bergweiler G, Lukas G et al (2020) Feature-based print method for multi-axis material extrusion in additive manufacturing. Procedia CIRP 93:85–89
26. Ezair B, Fuhrmann S, Elber G (2018) Volumetric covering print-paths for additive manufacturing of 3D models. CAD Comput Aided Des 100:1–13. https://doi.org/10.1016/j.cad.2018.02.006
27. Allen RJA, Trask RS (2015) An experimental demonstration of effective curved layer fused filament fabrication utilising a parallel deposition robot. Addit Manuf 8:78–87. https://doi.org/10.1016/j.addma.2015.09.001
28. Etienne J, Ray N, Panozzo D et al (2019) Curvislicer: Slightly curved slicing for 3-axis printers. ACM Trans Graph 38. https://doi.org/10.1145/3306346.3323022
29. Xu K, Li Y, Chen L, Tang K (2019) Curved layer based process planning for multi-axis volume printing of freeform parts. CAD Comput Aided Des 114:51–63. https://doi.org/10.1016/j.cad.2019.05.007
30. Fang G, Zhang T, Zhong S et al (2020) Reinforced FDM: Multi-axis filament alignment with controlled anisotropic strength. ACM Trans Graph 39. https://doi.org/10.1145/3414685.3417834
31. Dai C, Wang CCL, Wu C et al (2018)Support-free volume printing by multi-axis motion. ACM Trans Graph 37. https://doi.org/10.1145/3197517.3201342
32. Brell-Çokcan S, Braumann J (2011) Parametric robot control. Proc 31st Annu Conf Assoc Comput Aided Des Archit 242–251
33. Roschli A, Gaul KT, Boulger AM et al (2019) Designing for big area additive manufacturing. Addit Manuf 25:275–285. https://doi.org/10.1016/j.addma.2018.11.006
34. Hertle S, Drexler M, Drummer D (2016) Additive manufacturing of poly(propylene) by means of melt extrusion. Macromol Mater Eng 301:1482–1493. https://doi.org/10.1002/mame.201600259
35. Duty CE, Kunc V, Compton B et al (2017) Structure and mechanical behavior of Big Area Additive Manufacturing (BAAM) materials. Rapid Prototyp J 23:181–189. https://doi.org/10.1108/RPJ-12-2015-0183
36. Elber G, Cohen E (1996) Adaptive isocurve-based rendering for freeform surfaces. ACM Trans Graph 15:249–263. https://doi.org/10.1145/231731.231736
37. Dizon JRC, Espera AH, Chen Q, Advincula RC (2018) Mechanical characterization of 3D-printed polymers. Addit Manuf 20:44–67. https://doi.org/10.1016/j.addma.2017.12.002

3D PRINTING AND ADDITIVE MANUFACTURING
Volume 00, Number 00, 2022

DOI: 10.1089/3dp.2022.0097

Method of Multiaxis Three-Dimensional Printing with Intralayer Height Variation for Stairstep Effect Compensation

Martin Krčma,[1] David Paloušek,[2] David Škaroupka,[1] Johannes Braumann,[3] and Daniel Koutný[1]

Abstract

The recent developments in multiaxis three-dimensional (3D) printing have got a large potential for expanding the capability of material extrusion based methods. Especially curved and nonplanar methods can improve buildability, surface quality, and mechanical performance. However, the challenges that arise from using them complicate their deployment. In this article, we propose a hybrid planar method, based on varying the layer height and deposition speed in combination with tool reorientation, that allows us to get a lot of the same benefits that come from using nonplanar layers. The goal of the method is to keep the deposition constant regardless of the overhang angle. This is achieved by simultaneous control of layer height, deposition speed, and tool orientation. The method is the most beneficial for large-scale, single-wall 3D printing, such as clay, concrete, and other composites. The main restriction of the method depends on the minimum/maximum ratio between the nozzle diameter and layer height. A description of the method is provided, and sample objects are evaluated either as trajectories or as test prints. The claims are confirmed by microscopy measurement of the contact patch width. The method as presented allows printing of overhangs up to 82.34°, can be applied to complex geometry without difficulties, and further possibilities of limit expansion are discussed. The contact patch width decreases only by 20% at the 80° of overhang.

Keywords: multiaxis, 3D printing method, variable layer height, intralayer height variation, process planning

Introduction

Material extrusion (MEX) based three-dimensional (3D) printing is the most common type of 3D printing today, uniting techniques such as Fused Deposition Modeling, Free-form Filament Fabrication, or clay and concrete 3D printing. Its main benefits are the ease of implementation, wide variety of materials, and the capabilities of multimaterial or composite printing. The method also has intrinsic properties such as stair stepping, limited buildability, and anisotropy—most significantly in the direction of the build—all caused by the rasterized nature of the layer-by-layer process.[1]

Multiaxis 3D printing, and especially nonplanar 3D printing, has the potential to expand the boundaries of MEX based methods. These methods can completely or partially solve the problems caused by the layer-by-layer printing process. However, they also bring new difficulties in process planning, computation, and design limitations.[2,3]

Overhang buildability of conventional FDM 3D printing is limited due to the ability of subsequent layers to adhere to each other. This ability decreases as the contact patch width becomes smaller with increasing overhang angle—the common limit is 45°, but the actual value is dependent on the width/height ratio of the deposition. Users of FDM machines report printable overhangs in excess of 60° with the use of high ratios. However, this is a long-standing limitation of FDM printing.[4]

This article aims to present an easy to implement transitionary approach, which may be most beneficial for use with large nozzle sizes and single wall deposition, a strategy commonly deployed with screw extruders. This approach

[1]Institute of Machine and Industrial Design, Faculty of Mechanical Engineering, Brno University of Technology, Brno, Czech Republic.
[2]One3D s.r.o., Mohelnice, Czech Republic.
[3]Creative Robotics, University of Art and Design Linz, Linz, Austria.

Opposite page: A robot arm equipped with a pellet extruder in process of multiaxis 3D printing. *Image Credit:* Martin Krčma.

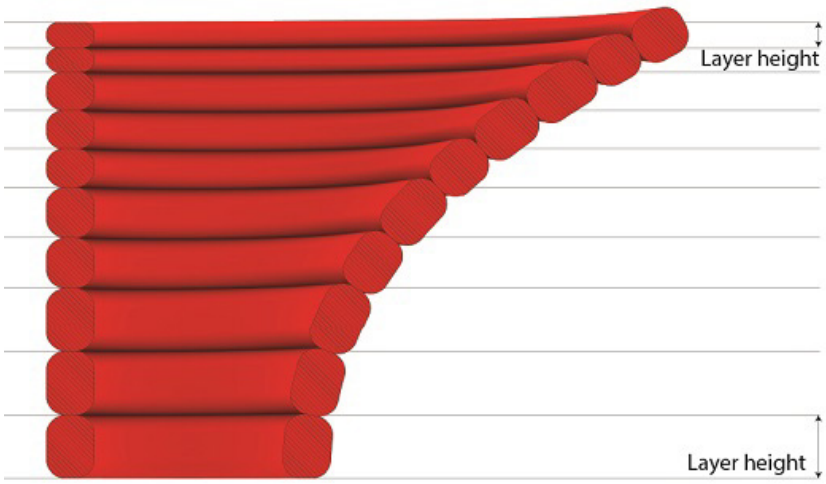

FIG. 1. Intralayer variable thickness depositions resulting from the method.

combines variable layer height, deposition speed, and tool orientation with planar layers and should significantly expand the buildability while being easy to implement and combine with other methods. The potential in expanding planar multiaxis methods has been noticed by other researchers.[2]

State of the art

Keeping the height constant independently on the overhang angle and orienting the extruder along the surfaces' local tangent is not a novel idea and has been previously demonstrated, for example, by Gosselin et al.[5] However, slicing objects in a way that maintains equal layer height introduces curvature into the layers, due to differences in geodesic distances. This makes it a necessity to deal with collision checking due to nozzle interference when moving on slopes or collision of the extruder or machine with the print for multiaxis strategies. Methods to generate these layers, as well as potential limitations of the process, were presented by Xu et al[6] and by Shan et al using isothermal simulation.[7]

A strategy to avoid the possibility of interference was presented by Dai et al,[8] ensuring accessibility by only generating convex layers, but this strategy has to balance with requirements on surface quality. Another nonplanar method to improve buildability works with splitting the model by its local geometry and varying the build orientation for the components.[9,10] Limitations of curved layer methods include inability to print certain objects with branched topology, the possibility of collision limiting buildable geometry, and low surface quality caused by curved layer stacking.[11]

In the literature, few examples of intentional in-layer height variations have been found. One of these works is presented by Pelzer and Hopmann,[12] applied to regular scale FDM machinery and focuses on accurately filling the space between top and bottom curved layers with variable layer height infill, as well as using this infill for better part reinforcement. A work that takes advantage of intralayer height variations to achieve better surface quality and detail preservation with a lower layer count for desktop FDM is the CurviSlicer.[13] Another work focusing on accurate printing of top and bottom curved shells was presented by Chen et al.[14] This work incorporates five-axis movements and presents an approach to print thin shells with curved variable thickness layers. Both articles mention collision avoidance problems and possible solutions. A new method called Continuously Varied Extrusion focuses on a related topic: 3D printing with an intralayer path width variation, to achieve better infill coverage.[15] Full Control G-Code Designer is a freely available tool that allows for these approaches to be implemented, but requires parametric definition of a model.[16] Changes in layer height also occur as a side effect of iso-parametric slicing approaches, but do not disturb the print if the differences are small enough.

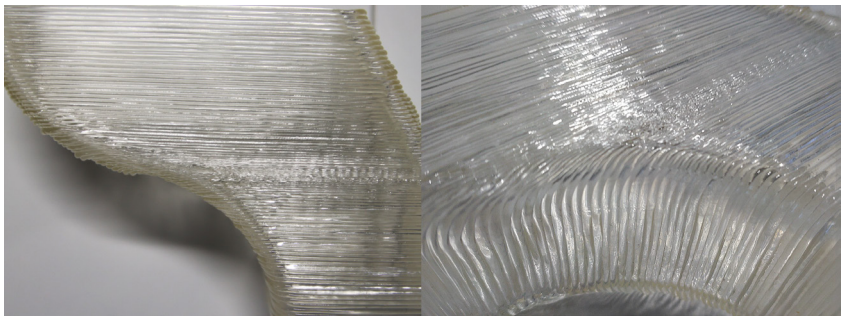

FIG. 2. Proof of concept print with a closeup of the intralayer height changes.

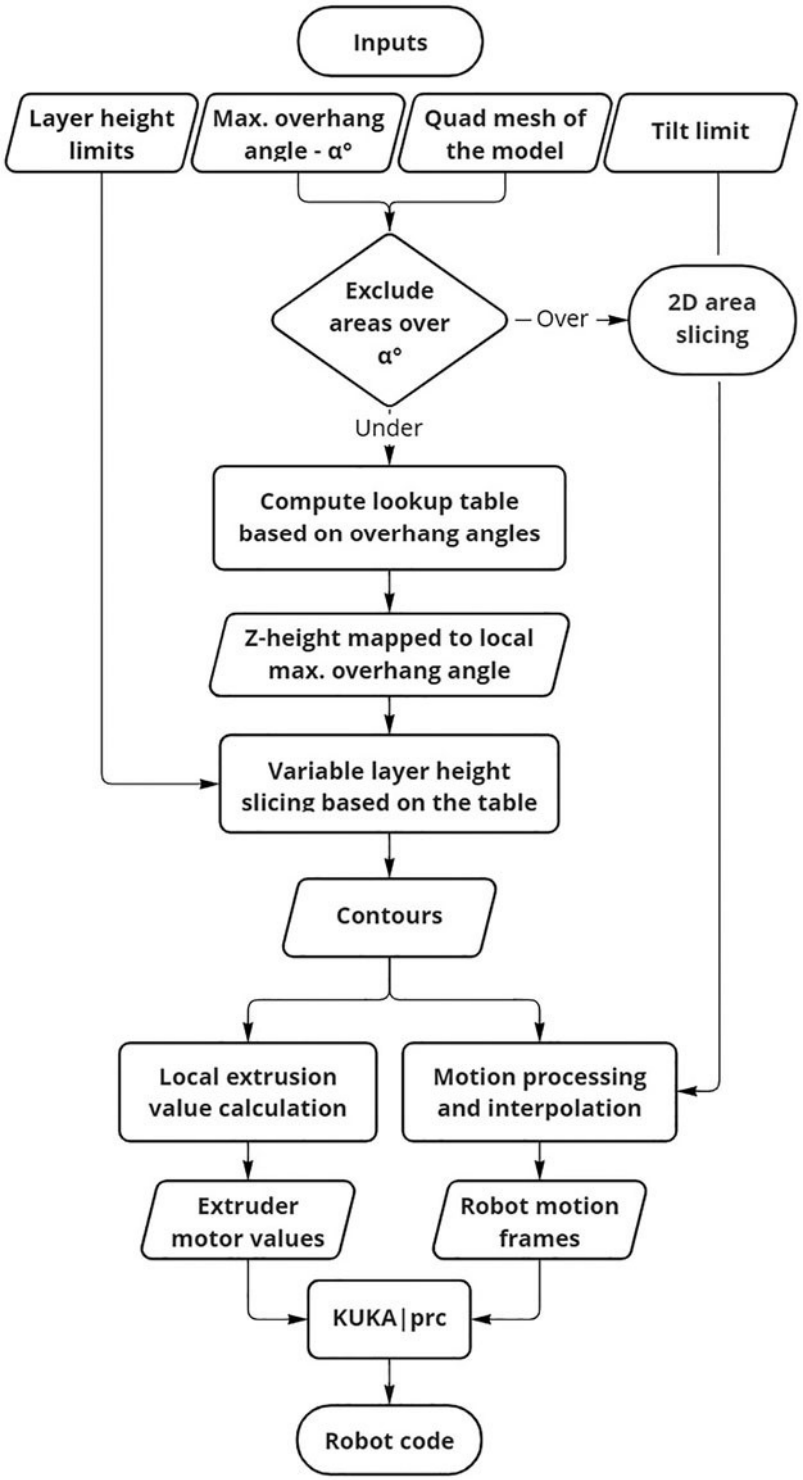

FIG. 3. Flowchart of the algorithm, from data input to variable height slicing and motion planning.

Variable layer height slicing is usually done according to the ''cusp height'' measure, either through the entire model or adaptively, with the layer height changing based on local geometry.[17] The cusp height describes the maximum deviation of the error from the original surface. A number of slicing algorithms were developed, for example, an efficient approach of slicing based on profile analysis, or by surface roughness (*Ra*), or by a combination of previous criteria.[18–20] Adaptive layer height and curved layer slicing have also been combined and tested for printing specific objects to bring both mechanical and surface quality improvements.[21]

Methods

The proposed method avoids the issues of self-collision and surface coverage by eschewing curved layers. Instead,

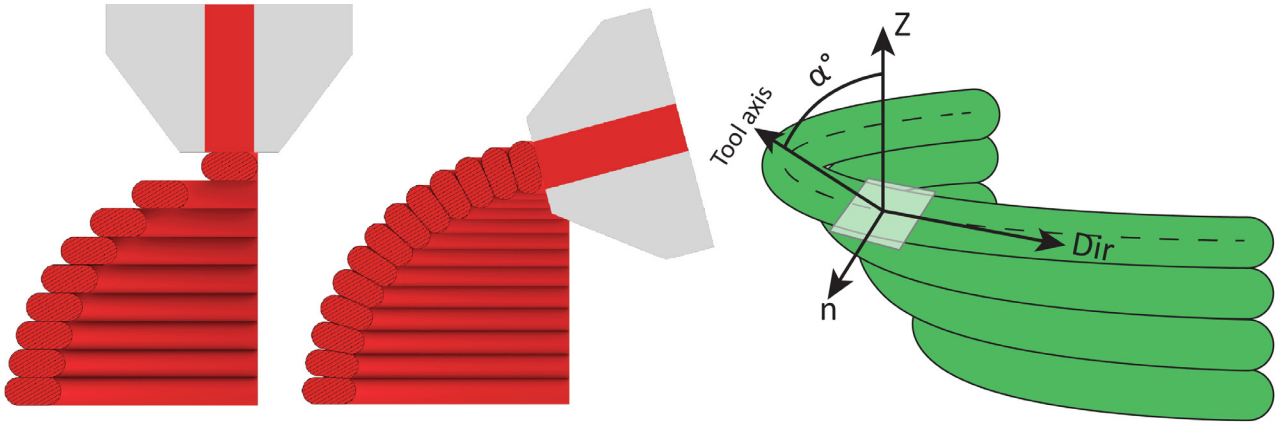

FIG. 4. *Left*: Conventional printing with constant layer height. *Middle*: Variable layer height with tilt (based on Krejcirik et al[27]). *Right*: Tool orientation vector.

we claim that the goal of all the methods is essentially to keep the amount of extruded material constant independent of overhang angle, resulting in constant wall thickness. To achieve the required actual material deposition rate, we propose varying the extrusion to movement speed ratio based on local overhang angle. This is coupled with reorientation of the nozzle by five-axis motion, to keep the expanded deposition aligned with local surface tangent direction, and with variable layer height slicing, to expand the buildability achieved by the method. The resulting slightly nonplanar depositions are shown in Figure 1, and a sample part is shown in Figure 2. While the tool path is planar, the width of the deposition causes slight out of plane effect, more prominent as the overhang increases.

The method, its flowchart pictured on Figure 3, is described in the following paragraphs.

Maximum and minimum layer height

Variable layer height slicing is used. The limits for layer height (h) are adapted from previous research and industry practices, and for the purpose of this study, the range of 10–75% of the nozzle diameter was used.[22,23] This ratio determines the maximum overhang angle (α) that is printable by this method, utilizing no additional strategies: $\cos\alpha = \frac{h_{\min}}{h_{\max}}$, which gives us the maximum overhang angle of 82.34°. The practical explanation of this limit is that in a layer at this overhang angle, both the minimum and the

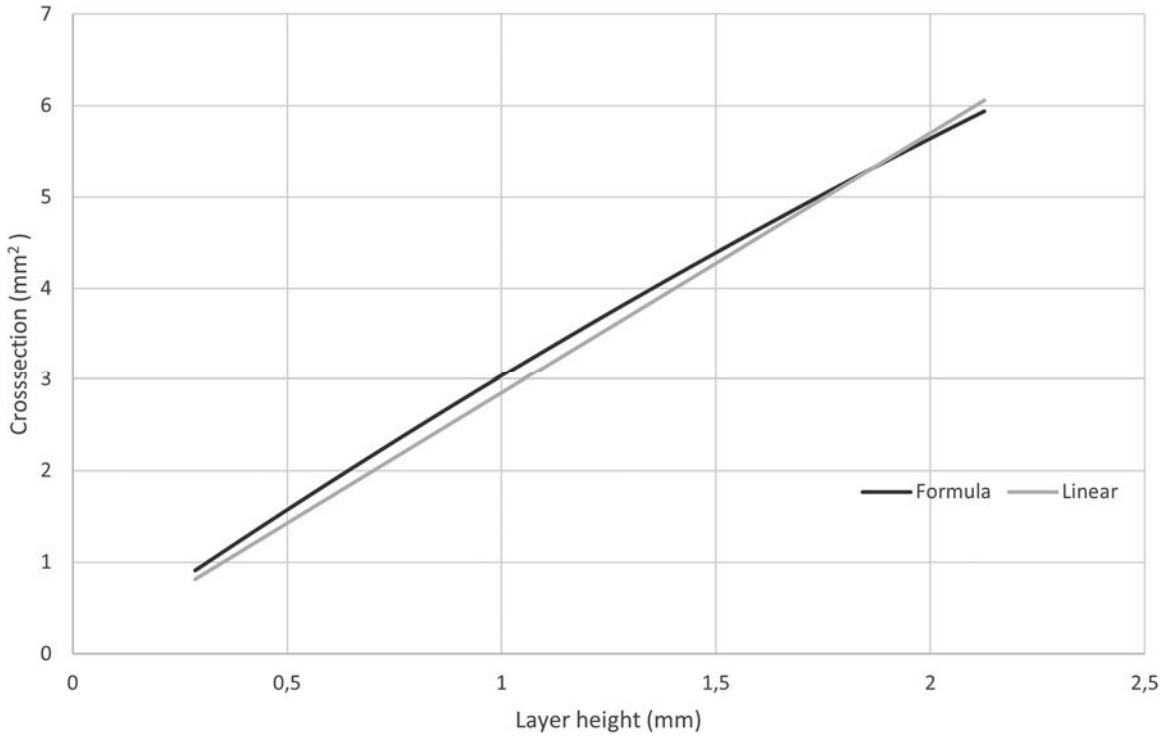

FIG. 5. Comparison of extrusion ratio from the linear and formula-based calculations.

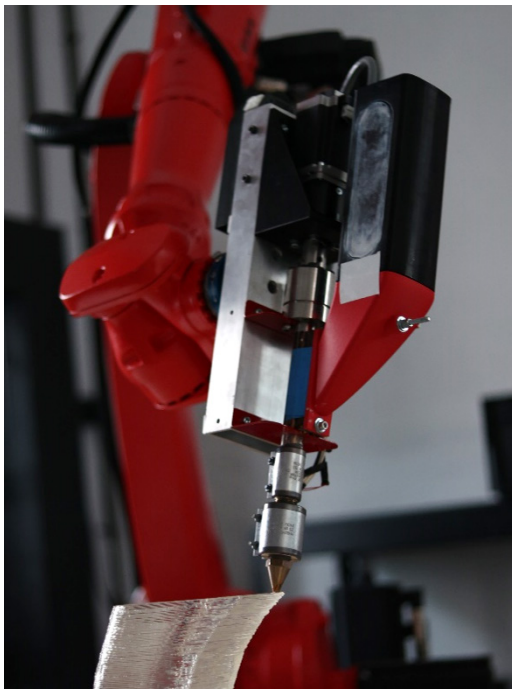

FIG. 6. The assembly during a print.

maximum layer heights are present. Up until this point, overhangs should be printable without any compromise in wall thickness.

Slicing algorithm

All slicing, computation, and motion planning is performed in McNeels Rhinoceros 7, its Grasshopper environment, built-in Iron Python interpreter, and KUKA|prc plug-in.[24]

Precalculation. The input data in either B-rep or mesh form are processed using Rhinos Quadmesh command, allowing processing without the influence of poor quality meshes, such as faces with high aspect ratio. If the mesh contains faces whose overhang angle is higher than the limit of this method, they are excluded from the precalculation mesh, and these areas would have to be processed otherwise.

Variable layer height slicing is then performed by a custom algorithm (Fig. 3), considering the maximum overhang angle at any given model height. For this, a table of height coordinate matched to corresponding max. angle is calculated and used during the iterative slicing process to decide on the next layer height. A sample table is included as Supplementary Data. The relationship between the overhang angle and the layer height is linear with the sine value of the angle between the Z axis and the local normal. The initial layer height is used for 0° of overhang, and the $h_{\min}$ is used for the maximum overhang angle. The resulting contours can be computed either from the quad mesh or from the original mesh if available.

Motion planning. The quad mesh is also used for the tool orientation planning. The tool orientation for each point is composed of a cross product between a normal vector of the quad mesh and a vector that is tangent to the tool path and oriented to the direction of travel. The orientation is explained in the Figure 4, right. In addition to the tool path interpolation provided by KUKA|prc, the tool orientation is interpolated as well to keep the robot motion consistent.

After calculating the five-axis motions, used to facilitate proper stacking of the print paths and increase surface quality (Fig. 4, left), a tilt limiter set at 45° is utilized. Tilt of 45° allows for full buildability of surfaces with up to 90° of overhang, if suitable (nonplanar) tool paths are used.[25] The tilt control algorithm works by evaluating the angle between the orientation of the intended tool axis and world Z axis. If the angle is higher than the threshold, the original vector is replaced by a one on an identical plane (described by the world Z direction and the original orientation vector), with the new angle equal to the threshold angle. As a side effect, if the extruder boundary cone is within this angle, any possibility of collision between the workpiece and the machine tool is eliminated.

Speed control. The extrusion ratio has to be continuously adjusted proportionally with varying layer height to ensure constant wall thickness. For each point of the tool path, the extrusion ratio is calculated from the local layer height—shortest distance to the following contour. For the evaluation prints, linear scaling was used. To increase precision, a scaling based on a cross-section formula could be used. The formula for a constant wall thickness is: $S = \pi\left(\frac{h}{2}\right)^2 + (w-h)h$; ($w$—width, h—layer height). The chart displayed on Figure 5 compares the differences between the two methods.

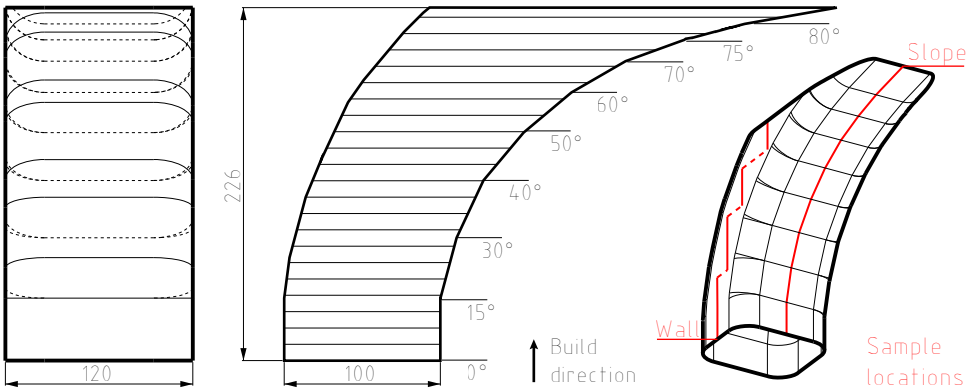

FIG. 7. Dimensions of the overhang tower and location of the samples.

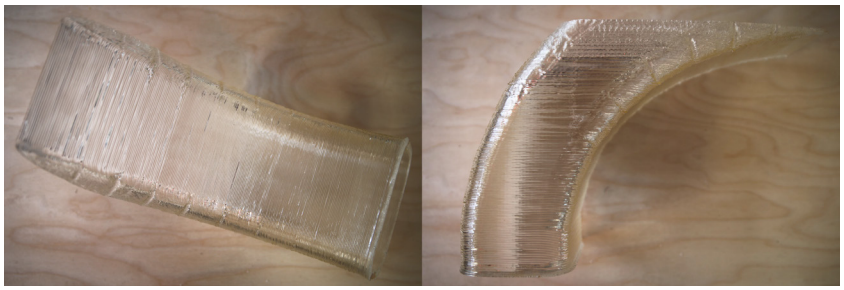

FIG. 8. The printed overhang tower after removal from build plate.

To avoid negative influence of the lag in material flow caused by changing Rotations Per Minute of the screw extruder, the setup has near constant RPM and it is only influenced by deviations in robot speed (e.g., when a rapid change in direction occurs). Instead, the tool center point speed changes depending on layer height. This also eliminates the influence of the nonlinear flow of the screw extruder. The speed control used to demonstrate this process was tailored to the screw extruder used, it is not an integral part of the process, and other ways to ensure correct material deposition rate could be developed. In filament setups, optimization for maximum material flow/tool speed would be possible.

Materials and machines

The robotic arm used for printing is a Kuka Cybertech KR16R2010-2 with a KRC 5 control cabinet. The extruder is adapted from a NOZTEK Touch filament extruder unit but equipped with a robot-coupled stepper motor for precise extrusion control. The pellet material used in the demonstration is clear PLA. The nozzle size was ø2.85 mm, with the nozzle having an elongated geometry beneficial to this method. The tip angle of the nozzle is 37.5°, and the tip length is 25 mm (The nozzle can be seen in Fig. 6). The initial layer height was 1.5 mm, and the barrel temperature was set at 210° C for both zones of the extruder. The initial tool speed was 20 mm/s. The assembly is pictured in Figure 6.

To practically prove the presented method, an overhang tower was designed and printed; its dimensions and the location of the samples are pictured in Figure 7. Confirmation of the results was done by measuring the width of the wall and the contact patch at all tiers of the overhang tower to prove the constant material deposition independent of overhang. For this purpose, samples were taken from the towers' overhangs (Slope) and from the vertical walls (Wall). The tower was cut apart, and the samples were milled to expose the cross section. The width was then measured optically, using an Olympus 8ZX7 microscope equipped with a Canon EOS 1200D at 16× magnification. For measurement and statistics, its accompanying software, QuickPHOTO Micro, was used.

In addition, an object with a complex topology—a chain link sample—was sliced and printed to show the capability to process objects with multiple cross sections.

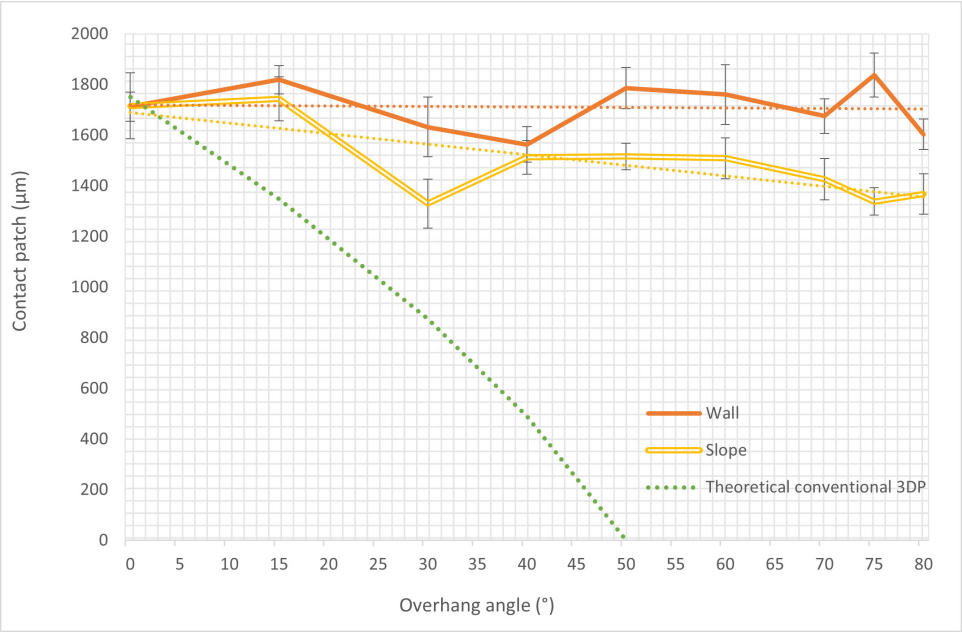

FIG. 9. Contact patch thickness chart comparing the Wall and Slope samples based on overhang angle with theoretical values of a conventional print with the same initial parameters.

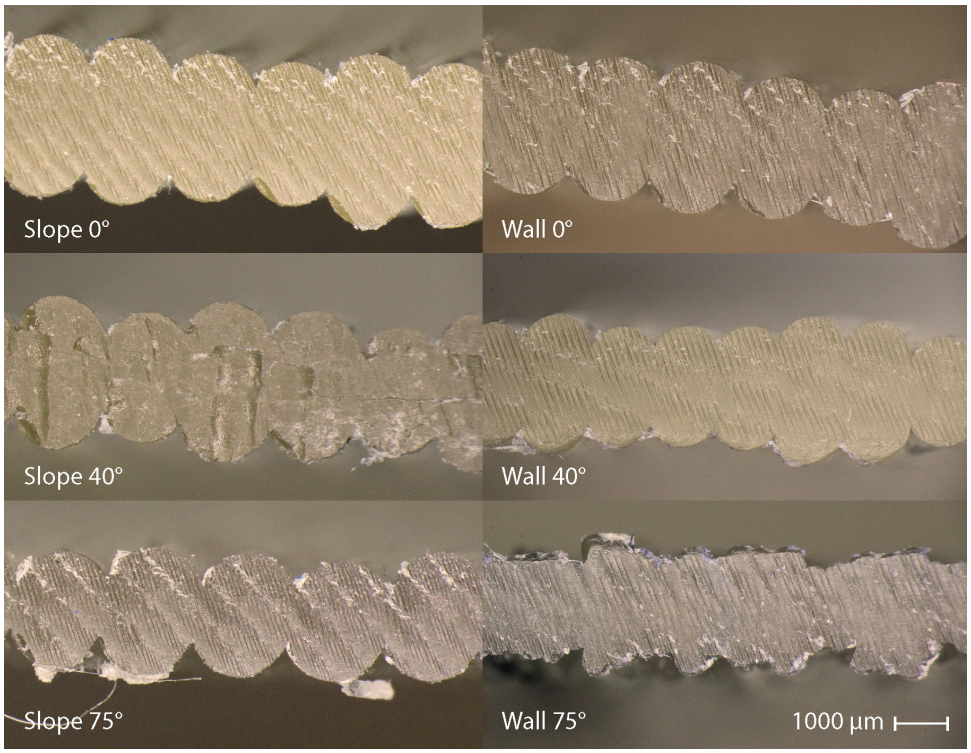

FIG. 10. Overview of contact patch samples displaying a selected sample from the 0°, 40°, and 75° Slope sections and the corresponding Wall samples.

Results and Discussion

The printed overhang tower can be seen in Figure 8. The confirmation objects were printed successfully. Some reduction of quality was recorded in sections with the lowest layer height. Causes of this effect are unknown as the setup was able to print the lowest layer height in an isolated sample. The reduction in quality might be due to the front face of nozzle contacting the deposition. This might be reduced by reducing the external nozzle tip diameter or by slightly modifying the tilt orientation to add a tilt in the direction of travel.

Contact patch thickness

The goal of this method is to keep the deposition thickness constant and independent of the overhang angle. The results of the microscopy can be seen in Figure 9. The contact patch

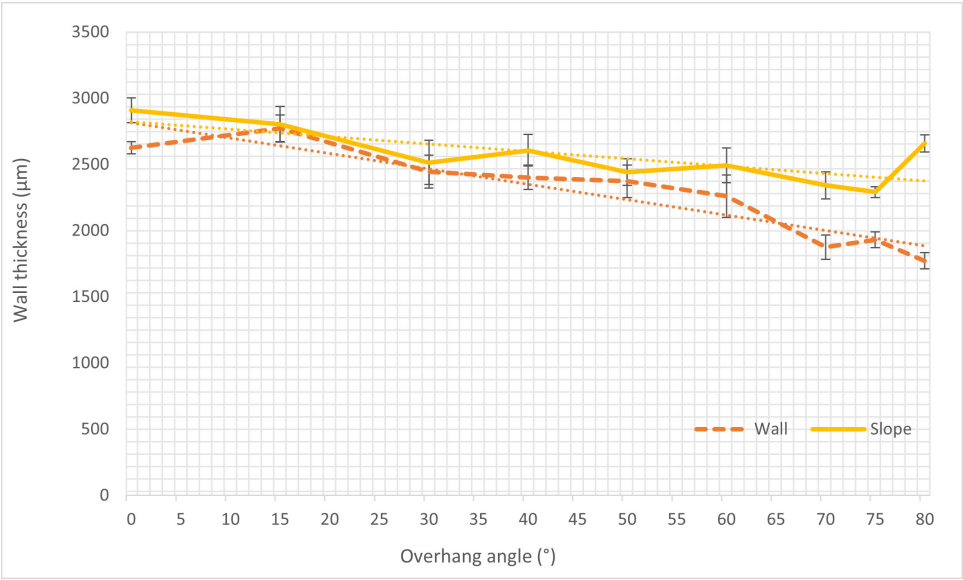

FIG. 11. Wall thickness chart comparing the Wall and Slope samples based on overhang angle.

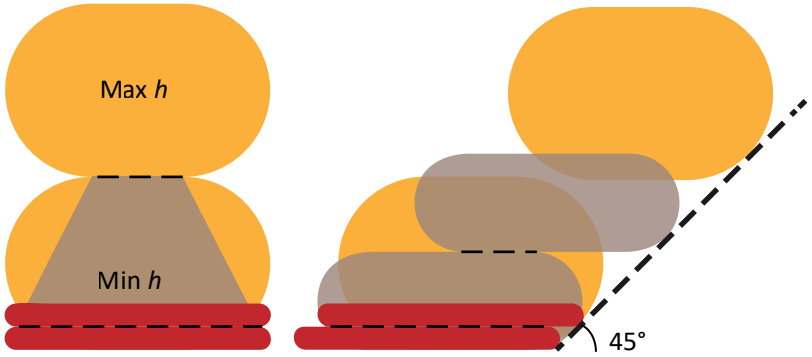

FIG. 12. *Left*: Width of the contact patch correlated to layer height—the lower the layer, the wider is the contact patch; *Right*: The impact of this effect on buildability.

thickness was close to constant for the wall samples. The decrease of the contact patch thickness for the sloped samples was 20% at the 80° overhang segment and 12% at the 50° overhang segment. This is a significant increase over the theoretical width of the contact patch for a conventional 3D printing, which would be 0 μm at 50° of overhang for a print with the same nozzle diameter (2.85 mm) and layer thickness (1.5 mm). The conventional patch thickness was modeled based on previous research.[9,26,27] The microscopy images can be seen in Figure 10. The drop at 30° of overhang is unexpected. Its appearance in both the Wall and the Slope samples suggests that it might not be related to the slicing method.

Wall thickness

There was a slight decrease in the wall thickness of the samples (see Fig. 11). The slope samples had a consistent decrease by $\sim$15% from 0° to 80° of overhang. The wall sample width had decreased by about 30%, with the most noticeable decrease during the last segments; these segments also showed the decrease in print quality. The overall decrease is probably caused by sagging or shrinkage of the deposition during the print, while the decrease in the last wall segment is probably caused by the higher level of variance at low layer heights. The contact patch remained more consistent partially due to the correlation of the contact patch thickness to layer height, explained in Figure 12, and possibly due to a partial sagging of the depositions.

Known limitations and capability extension

The method as described is capable of printing objects up to the buildability limit, which is 82.34° of overhang. This angle is based on the combination of minimum and maximum layer height, which was 10–75% of nozzle diameter. The limit would change if other values were used, based on specific printer capabilities. The limit as used has no relation to the sliced geometry, and other parts of the method are not dependent on in either. There is no risk of extruder–geometry collision due to the applied tilt limiter. One area where problems might arise based on sliced geometry are sharp internal corners, especially in lower layer height. If internal corner radii are limited to nozzle diameter or more, this risk is significantly reduced.

The current approach works by calculating the layer heights as if each layer includes a 0° overhang segment—in other words, as if the h_{min} was applied to a vertical segment. An extension of this method could be gained by considering

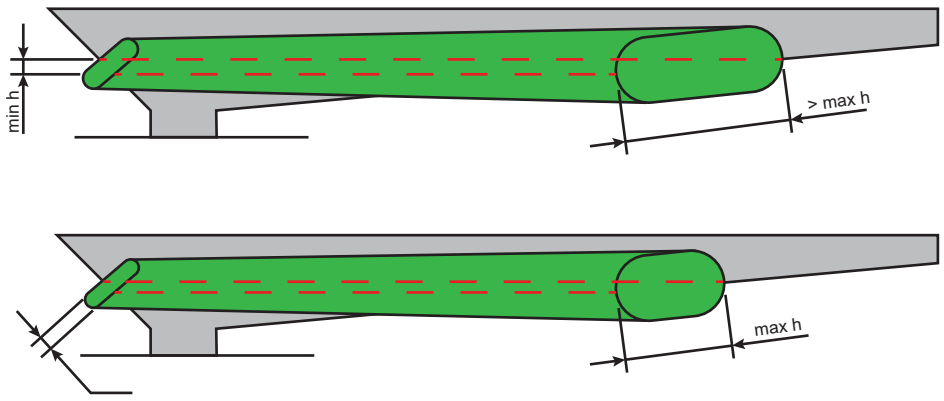

FIG. 13. Capability extension for specific geometries. **(A)** An unbuildable case without taking the actual inclination at the location of h_{min} into consideration. **(B)** The same geometry becomes buildable if the inclination of h_{min} is taken into account, extending the buildability limit.

FIG. 14. Sliced glass with zones to be printed with 2D slicing marked in *black*; toolpaths are thickened for visibility. 2D, two-dimensional.

the actual lowest overhang angle in each layer—and applying the minimum layer height at that value—in regard to the actual layer height at that overhang. This will enable higher printable overhangs based on geometry, up to and excluding 90° in specific cases. A case where the build limit could be expanded is pictured in Figure 13.

Multiaxis 3D printing can function even beyond the slicing limit of the described method. The near-flat areas that are uncovered by the slicing algorithm could be sliced as an actual flat area, using common approaches such as contour offsetting. This would make overhangs over 90° printable. The only modification from the two-dimensional (2D) methods currently in use would be the need to avoid printing in mid-air by only generating paths that maintain contact with previously deposited material. A sliced object that combines both types of trajectories can be seen in Figure 14.

As previously mentioned, the method can be used on geometry with a complex topology. To demonstrate this, a chain link sample with sections that both branch apart and connect back together was printed. The finished print (after postprocessing) can be seen in Figure 15, together with a flower planter stand that features functional, load bearing surfaces at 80° of overhang.

In addition to the abovementioned optimization for maximum tool speed, optimization for layer height could be added. Currently, layers with 0° overhang angle are printed with the nominal layer height, optimized for quality. Instead, the

FIG. 15. *Left*: The chain link sample sliced and printed with the described method (Leftovers after retractions removed). *Right*: Flower planter stand printed with the described method, as printed and in use.

max. layer height could be used. This would reduce build time for setups where movement speed is the limiting factor, instead of the extruder.

A future study of effects of this method on mechanical properties should show improvements. The expectation is that samples printed with this method would outperform conventional samples but be bested by nonplanar/curved methods, as those offer more contact between layers. The effect on solid parts could also be explored, the methods is expected to be less beneficial, as it will have no effect on internally facing walls, and will bring only a minor benefit over variable layer height printing—the overhang buildability of external contours should improve.

Conclusions

A new multiaxis 3D printing method for thin shells is presented in this article as an alternative to nonplanar/curved layer methods. It combines approaches of adaptive layer height slicing and multiaxis 3D printing and presents the concept of using in-layer layer height variation intently. The result is a significant expansion of buildability and elimination of supports while keeping the deposition width stable at the same time. The processing is straightforward, as the combination of limited tilt and planar layers ensures that any geometry can be printed without the need for collision or coverage checking. The method as presented only works for objects within the buildability limit (82.34°, derived from the maximum and minimum printable layer height) and has been verified by a realized 3D print, with up to 80° of overhang printed. The method was verified by measuring the width of the contact patch throughout the print. Using the method, the width decreased by 20% at 80° of overhang, while conventionally, the width would be 0 at 50°.

The method can be combined with additional approaches to expand the buildability limit, and some of them were presented, including a way to expand the limit for specific geometry and an approach combining the method with 2D filling patterns for near-horizontal areas. The method was realized in the Grasshopper plug-in but should be feasible in any other environment. The method as described brings the most benefit to large scale single wall printing, commonly in use with screw extruders, and for vase mode printing on FDM machinery. In future, it could be promising even for printing outer contours of dense parts as the same benefits would be applicable.

Authors' Contributions

M.K.: Conceptualization, methodology, validation, software, writing—original draft. D.P.: Supervision, conceptualization, writing—review and editing. D.Š.: Writing—review and editing. J.B.: Software, writing—review and editing. D.K.: Supervision, funding acquisition.

Author Disclosure Statement

The authors report that there are no competing interests to declare.

Funding Information

Part of the work was sponsored by the faculty project of the FME BUT, FSI-S-20-6296, and part of the work was carried out during a research stay sponsored by Aktion Österreich-Tschechien, AÖCZ-Semesterstipendien, MPC-2021-00465.

Supplementary Material

Supplementary Data

References

1. Dizon JRC, Espera AH, Chen Q, et al. Mechanical characterization of 3D-printed polymers. Addit Manuf 2018;20:44–67; doi: 10.1016/j.addma.2017.12.002.
2. Nayyeri P, Zareinia K, Bougherara H. Planar and nonplanar slicing algorithms for fused deposition modeling technology: A critical review. Int J Adv Manuf Technol 2022;119:2785–2810; doi: 10.1007/s00170-021-08347-x.
3. Nisja GA, Cao A, Gao C. Short review of nonplanar fused deposition modeling printing. Mater Des Process Commun 2021;3(4):e221; doi: 10.1002/mdp2.221.
4. Zhao HM, He Y, Fu JZ, et al. Inclined layer printing for fused deposition modeling without assisted supporting structure. Robot Comput Integr Manuf 2018;51(2016):1–13; doi: 10.1016/j.rcim.2017.11.011.
5. Gosselin C, Duballet R, Roux P, et al. Large-scale 3D printing of ultra-high performance concrete—A new processing route for architects and builders. Mater Des 2016;100:102–109; doi: 10.1016/j.matdes.2016.03.097.
6. Xu K, Li Y, Chen L, et al. Curved layer based process planning for multi-axis volume printing of freeform parts. CAD Comput Aided Des 2019;114:51–63; doi: 10.1016/j.cad.2019.05.007.
7. Shan Y, Gan D, Mao H. Curved layer slicing based on isothermal surface. Procedia Manuf 2021;53:484–491; doi: 10.1016/j.promfg.2021.06.081.
8. Dai C, Wang CCL, Wu C, et al. Support-free volume printing by multi-axis motion. ACM Trans Graph 2018;37(4):1–14; doi: 10.1145/3197517.3201342.
9. Fry NR, Richardson RC, Boyle JH. Robotic additive manufacturing system for dynamic build orientations. Rapid Prototyp J 2020;26(4):659–667; doi: 10.1108/RPJ-09-2019-0243.
10. Murtezaoglu Y, Plakhotnik D, Stautner M, et al. Geometry-based process planning for multi-axis support-free. Proc CIRP 2018;78:73–78; doi: 10.1016/j.procir.2017.04.009.
11. Zhao G, Ma G, Feng J, et al. Nonplanar slicing and path generation methods for robotic additive manufacturing. Int J Adv Manuf Technol 2018;96(9–12):3149–3159; doi: 10.1007/s00170-018-1772-9.
12. Pelzer L, Hopmann C. Additive manufacturing of non-planar layers with variable layer height. Addit Manuf 2021;37(2020):101697; doi: 10.1016/j.addma.2020.101697.
13. Etienne J, Ray N, Panozzo D, et al. Curvislicer: Slightly curved slicing for 3-axis printers. ACM Trans Graph 2019;38(4):1–11; doi: 10.1145/3306346.3323022.
14. Chen L, Chung MF, Tian Y, et al. Variable-depth curved layer fused deposition modeling of thin-shells. Robot Comput Integr Manuf 2019;57(2018):422–434; doi: 10.1016/j.rcim.2018.12.016.
15. Moetazedian A, Budisuharto AS, Silberschmidt VV, et al. CONVEX (CONtinuously Varied EXtrusion): A new scale of design for additive manufacturing. Addit Manuf 2021;37(2020):1–19; doi: 10.1016/j.addma.2020.101576.
16. Gleadall A. FullControl GCode Designer: Open-source software for unconstrained design in additive manufacturing.

Addit Manuf 2021;46:102109; doi: 10.1016/j.addma.2021.102109.
17. Mani K, Kulkarni P, Dutta D. Region-based adaptive slicing. CAD Comput Aided Des 1999;31(5):317–333; doi: 10.1016/S0010-4485(99)00033-0.
18. Mao H, Kwok TH, Chen Y, et al. Adaptive slicing based on efficient profile analysis. CAD Comput Aided Des 2019;107:89–101; doi: 10.1016/j.cad.2018.09.006.
19. Pandey PM, Reddy NV, Dhande SG. Real time adaptive slicing for fused deposition modelling. Int J Mach Tools Manuf 2003;43(1):61–71; doi: 10.1016/S0890-6955(02)00164-5.
20. Wasserfall F, Hendrich N, Zhang J. Adaptive slicing for the FDM process revisited. IEEE Int Conf Autom Sci Eng 2017;2017:49–54; doi: 10.1109/COASE.2017.8256074.
21. Huang B, Singamneni SB. Curved layer adaptive slicing (CLAS) for fused deposition modelling. Rapid Prototyp J 2015;21(4):354–367; doi: 10.1108/RPJ-06-2013-0059.
22. Kuznetsov VE, Solonin AN, Urzhumtsev OD, et al. Strength of PLA components fabricated with fused deposition technology using a desktop 3D printer as a function of geometrical parameters of the process. Polymers (Basel) 2018;10(3):1–11; doi: 10.3390/polym10030313.
23. Anonymous. Layers and perimeters. Available from: https://help.prusa3d.com/cs/article/vrstvy-a-perimetry_1748 [Last accessed: June 10, 2022].
24. Braumann J, Brell-Çokcan S. Parametric robot control. Proc 31st Annu Conf Assoc Comput Aided Des Archit 2011;242–251; doi: 10.52842/conf.acadia.2011.242.
25. Wüthrich M, Gubser M, Elspass WJ, et al. A novel slicing strategy to print overhangs without support material. Appl Sci 2021;11(18):1–21; doi: 10.3390/app11188760.
26. Krčma M, Paloušek D. Comparison of the effects of multiaxis printing strategies on large-scale 3D printed surface quality, accuracy, and strength. Int J Adv Manuf Technol 2022;119:7109–7120; doi: 10.1007/s00170-022-08685-4.
27. Krejcirik P, Skaroupka D, Palousek D. Free directional robotic deposition—Influence on overhang printability. MM Sci J 2018;12(2018):2715–2721; doi: 10.17973/mmsj.2018_12_2018119.

Address correspondence to:
Martin Krčma
Institute of Machine and Industrial Design
Faculty of Mechanical Engineering
Brno University of Technology
Technická 2896/2
616 00 Brno-Královo Pole
Czech Republic

E-mail: martin.krcma1@vut.cz